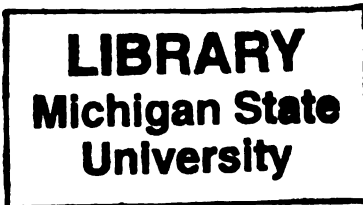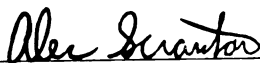This is to certify that the

thesis entitled

Kinetic Studies for Cationic Photopolymerization
of Epoxides

presented by

Nguyen, Khanh Phuong

has been accepted towards fulfillment
of the requirements for

__Masters__ degree in __Chemical Engineering__

Alex Scranton
Major professor

Date ___6/12/00___

O-7639

MSU is an Affirmative Action/Equal Opportunity Institution

PLACE IN RETURN BOX to remove this checkout from your record.
TO AVOID FINES return on or before date due.
MAY BE RECALLED with earlier due date if requested.

DATE DUE	DATE DUE	DATE DUE

KINETIC STUDIES FOR CATIONIC
PHOTOPOLYMERIZATION OF EPOXIDE MONOMERS

By

Khanh P. Nguyen

A THESIS

Submitted to
Michigan State University
in partial fulfillment of the requirements
for the degree of

MASTER OF SCIENCE

Department of Chemical Engineering

2000

ABSTRACT

KINETIC STUDIES FOR CATIONIC PHOTOPOLYMERIZATION OF EPOXIDE MONOMERS

By

Khanh P. Nguyen

The general objective of this research is to provide a more thorough understanding of the reaction kinetics of cationic photopolymerizations. Photo-differential scanning calorimetry (PDSC) experiments will be performed to systematically characterize the effects on the rate of polymerization and the ultimate limiting conversion by a host of variables in reaction mixtures containing an epoxide monomer, which may have different number of epoxide rings in the monomer molecule. The variables are temperature, type and concentration of photoinitiator; type and concentration of photosensitizer, initiating light intensity, and finally monomer structure and functionality.

The initiating light intensity above 52 mW/cm^2 produces a large increase in the observed rate of polymerization, but only about 2 % increase in final conversion. Among the three photoinitiators studied, tolycumyl iodonium tetrakis pentafluorophenyl borate and diaryliodonium hexafluoroantimonate have the comparable effects; whereas the triarylsulfonium hexafluorophosphate is the least effective. The optimum photoinitiator concentration is 8.0 x 10^{-3} molal. When the reaction is photosensitized by 8.0 x 10^{-4} molal, the reaction rate increases dramatically, but the final conversion improves by only a few percent. CPTX is determined to be a better photosensitizer than anthracene. The

effects of temperature are investigated over a range of 30°C to 40°C and finally to 50°C. Both reaction rate and final conversion increase accordingly; however, the effect is much greater in reaction rate than in conversion.

In short, the rate of polymerization and the ultimate limiting conversion increase when the magnitude of the testing variable is increased; however, the relatively small increase in conversion may be attributed to the monomer structure and functionality. The reactivity of the three mono-epoxides investigated is as follows: phenyl glycidyl ether > butyl glycidyl ether > octyl glycidyl ether; but for conversion: PGE > OGE > BGE. With respect to monomer functionality, the reactivity is determined in this order: di-epoxides ≥ tri-epoxides > mono-epoxides; and for conversion: mono-epoxides > di-epoxides > tri-epoxides.

ACKNOWLEDGMENTS

First and foremost, I would like to thank my major advisor, Dr. Alec B. Scranton for giving me the opportunity to work in the area of cationic photopolymerization. His knowledge, guidance, and support have been instrumental to the successful completion of my thesis project. I feel very fortunate to have the opportunity to work with and learn from him. Next, I would like to especially thank Dr. Hawley and Dr. Worden for serving as committee members. The assistance and suggestions they offer have contributed to the enhancement of my knowledge base.

I would like to thank Mr. Long Le and Mr. Ruiping Huang for their training and assisting me in the usage of the NMR and FTIR spectrometers respectively. Their expertise and experience help me learn and operate those instruments more efficiently. I would like to thank the two student assistants, Elena Tran and Steve Shubuski, for their contribution in performing some of the experiments. The results obtained are significant to the progress and timely completion of this research project.

I would like to thank my colleagues in our research group: Kiran Baikerikar, Bernhard Drescher, Julie Jessop, and Katy Padon. Our friendship has grown strongly over the last three years by the support we have for and the anecdotes we share with each other. These special times will remain in my fondest memories. My special appreciation goes to the staff members of the chemical engineering department, Julie Caywood and Candy Master, for their enthusiasm and assistance.

Last but not least, I would like to thank my parents who have instilled in me the values of hard work. Their love and words of encouragement have always given me comfort and strength.

TABLE OF CONTENTS

LIST OF TABLES

x

LIST OF FIGURES

xv

Chapter 1

Introduction

1.1. Overview and Motivation for Photopolymerizations

The emission of volatile organic components (VOCs) from curing inks, films and coatings can contribute to atmospheric pollution. Typically, an ink or coating formulation must be sufficiently fluid to be easily applied (usually onto a rapidly moving substrate through a series of transfer rollers), but must cure rapidly to a hard film. These processing demands have been traditionally met through the use of a rapidly evaporating organic solvent in the ink and coating formulations. However, when these volatile organic solvents enter the atmosphere, they result in the formation of smog and air pollution. Therefore, there is an urgent need for the development of high-performance inks and coatings that will not emit VOCs to the atmosphere.

The curing of an ink or coating formulation to form a highly crosslinked polymer film could be initiated by a variety of energy sources, including heat, electromagnetic radiation, and electron beam irradiation. Unfortunately, heat-initiated thermal systems typically require high temperatures to achieve reasonable cure rates. The elevated temperatures not only lead to high energy costs, but can also result in significant distortions in substrate dimensions in many cases.[1] High-energy irradiation such as gamma radiation and electron beam radiation can lead to rapid cure rates in a variety of systems; however, these techniques will likely have very limited applications because they would typically result in degradation of the substrate[2-5]. Light-induced

1

photopolymerizations have many potential advantages for ink and coating formulations including very high reaction rates at room temperature, low energy requirements, and versatility since a wide variety of monomers may be initiated photochemically. In addition, degradation of the substrate can be avoided when use with appropriate choice of the wavelength of the light source.

1.2. UV-Initiated Photopolymerizations

Photopolymerizations initiated by ultraviolet (UV) light have gained prominence in recent years for the rapid, pollution-free curing of polymer films.[6-9] These solvent-free polymerizations proceed very rapidly with a fraction of the energy requirements of thermally cured systems, and create films with excellent properties. Ultraviolet light is a convenient energy source for photopolymerization because a variety of readily available compounds will initiate chain polymerizations upon absorption of UV light.[6-12] UV-sensitive photoinitiators are currently available for free-radical or cationic polymerizations. These photoinitiators are typically effective for a variety of incident wavelengths.[6-12] This feature is useful for UV-curable inks and coatings because the commonly used pigments may be strong absorbers of light in the visible and ultraviolet wavelengths, and an initiator which will be effective at a wavelength outside this window must be chosen.

Free-radical photopolymerizations were first reported in the literature nearly fifty years ago,[13] and are currently receiving considerable attention.[6-8,13] By far the most widely used classes of monomers for UV-initiated free-radical photopolymerizations are

multifunctional acrylates and methacrylates. These monomers polymerize very rapidly, and are easily modified on the ester group, allowing materials with a variety of properties to be obtained.[6] However, the acrylates are relatively volatile and have an unpleasant odor.[6] Moreover, recently there has been growing concern over potential health hazards associated with the acrylates.[7,8,14] Several recent investigations have demonstrated that free-radical polymerizations of multifunctional acrylates and methacrylates exhibit unusual kinetic behavior, including immediate onset of autoacceleration with the formation of heterogeneous polymers,[6,15-20] and the attainment of a maximum conversion significantly less than unity.[6,21-24] Finally, the free radical photopolymerizations are inhibited by oxygen and must be carried out under an inert atmosphere,[6,7,13] such as nitrogen.

UV-initiated cationic photopolymerizations display several advantages when compared with the free-radical photopolymerization discussed above. First of all the cationic photopolymerizations are not inhibited by oxygen.[7,13,14,25] This feature provides an important practical advantage for industrial processes since it is not necessary to blanket the system with nitrogen to achieve rapid cure rates. Secondly, in contrast to the free-radical polymerizations which experience a rapid decrease in polymerization rate when the light source is removed (due to radical-radical termination reactions), the cationic polymerizations will proceed long after the irradiation has stopped, consuming nearly all of the monomer.[13,28] Finally, cationic photopolymerization is a very versatile technique, and may be used to polymerize important classes of monomers, including epoxides and vinyl ethers.[14,25-30] Although these classes of monomers cannot cure by free-radical polymerizations, they exhibit many desirable properties, including low volatility, good

rheological properties and negligible toxicity.[7] Furthermore, the cured polymer films associated with these monomers exhibit excellent clarity, adhesion, abrasion resistance, and chemical resistance.[13,14,29,30]

Despite the advantages of UV-initiated photopolymerizations discussed above, cationic photopolymerizations have received considerably less attention than the analogous free-radical reactions. This fact may be attributed to the lack of suitable UV-sensitive cationic photoinitiators until decades after radical photoinitiators were available.[26,27] Crivello and Lam reported two classes of thermally stable photoinitiators for cationic polymerizations: diaryliodonium and triarylsulfonium salts.[10] Upon photolysis, these compounds undergo irreversible fragmentation in which the carbon-iodine or carbon-sulfur bond is cleaved to produce an aryliodonium or an arylsulfonium cation-radical capable of initiating cationic polymerization.[12] While the diaryliodonium and triarylsulfonium salts actively initiate cationic polymerization in the presence of UV light, they are remarkably latent in the absence of light. In fact, fully formulated solutions of these salts in epoxide monomers have shelf lives of several years.[12]

The wavelength at which the diaryliodonium and triarylsulfonium salts indicate their maximum UV absorbance depends somewhat upon substituents attached to the ring, but typically falls between 225 and 275 nm.[9,28] Although the initiators absorb strongly at wavelengths near 250 nm, their absorption diminishes at longer wavelengths.[9,27] This fact could limit the efficiency of the initiators for photopolymerizations driven by mercury lamps which provide most of their emission at wavelengths above 300 nm.[9,28] However, the spectral region over which the initiators are effective may be expanded by the addition of a variety of photosensitizers, including hydrocarbons, ketones and

4

heterocyclic compounds.[9] These compounds actively sensitize the iodonium and sulfonium initiators by an electron transfer process, rendering them effective in the long UV and visible wavelengths of light.[9,27,28]

1.3. Motivation for Research on Cationic Photopolymerizations

UV-initiated cationic photopolymerizations have considerable potential for the development of improved coatings and inks. These reactions may be used to rapidly form highly crosslinked polymer films exhibiting excellent adhesion, abrasion resistance, and chemical resistance without emitting volatile organic components and using a fraction of the energy requirements of thermal systems. Unlike free radical photopolymerizations, the cationic reactions are not inhibited by atmospheric oxygen, and may be used to polymerize epoxides and vinyl ethers. These monomers exhibit many desirable properties, including low volatility, good rheological characteristics and negligible toxicity.[7,28] Fully formulated systems containing monomer, pigment and initiator exhibit shelf lives of more than a year,[12] and initiators may be chosen to be effective for wavelengths at which the pigments have low extinction coefficients. Finally, the UV irradiation will not significantly degrade the substrate (unlike electron beam curing) and the cationic polymerization can withstand moderate amounts of water without a significant decrease in reaction rate.[13,28]

Despite the promise of UV-initiated cationic photopolymerizations, these reactions have received only limited attention. This fact may be attributed primarily to the lack of suitable initiators until recent years. In fact, most of the work on cationic

photopolymerizations reported in the literature focuses on the initiation step of the reaction.[8-12,25-29] The development of thermally stable UV-sensitive cationic photoinitiators has led to increased interest in the cationic photopolymerizations of epoxides and vinyl ethers in the last ten years;[26-32] however, the field is significantly less developed than that of free-radical photopolymerizations. For example, the reaction kinetics of free radical photopolymerizations of multifunctional acrylates and methacrylates have been extensively investigated,[6,15-25] revealing anomalous kinetic behavior, including immediate onset of autoacceleration, the formation of heterogeneous networks, and the attainment of a maximum conversion significantly less than unity. However, similar experiments have not been reported for cationic photopolymerizations. The reaction kinetics of cationic photopolymerizations of diepoxides and bisvinyl ethers typically have been characterized only macroscopically in terms of the tack-free time of the polymer film.

The broad objective of this thesis is to provide a more detailed characterization of the kinetics of cationic photopolymerizations. The specific aims of this research effort will be outlined in Chapter 3. A number of parameters will be investigated for their effects on the rate of polymerization and the final conversion. The parameters are temperature, type and concentration of photoinitiator, type and concentration of photosensitizer, initiating light intensity, and finally the structure and functionality of the epoxide monomer. There are three different classes of epoxide monomers that will be investigated: 1) each of the three mono-epoxide monomers has only one epoxide ring in the molecule, but they differ from each other by the length and type of pedant group attached to the epoxide ring; 2) each of the two di-epoxide monomers has two groups of epoxide rings in the molecule, and differs from each other by the middle group

connecting the two epoxide rings; and 3) one tri-epoxide monomer which has three epoxide rings in the molecule. The reactive mixuture must contain a photoinitiator and may contain a photosensitizer. There are three different photoinitiators and two distinct photosensitizers that will be investigated. All these components will be thoroughly characterized and the specific reasons for their selection in this research can be found in chapter 4. The primary experimental technique is called Photo-differential scanning calorimetry (PDSC). Based on the analysis and interpretation of the raw data provided by the PDSC experiments, substantial information can be obtained with regard to the kinetics of cationic photopolymerizations (chapter 5). In addition to PDSC, other techniques, such as ^{1}H-NMR spectroscopy is used to verify the monomer molecular structure, and the technique of Fourier Transform Infrared (FTIR) spectroscopy will be utilized to obtain degree of monomer conversion. All experimental techniques are described in chapter 2. Finally, chapter 6 presents valuable results and findings with respect to the kinetics of cationic photopolymerizations of epoxide monomers.

1.4. References

1. E. L. Graminski, "Fundamental Chemical and Engineering Issues in Paper Currency Production," National Science Foundation, Washington D. C., 1 (1991).

2. P. E. Sundell, S. Jonsson, and A. Hult, "Radiation Curing of Polymeric Materials," edited by C. E. Hoyle and J. F. Kinstle, ACS Symposium Series, Vol. 417, American Chemical Society, Washington D. C., 459 (1989).

3. H. C. Kim, A. M. El-Naggar, G. L. Wilkes, Y. Yoo and J. E. McGrath, "Radiation Curing of Polymeric Materials," edited by C. E. Hoyle and J. F. Kinstle, ACS Symposium Series, Vol. 417, American Chemical Society, Washington D. C., 474 (1989).

4. V. Stannett and A. Deffieux, "Cationic Polymerization and Related Processes," edited by E. J. Goethals, International Union of Pure and Applied Chemistry, Oxford, UK, 307 (1984).

5. J. Pacansky and R. J. Waltman, "Radiation Curing of Polymeric Materials," edited by C. E. Hoyle and J. F. Kinstle, ACS Symposium Series, Vol. 417, American Chemical Society, Washington D. C., 498 (1989).

6. J. G. Kloosterboer, *Adv. Polym. Sci.*, **84**, 1 (1988).

7. C. G. Roffey, "Photopolymerization of Surface Coatings," Wiley, New York, (1981).

8. S. P. Pappas, "UV Curing, Science and Technology," Vol. 2, Technology Marketing Corporation, Norwalk, CT, (1985).

9. J. V. Crivello, *Adv. Polym. Sci.*, **62**, 1 (1984).

10. J. V. Crivello and J. L. Lee, *J. Polym. Sci., Polym. Chem. Ed.*, **27**, 3951 (1989).

11. A. Ledwith, S. Al-Kass, and A. Hulm-Lowe, "Cationic Polymerization and Related Processes," edited by E. J. Goethals, International Union of Pure and Applied Chemistry, Oxford, UK, 275 (1984).

12. J. V. Crivello, "Cationic Polymerization and Related Processes," edited by E. J. Goethals, International Union of Pure and Applied Chemistry, Oxford, UK, 289 (1984).

13. A. Reiser, "Photoreactive Polymers," Wiley, New York, NY (1989).

14. S. P. Lapin, "Radiation Curing of Polymeric Materials," edited by C. E. Hoyle and J. F. Kinstle, ACS Symposium Series, Vol. 417, American Chemical Society, Washington D. C., 363 (1989).

15. H. M. J. Boots, J. G. Kloosterboer, and G. van de Hei, *Brit. Polym. J.*, **17**, 219 (1985).

16. H. Galina, B. Kolarz, P. Wieczorek, and M. Wojczynska, *Brit. Polym. J.*, **17**, 215 (1985).

17. W. Funke, *Brit. Polym. J.*, **21**, 107 (1989).

18. J. Bastide and L. Leibler, Macromolecules, **21**, 2649 (1988).

19. A. Matsumoto, H. Matsuo, H. Ando and M. Oiwa, *Eur. Polym. J.*, **25**, 237 (1989).

20. J. Baselga, M. Llorente, I. Hernandez-Ruentes, and I. Pierola, *Eur. Polym. J.*, **25**, 471 (1989).

21. D. Turner, Z. Haque, S. Kalachandra and T. Wilson, *Polym. Mater. Sci. Eng. Proceed*, **56**, 769 (1989).

22. G. P. Simon, P. E. M. Allen, D. J. Bennett, D. R. G. Williams and E. H. Williams, *Macromolecules*, **22**, 3555 (1989).

23. J. G. Kloosterboer, G. F. C. M. Lijten and C. P. G. Zegers, *Polym. Mater. Sci. Eng. Proceed*, **60**, 122 (1989).

24. P. E. M. Allen, D. J. Bennett, S. Hagias, A. Hounslow, G. Ross, G. P. Simon, D. R. G. Williams and E. H. Williams, *Eur. Polym. J.*, **25**, 785 (1989).

25. J. G. Kloosterboer, G. F. C. M. Lijten and H. M. J. Boots, *Makromol. Chem., Macromol. Symp.*, **24**, 223 (1989).

26. J. V. Crivello and J. H. W. Lam, "Epoxy Resin Chemistry," edited by R. S. Bauer, ACS Symposium Series, Vol. 114, American Chemical Society, Washington D.C., 1 (1979).

27. S. P. Pappas, Prog. Org. Coat., **13**, 35 (1985).

28. J. V. Crivello, "Organic Coatings, Science and Technology," Vol. 5 edited by G. D. Parfitt and A. V. Patsis, Marcel Dekker, Inc., New York, NY, 35 (1983).

29. W. R. Watt, "Epoxy Resin Chemistry," edited by R. S. Bauer, ACS Symposium Series, Vol. 114, American Chemical Society, Washington D.C., 17 (1979).

30. F. Loshe and H. Zweifel, *Adv. Polym. Sci.*, **78**, 61 (1986).

31. J. V. Crivello, J. L. Lee and D. A. Conlon, *J. Polym. Sci., Polym. Chem. Ed.*, **21**, 1785 (1983).

32. J. V. Crivello, J. L. Lee and D. A. Conlon, *J. Polym. Sci., Polym. Chem. Ed.*, **28**, 479 (1990).

Chapter 2

Background

2.1. Photopolymerizations: Characteristics and Applications

Photopolymerizations are reactions initiated by light. Photoinitiation is a photochemical event in which the initiator produces active centers (usually free radicals or cations) upon absorption of a photon of the appropriate wavelength. This wavelength typically lies in the ultraviolet (UV) or visible region of the light spectrum.[1] Once the active centers are produced, the polymerization reaction proceeds rapidly by propagation of the active center with successive monomer units in the same manner as traditional thermal polymerizations.

Photopolymerizations offer many advantages that may be suitable for a variety of applications. First, these polymerizations can rapidly form polymer without the use of diluting solvents at a fraction of the energy of traditional thermal systems. Second, photopolymerizations provide significant spatial control over the reaction since the initiating light may be directed to locations of interest in the reactive system, and temporal control since the light may be appropriately shuttered on or off during the reaction. These advantages have been exploited in many applications, including films, inks and coatings; a host of emerging high-tech systems such as fabrication of printed circuit boards, coatings for optical fibers, and replication of optical disks; and recently in stereolithography for the production of three dimensional parts.

2.2. Cationic Polymerizations

Cationic polymerizations are chain reactions in which a propagating cationic center successively reacts with many monomer units to form long polymer chains. Classes of monomers which will undergo cationic polymerizations include α-olefins, 1,3-dienes, vinyl ethers, and epoxides. Cationic polymerizations are not as well characterized as radical polymerizations partially because they proceed at very rapid rates, and may be sensitive to small concentrations of impurities.[2] Cationic initiators are typically protonic or Lewis acids, and the resulting reactive cations are sufficiently stable to have a reasonable lifetime for chain growth by propagation. The polymer chain growth may be terminated by chain transfer of the reactive center, or occasionally by counterion combination. Compounds such as water, alcohols, and esters are particularly effective chain transfer agents. Although chain transfer results in a decrease in the average primary polymer chain length, it typically will not affect the polymerization rate because the resulting cation will continue to propagate.[2]

Kinetic data for cationic polymerizations are difficult to interpret for several reasons.[2-4] First of all, the reactions often proceed so rapidly that the steady-state assumption is not valid for the reactive centers.[2] The analysis is further complicated by the fact that the nature of the propagating center and the counterion are often unclear.[2-4] For kinetic modeling of these reactions, it is common to assume several types of propagating centers ranging from completely free (unpaired) ions to covalent species. The unpaired species typically exhibit much higher kinetic constants for propagation than pair species. Cationic polymerization rates are often higher than those for free radical polymerizations for a variety of reasons. For cationic polymerizations of unsaturated

monomers the kinetic constants for propagation are usually higher than those for free radical reactions, while the rate constants for termination are lower. Both of these trends contribute to higher reaction rates for the cationic reactions. Furthermore, the concentration of propagating species is usually two orders of magnitude higher for cationic polymerizations than for free radical polymerizations.

While cationic polymerizations are not used extensively for the commercial synthesis of long polymer chains, they show considerable promise for photopolymerizations of highly crosslinked polymer films. Due to the predominance of transfer processes during the course of the reaction, linear cationic polymerizations tend to yield polymers of moderate molecular weight and relatively broad molecular weight distribution. These facts tend to limit the usefulness of the reactions for the synthesis of linear high polymers. However for photopolymerizations of multifunctional monomers, a high linear primary chain length is not necessary because the resulting highly crosslinked polymers derive their excellent properties from the network structure, not from long linear chains. For these systems the insensitivity to oxygen and high reaction rates exhibited by cationic polymerizations represent significant advantages.

2.3. Cationic Photopolymerizations of Epoxides

The development of thermally stable cationic photoinitiators in the late 1970s has lead to increased interest in cationic photopolymerizations. Most of the work reported in the literature has focused on the synthesis and development of appropriate monomers and initiators for cationic photopolymerizations of high performance polymer films.[5-13] Several classes of monomers exhibiting desirable properties and rapid polymerization

rates have been reported, including epoxides,[10,11-13] novel silicon-containing epoxy resins[15,17,20] and urethane bisvinyl ethers.[10,15,16] The selection of appropriate monomers and initiators is now reasonably broad, however the characteristics of the cationic photopolymerization reactions have received only limited attention. There is a need for fundamental studies of the kinetics of the reactions, as well as the structure and physical properties of the resulting highly crosslinked polymer networks. Such studies would allow the optimum formulations and curing procedures to be established.

Experimental studies of the cationic photopolymerizations of epoxides and vinyl ethers have provided information about the salient features of the reactions. The observed polymerization rate depends upon several variables including the type and concentration of the initiator, the intensity and wavelength of the UV light source, temperature, and the structure of the monomer. Until now, most investigators have used mercury lamps for the UV light source.[10,13] Many monomers exhibit a substantial increase in cure rate as temperature is increased.[10,11,18] This fact presents potential complications for kinetic studies of extremely rapid cationic photopolymerizations. Polymerization reaction of epoxides and vinyl ethers are highly exothermic and can liberate significant amounts of heat in a very short period of time. The cure rate of cationic photopolymerizations is typically characterized by the tack-free time of the polymer film. Reported tack-free times range from less than one second to several minutes;[11-13] however the meaning of the tack-free time in terms of the degree of cure is unclear. Differential scanning calorimetry experiments[13] indicate that reaction proceeds long after the tack-free time. The studies also indicate that UV cured epoxides typically exhibited a cure rate which passed through a maximum, then rapidly decreased to smaller

values. This behavior was attributed to diffusion limited propagation upon vitrification in the highly crosslinked films.[18,21] This interpretation is supported by the fact that tack free time may be decreased by the addition of chain transfer agents which delay vitrification.[18] Unfortunately the chain transfer agents cause a reduction in crosslink density, undermining the mechanical properties and the chemical resistance of the cured film.[10]

2.4. UV-initiated Cationic Photopolymerizations

In recent years, cationic photopolymerizations have been given special attention. This technique has made tremendous progress due to its many advantages: high reactivity, efficiency, and non-polluting. Therefore, cationic photopolymerization is a technique applied in many fields, such as release paper, photodoping, the graphic arts, microlithography, and holography. A host of highly efficient cationic photoinitiators is commercially available, especially the onium salts: triarylsulfonium and diaryliodonium salts.

2.4.1. Diaryliodonium and Triarylsulfonium Salt Photoinitiators

2.4.1.1. General Characteristics and Synthesis Methods

Diaryliodonium salts are generally colorless to yellowish white crystalline compounds, which are stable in the absence of light at temperatures up to their melting points. They are often soluble in many common organic solvents. Compounds containing weakly nucleophilic anions such as SbF_6^-, BF_4^- are ionic salts, while those with simple halide anions exhibit some covalent character.[22]

$$Ar\!-\!\overset{+}{Y}\!-\!Ar'$$

$$\overset{-}{X} \qquad\qquad \overset{+}{Y} = I, Br, Cl ; \qquad \overset{-}{X} = SbF_6^-, BF_4^-$$

The major reactions of diaryliodonium salts include the attack at the positively charged iodine atom by nucleophiles X^-, resulting in the displacement of an aryl group.

Triarylsulfonium salts are generally colorless crystalline compounds, which are soluble in common organic solvents and slightly soluble in water. The triphenylsulfonium cation adopts a pyramidal configuration with all the carbon-sulfur bonds lying nearly in the same plane.[23] There is considerable positive charge dispersal throughout the molecule because of the significant $p\pi\!-\!d\pi$ bonding between the sulfur atom and the aromatic rings. For the same reason, these compounds are thermally stable and the cations are not

$$\begin{array}{c} Ar \\ | \\ Ar\!-\!\overset{+}{M}\overset{-}{X} \qquad\qquad \overset{+}{M} = S, Se, Te; \qquad \overset{-}{X} = PF_6^-, SbF_6^- \\ | \\ Ar \end{array}$$
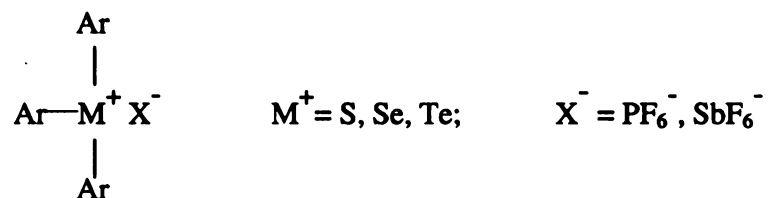
readily susceptible to nucleophilic displacement reactions at the sulfur atom. The synthesis methods for both types of onium salts have been well characterized. In addition, the preparative methods for triarylsulfonium salts are more easily done than those for the diaryliodonium salts.[23-26]

2.4.1.2. Photochemistry : Photolysis of Photoinitiators

Upon absorption of a photon of the appropriate wavelength, the photoinitator undergoes an irreversible fragmentation to generate the active centers, the radical-cations. Crivello and Lam[27] proposed the following mechanistic pathway to account for the photoproducts which had been observed.

Scheme 1

$$Ar_2I^+X^- \xrightarrow{\ hv\ } [\,Ar_2I^+X^-\,]* \qquad\qquad (2.1)$$

$$[\,Ar_2I^+X^-\,]* \longrightarrow ArI + X^- + Ar\cdot \qquad\qquad (2.2)$$

In this mechanism, light is absorbed first to produce an electronically excited diaryliodonium salt. Rapid decay of the photoexcited species then takes place with the resultant cleavage of a carbon-iodine bond to give an aryliodonium cation-radical and an aryl radical.

A similar mechanistic pathway has been proposed for the photolysis of triarylsulfonium salts as follows.

Scheme 2

$$Ar_3S^+X^- \xrightarrow{\ hv\ } [\,Ar_3S^+X^-\,]* \qquad\qquad (2.3)$$

$$[\,Ar_3S^+X^-\,]* \longrightarrow Ar_2S + X^- + Ar\cdot \qquad\qquad (2.4)$$

The evidence for the formation of these active species in both reaction schemes had been shown by the works of Pappas[28] and coworkers and Crivello and Lee.[29]

2.4.1.3. Mechanisms of Photoinitiation and Propagation

The cation-radicals produced by photolysis are capable of directly initiating polymerization. Crivello and Lam[30] have suggested that the cation-radicals interact with the solvent or monomer, R—H, by hydrogen abstraction to generate the strong protonic acid, HX^- (Eq. 2.5).

$$\text{ArI+X}^- + \text{Ar}\cdot \xrightarrow{\text{R-H}} \text{HX}^- + \text{products} \qquad (2.5)$$

Initiation then occurs by the addition of the acid to the monomer (M) with the formation of a carbenium species (Eq. 2.6). Propagation then follows suit (Eq. 2.7).

Scheme 3

$$\text{HX}^- + \text{M} \longrightarrow \text{HM}^+\text{X}^- \qquad (2.6)$$

$$\text{HM}^+\text{X}^- + n\text{M} \longrightarrow \text{H(M)}_{n-1}\text{M}^+\text{X}^- \qquad (2.7)$$
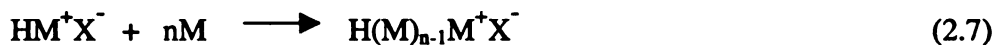
2.4.1.4. Photosensitization

The majority of the diaryliodonium and triarylsulfonium salts absorb strongly the wavelength range of 230 ⁻ 250 nm. Even the introduction of simple substituents on the aryl rings does not markedly alter their spectral sensitivity. The poor absorptivity of these onium salts in the 300-450 nm region is of great concern since it severely limits their efficiency or light utilization in the region in which the commonly available medium and high pressure mercury arc lamps provide a substantial portion of their emission. In addition, the products of photolysis also display absorption bands at or near those of the photoinitiators. Thus, as they are formed, these products suppress further photolysis of the photoinitiators due to screening effects. One solution to these difficulties is to synthesize photoinitiators which incorporate chromophores that allow absorption at longer wavelengths. Another method is through the use of photosensitization. In the photosensitization process, the function of the photosensitizer is to absorb energy of specific wavelengths and to mediate its transfer to the initiator.

Based on the work of several investigators,[31-33] The two possible mechanisms for photosensitization have been investigated and characterized: 1) electron transfer, and 2)

18

free-radical induced decomposition. The electron transfer mechanism was investigated by Pappas and co-workers[33] using diaryliodonium and triarylsulfonium salts. They have showed that diaryliodonium salts, which have lower oxidation potentials, are more easily photosensitized than triarylsulfonium salts. Working with divinyl ethers, Nelson *et. al* have also demonstrated that the electron transfer occurs from the triplet state of the sensitizer anthracene to the initiator.[34]

2.4.2. Development and Applications of Onium Salt Photoinitiators

A typical photopolymerizable formula contains monomer resin, a photoinitiator, and may contain an additive (photosensitizer, dye, filler, diluent, etc.). The first two components are the basic requirements for the reaction to occur. The overall reaction kinetics of cationic photopolymerization may be characterized in terms of the reactivity of these components.

2.4.2.1. Effect of photoinitiator

The aryldiazonium salts formed the first class of photoinitiators that could efficiently induce cationic polymerization. However, they were thermally unstable, and the resultant short shelf lives had precluded their use in practical UV-curing applications. During the 1970's, three new classes of cationic photoinitiators were developed, namely diaryliodonium,[35-37] triarylsulfonium,[38-40] and ferrocenium salts.[41,42] Subsequent advances have focused on modifying these onium salts to tailor their absorption characteristics, to enhance solubility, and to reduce toxicity. With respect to absorptivity, Crivello has shown that for triarylsulfonium salts, their spectral responses to the initiating light depend directly on the structure of the aromatic groups attached to the positively

19

charged sulfur atom. One strategy was to incorporate long-wavelength chromophores; however, the synthetic complexities of this method make it impractical in real-life applications. A much better alternative is through photosensitization, as discussed in section 2.4.1.4.[43]

The reactivity of the initiating species generated from the photolysis of the onium salt with a monomer in (Eq. 2.6) depends to a great extent on the character of the anion X^-. These anions or counterions can participate in the nucleophilic attack on the reactive species, thus terminating the polymerization. In order to avoid this complication, the least nucleophilic anions such as SbF_6^-, AsF_6^-, PF_6^-, and BF_4^- have been used. However, these essentially non-nucleophilic anions could still show considerable variation in the reactivity of their corresponding onium salt photoinitiators. For the same reason, water or many bases can effectively terminate polymerization.

Since the majority of the onium salts are ionic, solubility could become a problem for non-polar monomer resins. The solutions could include clever substitutions on the aromatic groups without compromising the absorption properties of the photoinitiators. For example, the long alkyl groups attached to the phenyl rings can greatly enhance solubility.

Toxicity is also a concern for some onium salts, specifically those carrying the heavy metals such as antimony (Sb) or arsenic (As) in their counterions. For example, diphenyliodonium hexafluoroantimonate has an oral LD_{50} of 40 mg/Kg (rats).[44] In addition, the hexafluoroantimonate anion is sensitive to humidity,[45] which poses a problem for long-term storage. Those problems dealing with solubility and toxicity could be eliminated with the relatively recent invention[46] of a new kind of iodonium salt,

namely diaryliodonium tetrakis (pentafluorophenyl) borate salts. These borate-based salts also display high reactivity, low toxicity and relative insensitivity to humidity.

2.4.2.2. Effect of Monomer Structure and Functionality

The structure of an epoxide molecule can affect its rate of ring-opening in cationic photopolymerization. Therefore, the monomer's reactivity depends directly on the degree of strain brought about by the three-member ring. For example, it is a fact that epoxy cyclohexanes possess greater ring strain than their open-chain counterparts.[47,48] In addition, Crivello and coworkers have recently shown that the presence of ester and ether group in the monomer tend to depress their reactivity.[49] Their works have proven without a doubt that the monomer's structure and its degree of ring strain significantly contribute to the overall polymerization reactivity.[49-52] They successfully engineered a series of novel epoxies, including a novel hybrid monomer having both oxirane and vinyl moieties.

2.4.2.3. Other factors affecting reaction rates in cationic photopolymerization

In addition to the reactivity of specific monomer and photoinitiator used, other factors like temperature, initiating light intensity, and even level of impurities present in the reactive mixture can affect the overall rate of polymerization.

21

2.5. Experimental Techniques

2.5.1. Photo-Differential Scanning Calorimetry

Photo- differential scanning calorimetry (PDSC) is the primary technique used throughout this research effort. Along with the technique of real-time infrared (RTIR) spectroscopy, photo-differential scanning calorimetry (PDSC) has been applied widely for in situ characterization of reaction kinetics and polymerization rate constants involving photopolymerizations.[53-59] The response time of PDSC is relatively fast, about 2-3 seconds.[58] Therefore, it can be used to monitor the kinetics of cationic photopolymerizations for divinyl ethers[57] and epoxies.[55-58] The DSC experiments can be run at isothermal conditions or with temperature ramped with time as in the determination of glass transition temperature, T_g. Photo-DSC requires the use of light to initiate the reaction.

The basic operating principle for DSC is relatively straightforward. It measures the difference between sample and reference cells during a thermal event, such as a chemical reaction or a controlled temperature change.[59] Changes in the heating rates of the sample relative to the reference can be converted into heat capacity and enthalpy change. The DSC typically uses temperature sensors placed in heat sinks, which are located just below the sample and reference cells to monitor changes in temperature. Because the cells are maintained independently, heat flow can be controlled for each cell. Heat can either be removed from or supplied to either or both cells depending on the system being tested. In other words, DSC can characterize both exothermic and endothermic reactions. Therefore, DSC is well suited for kinetics characterization of

cationic photopolymerizations, which are highly exothermic.

The heat of reaction profile obtained from DSC can be calculated to obtain several kinetics features, such as the rate of polymerization, the product of polymerization rate constant and concentration of active centers. In addition, the conversion profile as a function of time and the final conversion of a given formulation can be calculated. Another useful application of photo-DSC is the determination of the termination rate constant in the "dark" reaction. The sample is illuminated to initiate the reaction, and then the light is shuttered off in order to monitor the dark reaction.

In short, the versatility of DSC will be utilized in this research to study the effects of temperature, type and concentration of photoinitiator, type and concentration of photosensitizer, and light intensity for various systems of epoxy resin, initiator, and sensitizer. The experimental set-up for PDSC is shown in Figure 2.1 below.
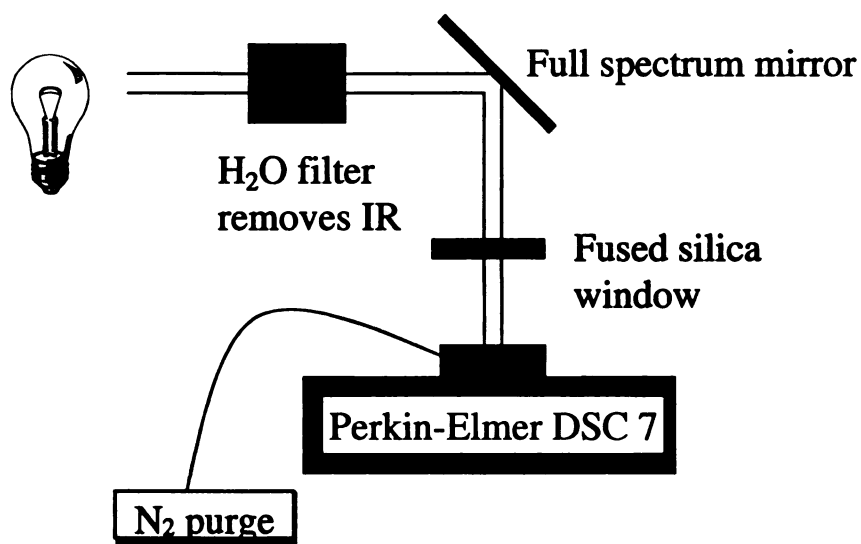
Figure 2.1. Experimental set-up for the Photo-differential scanning calorimetry (PDSC) experiments.

2.5.2. Fourier Transform Infrared (FTIR) Spectroscopy

A general introduction to the basic principles of infrared spectroscopy is presented here. Detailed discussion on the physics, development, and applications of FTIR can be found in many textbooks and published articles.[60-62] The infrared (IR) region of the light spectrum covers the wavenumbers between 10,000 cm^{-1} and 10 cm^{-1}. The region of interest for this research is the mid-infrared, spanning 4000 to 400 cm^{-1}. The basic operating principle behind IR spectroscopy is that when infrared light is passed through a sample, certain frequencies are absorbed while others are transmitted, resulting in an absorption (or transmittance) spectrum that is dependent upon the molecular vibrational frequencies of that sample.

In polymers, molecular bonds have different vibrational frequencies, which correspond to characteristic IR absorption bands. For example, for the di-epoxide monomer 3,4-epoxycyclohexylmethyl 3',4'-epoxycyclohexane carboxylate (cycloaliphatic di-epoxy ERL-4221), the characteristic absorption band is at 790 cm^{-1} corresponding to the C—H bond stretching vibration of the epoxide group.[63-65] By monitoring the change of this absorption band, the degree of conversion can be obtained. In addition, the C—H absorption band should lie in the region of 740 ‒ 850 cm^{-1}, depending on the molecular structure of a particular epoxide molecule.[66]

The technique of FTIR will be utilized in this research effort. The results in terms of the degree of conversion will be compared to those obtained from PDSC studies.

24

2.5.3. ^{1}H-NMR Spectroscopy

A brief introduction to the basic principles of NMR is presented here. Detailed discussion about the physics, development and applications of this technique can be found in many textbooks and published articles.[67-70] Nuclear magnetic resonance is a powerful technique that enables the user to deduce the molecular structure of a compound of interest based on the information given by a NMR spectrum.

NMR is based on the interactions between the nucleus of a particular atom with the applied magnetic field. The interacting atom is either a hydrogen (proton) or a carbon atom, thus giving the name *pmr* (proton magnetic resonance or ^{1}H-NMR) spectrum or *cmr* spectrum (based on ^{13}C nuclei). The following discussion is based on proton, but the same principles operate on the ^{13}C-NMR. The nucleus of a hydrogen atom, ^{1}H, has a net charge and can spin. The spinning generates a *magnetic moment* along the axis of spin. When a proton is placed in an external magnetic field, its magnetic moment can be aligned *with* or *against* the external field according to quantum mechanics. Alignment with the field is more stable, and aligning against the field is less stable because energy is absorbed to "flip" the proton magnet over. The exact amount of energy required to cause the flipping depends on the strength of the external magnetic field: the stronger the field, the greater the tendency to remain lined up with it, and the higher the frequency of the radiation needed to do the job because $\Delta E = h\nu$.

$$\nu = \frac{\gamma H_o}{2\pi}$$

where, ν = frequency in Hz; H_o = magnetic field strength in gauss

γ = the gyromagnetic ratio, a constant of 26,750 for proton

In principle, a substance can be placed in a magnetic field of constant strength, and its NMR spectrum is obtained by passing radiation of steadily changing frequency through the substance while observing the frequency at which radiation is absorbed. In practice, however, it is more convenient to keep the radiation frequency constant and to vary the strength of the magnetic field. At some value of the field strength, the energy required to flip the proton matches the energy of the radiation; absorption occurs and a signal is observed. Such a spectrum is called a nuclear magnetic resonance (NMR) spectrum.

The actual environment, that the proton is in a substance, is far more complex. Due to the electron density at the proton as well as presence of other protons, the frequency at which a proton absorbs depends on the magnetic field at which that proton feels, and this *effective* field strength is not exactly the same as the *applied* field strength. For example, at a given radiofrequency, all protons absorb at the same *effective* field strength, but they absorb at different *applied* field strength. It is this applied field strength that is measured, and against which absorption is plotted to produce a NMR spectrum.

The position of an absorption signal for a particular proton is plotted on the δ (*delta*) scale. The reference signal is from tetramethylsilane (TMS) and is taken to be 0.0 ppm. The position of an absorption signal can be shifted with respect to the TMS signal depending on the particular electronic environment the proton is in. Such shifts in the position of NMR absorptions are called chemical shifts. For a given molecule, protons with different electronic environments – non-equivalent protons – have different chemical shift; and protons with the same electronic environment – equivalent protons – have the

same chemical shift. Most chemical shifts have δ values between 0 and 10 ppm. A small δ value represents a small downfield shift, i.e., going to the left on the nmr spectrum chart and toward lower *applied magnetic field* strength. For example[71], a spectrometer operating at a frequency of 300 MHz or 300 x 10^6 Hz,

$$\delta = \frac{observed\ shift\ (Hz)\ x10^6}{300\,x10^6\,(Hz)}$$

For analysis of NMR spectra there are four basic features of the spectrum that can be used to characterize the molecular structure and composition of the sample: 1)the number of signals (or peaks), corresponds to the number different "kinds" of protons (as determined by electronic environment) there are in a molecule; 2) the positions of the signals, characterizes the electronic environment of each kind of proton; 3) the intensities of the signals (integral of the area beneath the peak), determines tell how many protons of each kind there are; and 4) the splitting of a signal into smaller peaks characterized the number of protons covalently bonded by a neighboring carbon.

2.6. References

1. D. F. Banks, *Chem. Revs*, **66 (3)**, 243, (1966).

2. G. Odian, *Principles of Polymerization*, 2nd Edition, Wiley, New York, NY (1981).

3. P. H. Plesch, *Cationic Polymerization and Related Processes*, edited by E.J. Goethals, International Union of Pure and Applied Chemistry, Oxford, UK, 1 (1984).

4. D. J. Dunn, *Developments in Polymerization*, edited by R.N. Haward, Applied Science Publishers, London, **1**, 45 (1979).

5. J. V. Crivello, *Adv. Polym. Sci.*, **62**, 1 (1984).

6. J. V. Crivello and J. L. Lee, *J. Polym. Sci., Polym. Chem.*, **27**, 3951 (1989).

7. A. Ledwith, S. Al-Kass, A. Hulme-Lowe, *Cationic Polymerization and Related Processes*, edited by E. J. Goethals, International Union of Pure and Applied Chemistry, Oxford, UK, 275 (1984).

8. J. V. Crivello, *Cationic Polymerization and Related Processes*, edited by E. J. Goethals, International Union of Pure and Applied Chemistry, Oxford, UK, 289 (1984).

9. A. Reiser, *Photoreactive Polymers*, Wiley, New York, NY (1989).

10. S. P. Lapin, *Radiation Curing of Polymeric Materials*, edited by C.E. Hoyle and J.F. Kinstle, ACS Symposium Series, Vol. 417, American Chemical Society, Washington D.C., 363 (1989).

11. S. P. Pappas, *Prog. Org. Coat*, **13**, 35 (1985).

12. J. V. Crivello, *Organic Coatings, Science and Technology*, Vol. 5 edited by G. D. Parfitt and A.V. Patsis, Marcel Dekker, Inc., New York, NY, 35 (1983).

13. W. R. Watt, *Epoxy Resin Chemistry*, edited by R. S. Bauer, ACS Symposium Series, Vol. 114, American Chemical Society, Washington D.C., 17 (1979).

14. J. V. Crivello and D.A. Conlon, *J. Polym. Sci., Polym. Chem.*, **21**, 1785 (1983).

15. J.V. Crivello and J. L. Lee, *Radiation Curing of Polymeric Materials*, edited by C.E. Hoyle and J.F. Kinstle, ACS Symposium Series, Vol. 417, American Chemical Society, Washington D.C., 398 (1989).

16. F. Loshe and H. Zweifel, *Adv. Polym. Sci.*, **78**, 61 (1986).

17. J. V. Crivello and J.L Lee, *J. Polym. Sci., Polym. Chem.*, **28**, 479 (1990).

18. J. V. Crvello, D. A. Conlon, D. R. Olson, and K.K. Webb, *Polym. Paint Colour J.*,

178, 696, (1988).

19. J. Pelgrims, *Pigm. Resin Technol.*, **16**, 4 (1987).

20. R. P. Eckberg and K. D. Riding, *Radiation Curing of Polymeric Materials*, edited by C. E. Hoyle and J. F. Kinstle, ACS Symposium Series, Vol. 417, American Chemical Society, Washington D.C., 382 (1989).

21. J. V. Crivello , D.A. Conlon, D.R. Olson, and K.K. Webb, *J. Rad. Cur.*, **13**, 3, (1986).

22. M. Simonetta and A. Garezotti, *The Chemistry of the Sulfonium Group*, Vol. 1, 13, C. J. M. Stirling and S. Patai (Eds), Wiley, New York, N. Y., 1981.

23. A. Ledwith *et. al.*, *Polymer*, **22**, 143 (1981).

24. P. A. Low, *The Chemistry of the Sulfonium Group*, Vol. 1, 267, C. J. M. Stirling and S. Patai (Eds), Wiley, New York, N. Y., 1981.

25. B. M. Trost and L. S. Melvin Jr., *Sulfur Ylides – Emerging Synthetic Intermediates*, Academic Press, London, 1975.

26. J. P. Marino, *Topics in Sulfur Chemistry*, Vol. 1, 1, A. Sennig (Ed), George T. Verlag, Stuttgart, 1976.

27. J. V. Crivello and J. H. W. Lam, *Macromolecules*, **10**, 1307 (1977).

28. S. P. Pappas *et. al.*, *Proc. Soc. Photogr. Sci. and Eng.*, 22nd Fall Symp., Washington D. C., Nov. 15 – 18, 1982, 46.

29. J. V. Crivello and J. L. Lee, Makromol. Chem., **184**, 463 (1983).

30. J. V. Crivello and J. H. W. Lam, *J. Polym. Sci., Polym. Chem. Ed.*, **17**, 977 (1979).

31. G. H. Smith, *US patent* 4,069,054 Jan. 17, 1978.
Chem. Abstract 94, 112539e, 1981.

32. J. V. Crivello and J. H. W. Lam, *J. Polym. Sci., Polym. Chem. Ed.*, **16**, 2441, (1978).

33. S. P. Pappas, L. R. Gatechair, and J. H. Jilek, *J. Polym. Sci.: Polym. Chem. Ed.*, **22**, 77, (1984).

34. E. W. Nelson, T. P. Carter, and A. B. Scranton, *J. Polym. Sci.: Polym. Chem. Ed.*, **33**, 247, (1995).

35. J. V. Crivello, *US patent* 3,981,897, 1976.

36. G. H. Smith, *Belgian patent* 837,782, 1975.

37. J. Nemcek, *US patent* 837,782, 1975.

38. J. V. Crivello and J. H. W. Lam, *US patent* 4,058,401, 1977.

39. J. V. Crivello and J. H. W. Lam, *J. Radiat. Curing*, **5** (1), 2, (1978).

40. G. H. Smith, *US patent* 4,069,054, 1978.

41. K. Meier, N. Buehler, H. Zweifel, G. Berner, F. Lohse, *Euro. Patent Appl.* 093915, 1979.

42. M. C. Polazzotto and W. A. Hendrickson, *Euro Patent Appl.* 109851, 1982.

43. J. V. Crivello, *Adv. Polym. Sci.*, **62** (1984).

44. J. V. Crivello and J. L. Lee, *J. Polym. Sci.: Polym. Chem. Ed.*, **27**, 3951, (1995).

45. P. Borthoul, R. Dolique, L. Domang, and P. Pascal, *Nouveau Traite de Chime Minerale*, Vol. XI, *Arsenic, Antimoine, Bismuth*, Masson, Paris, 560, 1958.

46. F. Castellanos, C. Priou, A. Soldat, and J. Cavezzan, *J. Coatings Tech.*, **67**, 71, (1995).

47. R. Grubbs and W. Tumas, *Science*, **243**, 158, (1989).

48. M. P. Kozina, L. P. Timofeeva, V. A. Luk'yanova, S. M. Pimenova, and L. I. Kas'yan, *Russ. J. Phys. Chem.*, **62**, 1203 (1988).

49. J. V. Crivello and Ramesh Narayan, *Macromolecules*, **29**, 439 (1996).

50. J. V. Crivello and Shaoshi Liu, *Chem. Mater.*, **10**, 3724 (1998).

51. S. K. Rajaraman, W. A. Mowers, and J. V. Crivello, *Macromolecules*, **32**, 36 (1999).

52. S. Liu and J. V. Crivello, *J. Polym. Sci.: Polym. Chem. Ed.*, **37**, 1199 (1999).

53. J. G. Kloosterboer and G. F. C. M. Lijen, *Polymer*, **28**, 1149 (1987).

54. J. P. Everett, D. L. Smith, G. D. Rose, P. Argritis, C. J. Aidinis, and M. Hatzakis, *Polymer*, **38** (7), 1719 (1997).

55. C. Priou, A. Soldat, J. Cavezzan, F. Castellanos and J. P. Fouassier, *J. Coatings Tech.*, **67** (851), 71 (1995).

56. J. V. Crivello and R. Narayan, *Macromolecules*, **29**, 439 (1996).

57. C. Decker and K. Moussa, *J. Coatings Tech.*, **62 (786)**, 55 (1990).

58. S. K. Rajaraman, W. A. Mowers, and J. V. Crivello, *Macromolecules*, **32**, 37 (1999).

59. E. W. Nelson, T. P. Carter, and A. B. Scranton, J. Polym. Sci., **33 (39)** (1995).

60. E. A. Grulke, Polymer Process Engineering, Prentice Hall, New York, 324 (1994).

61. N. B. Colthup, L. H. Daly, and S. E. Wiberley, *Introduction to Infrared and Raman spectroscopy*, 2nd ed., Academic Press, New York, 1975

62. J. D. Ingle and S. R. Crouch, *Spectrochemical Analysis*, Prentice Hall, Englewood Cliffs, New Jersey, 1988.

63. T. Herschfeld and B. Chase, "FT-Raman Spectroscopy: Development and Justification," *Appl. Spectrosc.*, **40**, 133 (1986).

64. C. Decker and K. Moussa, *J. Polym. Sci., A: Polym. Chem.*, **28**, 3429 (1990).

65. J. V. Crivello and U. Varleman, *J. Polym. Sci., A: Polym Chem.*, **33**, 2473 (1995).

66. S. Yan, J. S. Chen, H. Korner, T. Breiner, C. K. Ober, and M. D. Poliks, *Chem. Mater.*, **10**, 1475 (1998).

67. J. K. M. Sanders and B. K. Hunter, *Modern NMR Spectroscopy – A Guide for Chemists*, Oxford University Press, New York, 1987.

68. R. T. Morrison and R. N. Boyd, *Organic Chemistry*, 3rd ed., Allyn and Bacon, Inc., Boston, Massachusetts, 1973.

69. E. Breitmaier, *Structure Elucidation by NMR in Organic Chemistry – A Practical Guide*, John Wiley & Sons, New York, 1993.

70. R. Freeman and G. A. Morris, *Bull. Mag. Reson.*, **1**, pp. 1 - 28, 1979.

71. R. T. Morrison and R. N. Boyd, *Organic Chemistry*, 3rd ed., Allyn and Bacon, Inc., Boston, Massachusetts, pp. 420 – 422 (1973).

Chapter 3

Research Objectives

Based on the discussion above it is clear that there is a need to provide a more thorough understanding of the kinetics of cationic photopolymerizations. Therefore, the broad objective of this research effort is to perform a systematic series of experiments that will investigate the effects of a host of variables on the resulting polymerization kinetics and observed limiting conversion of epoxide monomers.

The specific objectives are as follows:

i. to obtain complete, time-resolved profiles of the rate of polymerization as a function of time using photo-differential scanning calorimetry to characterize the effects of the following variables:

  - temperature;

  - type of photoinitiator (and for a representative system, the effect of photoinitiator concentration);

  - type of photosensitizer (and for a representative system, the effect of photosensitizer concentration);

  - initiating light intensity;

ii. to obtain complete, time-resolved profiles of conversion as a function of time with respect to the same variables above;

iii. to investigate the effect of the monomer structure and functionality on the photopolymerization kinetics and limiting conversion.

Chapter 4

Characterization of the Photoinitiating Systems

4.1. Selection of the Components in the Photoinitiating Systems

A typical photopolymerizable formulation contains a monomer resin, an initiator, and may contain other additives such as a sensitizer, dye, filler, diluent, etc. It is obvious that the monomer resin and initiator are the basic requirements for the reaction to occur upon light irradiation. In order to use most efficiently the initiating power of the irradiating light, all these components except the initiator and/or the sensitizer should to be transparent to the initiating wavelength.

Three classes of monomers were investigated in this study as listed in Table 4.1: 1) epoxides containing a single epoxide group, 2) epoxides containing two epoxide groups, and 3) epoxides containing three polymerizable epoxide groups. These classes will henceforth be denoted mono-epoxide, di-epoxide and tri-epoxide monomers, respectively. Three different mono-epoxide monomers were investigated: 1) octyl glycidyl ether, 2) butyl glycidyl ether, and 3) phenyl glycidyl ether. These mono-epoxide monomers were chosen to investigate the effect of the length and type of the pendant group attached to the epoxide ring. Two different di-epoxide monomers were used: 1) 1,4-butanediol diglycidyl ether, 2) cyclohexane dimenthanol diglycidyl. The comparison of the results from the mono-epoxide studies and the di-epoxide studies will allow the effect of crosslinking to be investigated, while comparison among the two di-epoxide monomers will allow the effects of the length and flexibility of the chain between the two

reactive groups to be investigated. Finally, the tri-epoxide monomer trimethyol propane triglycidyl ether was investigated. All epoxide monomers were obtained from Shell Chemical Company.

As illustrated in Table 4.2, three different photoinitiators were used, including two iodonium salts and one sulfonium salt. The two iodonium salts were: 1) tolylcumyl iodonium tetrakis pentaflourophenyl borate, (B-$[F_5]_4^-$ counterion) from Rhodia Inc; 2) diaryliodonium hexafluoro-antimonate, ($[SbF_6]^-$ counterion) from Sartomer Company. These diaryliodonium salts differ from each other by the counterion. One is the (tolycumyl) iodonium with the bulky counter ion tetrakis (penta-fluorophenyl) borate. The other diaryliodonium salt has a relatively smaller counterion hexafluoroantimonate (Table 4.2). The third photoinitiator was triarylsulfonium hexafluorophosphate ($[PF_6]^-$ counterion) from Sartomer Company. The triarylsulfonium salt has the counterion hexafluorophosphate. Two photosensitizers from Aldrich Chemical Company, Inc. were used: 1) anthracene, and 2) 1-chloro-4-propoxy-9H-thioxanthen-9-one (CPTX).

As indicated by their absorption spectra (Figures 4.8 – 4.10), the photoinitiators absorb strongly in the deep UV region of 230 – 254 nm. In order to increase their spectral sensitivities, specific photosensitizers will be added to the initiating systems. The two photosensitizers are anthracene and 1-chloro-4-propoxy-9H-thioxanthen-9-one (CPTX) and their molecular structures are shown in Table 4.2. Figures 4.11 – 4.12 show that both anthracene and CPTX have absorption maxima in the 310 – 380 nm region, which coincides with the strong emission peaks of the emission spectrum of the initiating light source, a 200 Watt Hg-Xe arc lamp (Figure 4.1). Thus, these photosensitizers were selected due to their absorbance characteristics.

Table 4.1. Epoxide monomers used in the cationic photopolymerizations

Butyl glycidyl ether

Octyl glycidyl ether

Phenyl glycidyl ether

1,4-butanediol diglycidyl ether

Cyclohexane dimethanol diglycidyl ether

Trimethyol propane triglycidyl ether

35
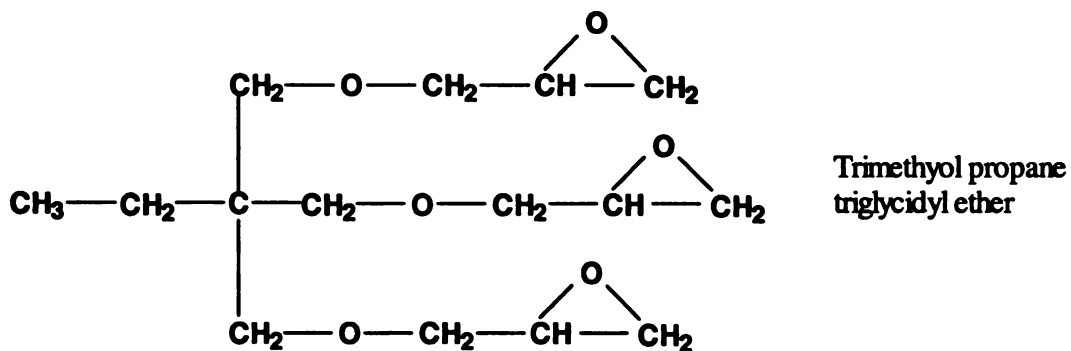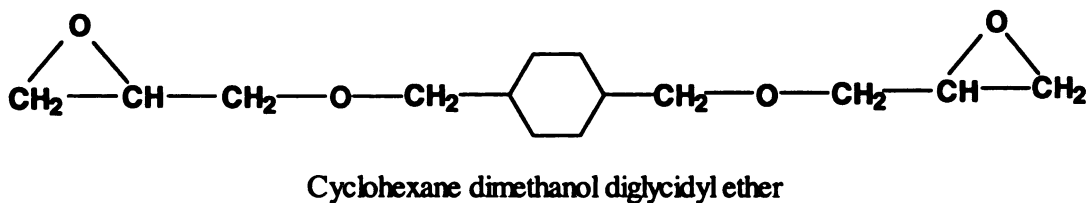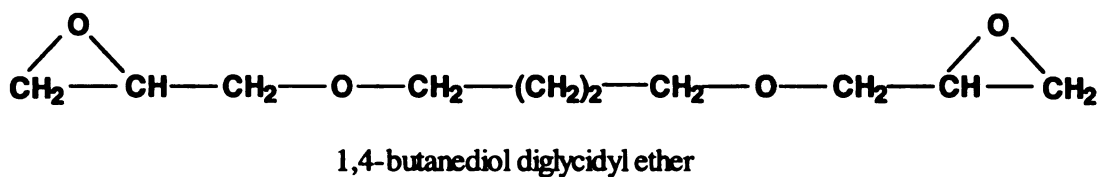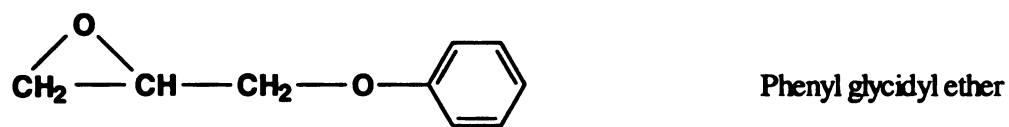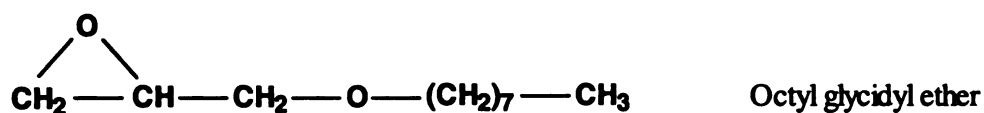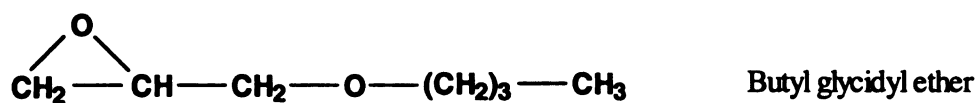
Table 4.2. Photoinitiators and photosensitizers for cationic photopolymerizations

Photoinitiators

(tolylcumyl) *iodonium* tetrakis
(pentafluorophenyl) borate
MW = 1015.7 g/mole

Diaryliodonium Hexafluoroantimonate
MW = 746.23 g/mole

Mixed Triarylsulfonium Hexaflourophosphate
Average* MW = 1693.44 g/mole
* a 50 wt% solution of propylene carbonate

MW = 846.72
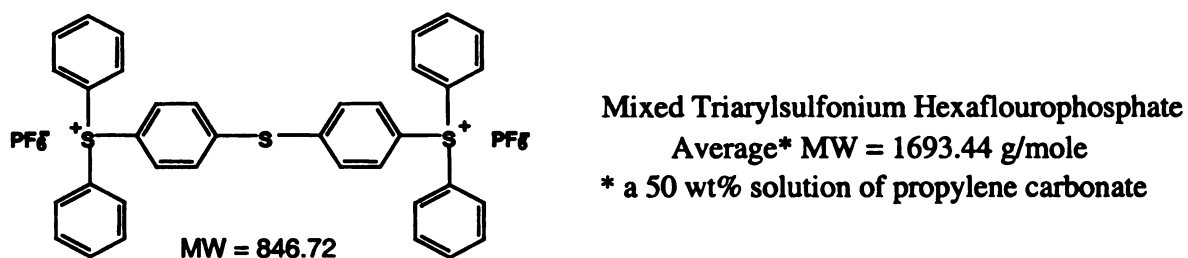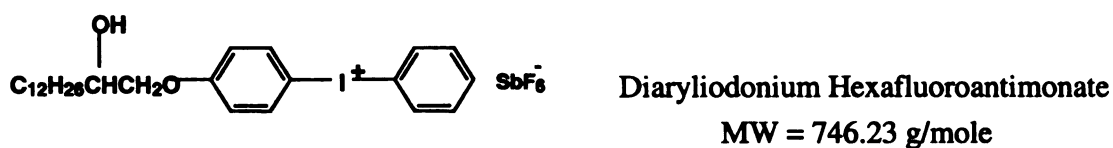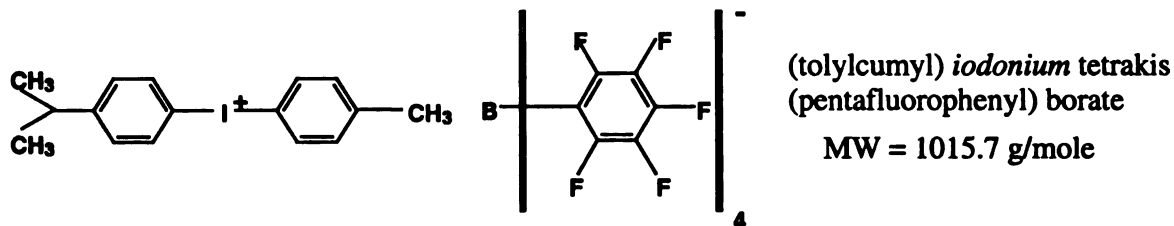
Photosensitizers
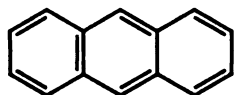
Anthracene, MW = 178.23 g/mole
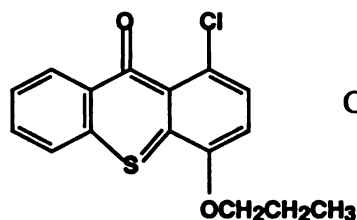
CPTX (1-chloro-4-propoxy-9H-thioxanthen-9-one)
MW = 304.80 g/mole

4.2. Absorption Spectra of the Photoinitiating System Constituents

One of the important parameters that can affect the overall kinetics of the polymerization reaction is the absorption of the incident light by the constituents in the reactive mixture. The knowledge of these absorption spectra is critical in the optimal selection of monomers, initiators and/or sensitizers. From the emission spectrum, obtained by Ocean Optics, of the light source, a 200 Watt Hg-Xe arc lamp, (Figure 4.1), the location of the strongest emission peaks and their associated wavelengths can be determined. The absorption spectra were obtained using the UV-vis spectrophotometer (HP8452A Diode Array). For example, an amount of initiator was weighed in the Metler 200 scale, with accuracy to 0.1 milligrams. The number of moles was calculated and then dissolved in the appropriate volume of the solvent methylene dichloride (CH_2Cl_2) to obtain the desired concentration. The absorbance was then taken. Serial dilutions were done to obtain an absorbance value of 2 or less. The extinction coefficient was calculated using Beer's Law,

$$Absorbance = \varepsilon cl \qquad (4.1)$$

Where, $\varepsilon \equiv$ extinction coefficient in $L.mole^{-1}.cm^{-1}$

$c \equiv$ concentration of monomer resin in mole / Liter

$l \equiv$ path length in cm

The absorption spectra of all of the system constituents are shown in Figures 4.2-4.12. From these absorption spectra, the wavelength of maximum absorbance and the corresponding extinction coefficient were calculated. Table 4.3 provides a summary of the absorption properties for all monomers, photoinitiators, and photosensitizers used in this research effort.

Table 4.3. Absorption properties of epoxide monomers, photoinitiators, and photosensitizers

Monomers	Absorbance	Peak Wavelength (nm)	Concentration (mol/L) in CH_2Cl_2	Calculated Extinction Coef. ($L*mole^{-1}*cm^{-1}$)
n-octyl glycidyl ether	0.463	232	1.000	0.463
n-butyl glycidyl ether	1.621	240	0.100	16.214
Phenyl glycidyl ether	1.313 1.668	228 270	0.001 0.001	1313.324 1668.045
1,4-butanediol diglycidyl ether	0.492	240	0.100	4.916
Cyclohexane dimethanol diglycidyl ether	0.652 0.615	228 240	0.100 0.100	6.520 6.153
Cycloalphatic diepoxies ERL 4221	0.502	228	0.010	50.166

Photoinitiators

(tolycumyl) *iodonium* tetrakis (pentafluorophen yl) borate	1.590 1.539	230 252	1.00E-3 1.00E-3	1.59E3 1.54E3
Diaryliodonium Hexafluoro- antimonate	1.131 1.294	230 260	5.00E-5 5.00E-5	2.26E4 2.59E4
Triarylsulfonium Hexafluoro- phosphate	1.542 0.674	232 298	5.00E-5 5.00E-5	3.08E4 1.35E4

Photosensitizers

1-chloro-4- propoxy-9H thioxathen-9-one (CPTX)	1.968 0.530 0.333	258 316 386	5.00E-5 5.00E-5 5.00E-5	3.94E4 1.06E4 6.66E3
Anthracene	3.217 0.412 0.379	248 358 378	5.00E-5 5.00E-5 5.00E-5	6.43E4 8.25E3 7.58E3
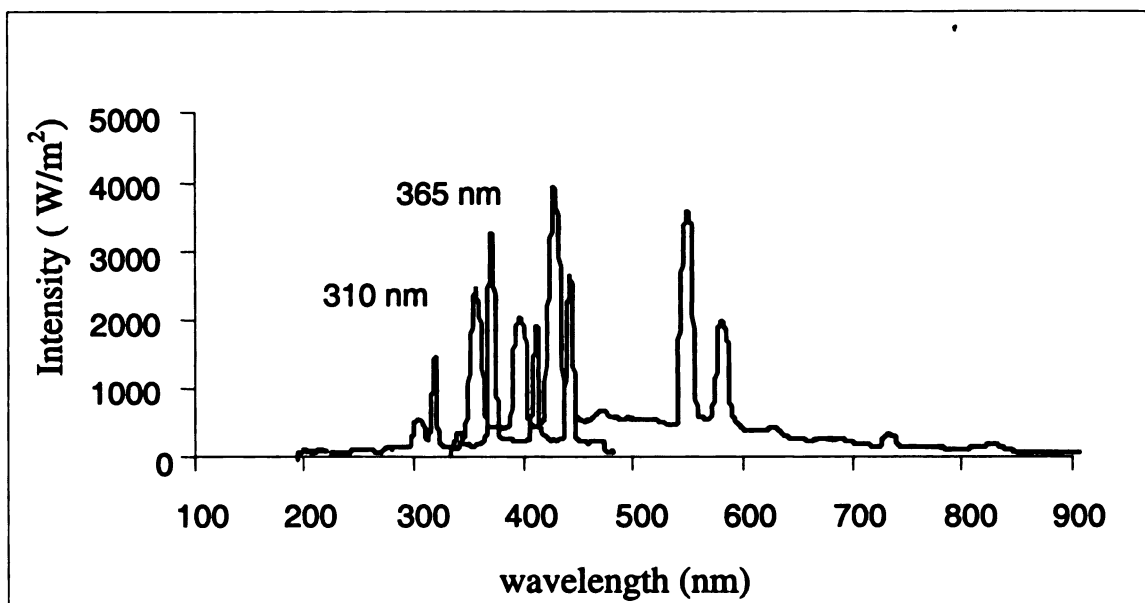
Figure 4.1. Emission spectrum of the 200 Watt Hg-Xe arc lamp for the photo-differential scanning calorimetry (PDSC) studies.

As shown in Figure 4.1, the emission spectrum has strong emission peaks at wavelengths of 310 nm and 365 nm, which are in the region where the photosensitizers strongly absorb. Figures 4.1 through 4.12 are presented in color.
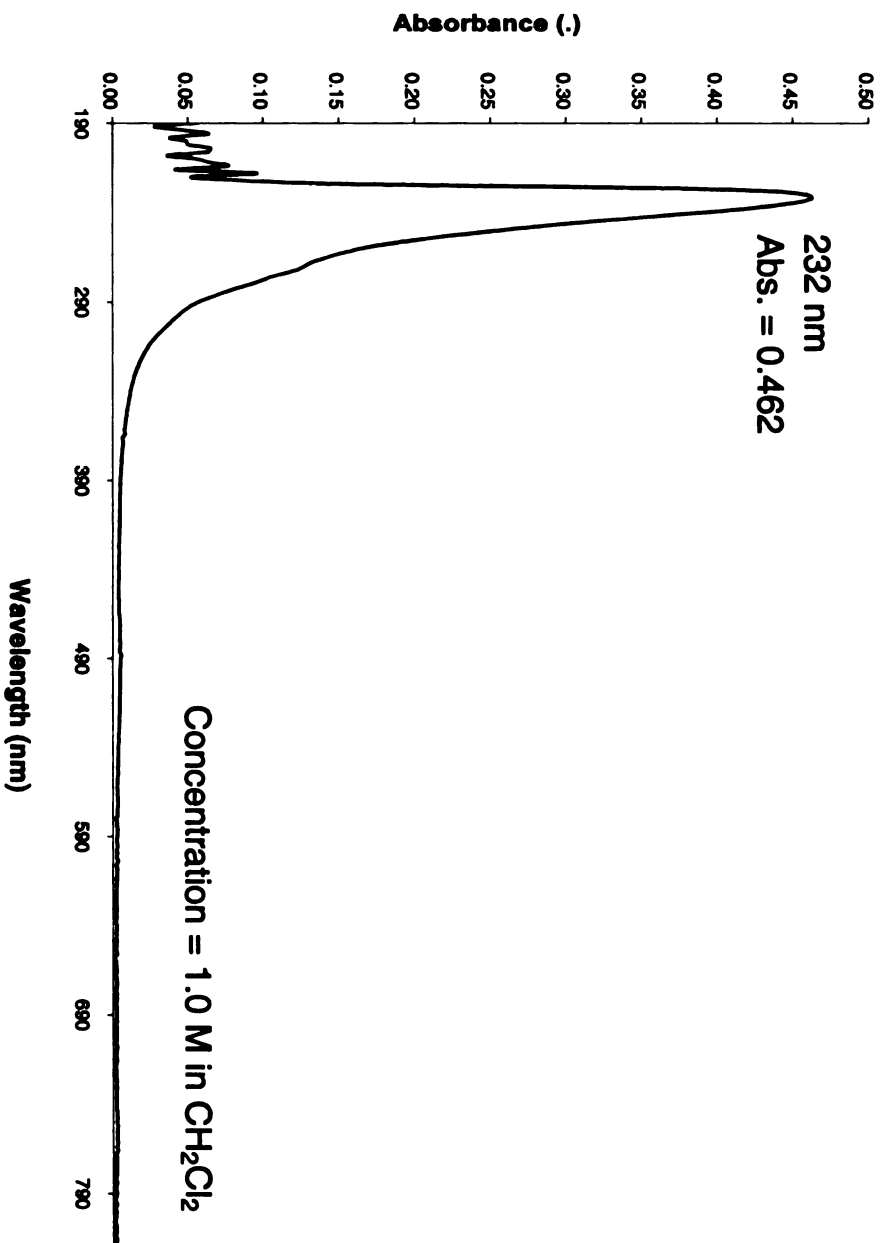
Figure 4.2. Absorption spectrum for the mono-epoxide monomer *octyl glycidyl ether*

232 nm
Abs. = 0.462

Concentration = 1.0 M in CH_2Cl_2
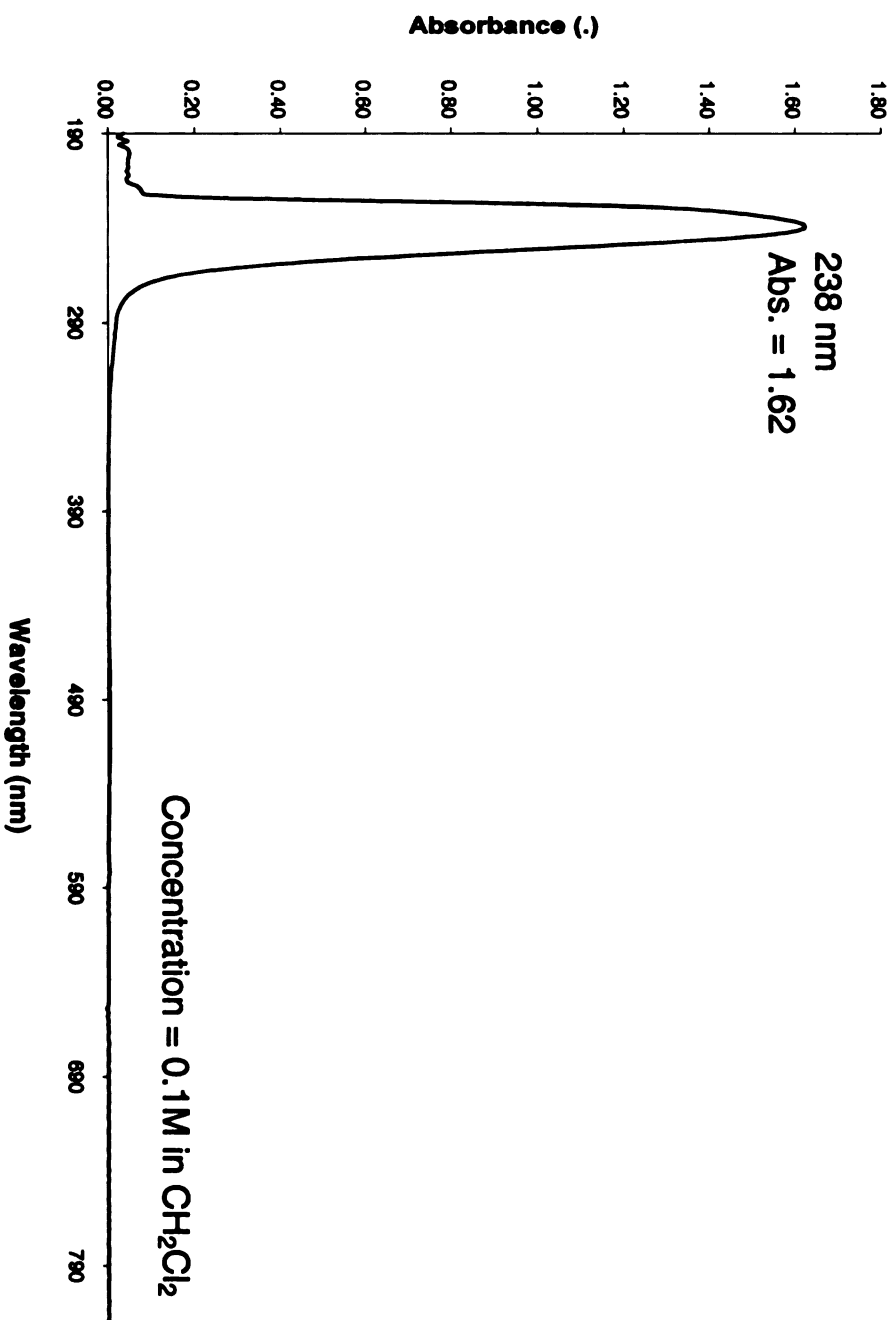
Figure 4.3. Absorption spectrum for the mono-epoxide monomer *butyl glycidyl ether*
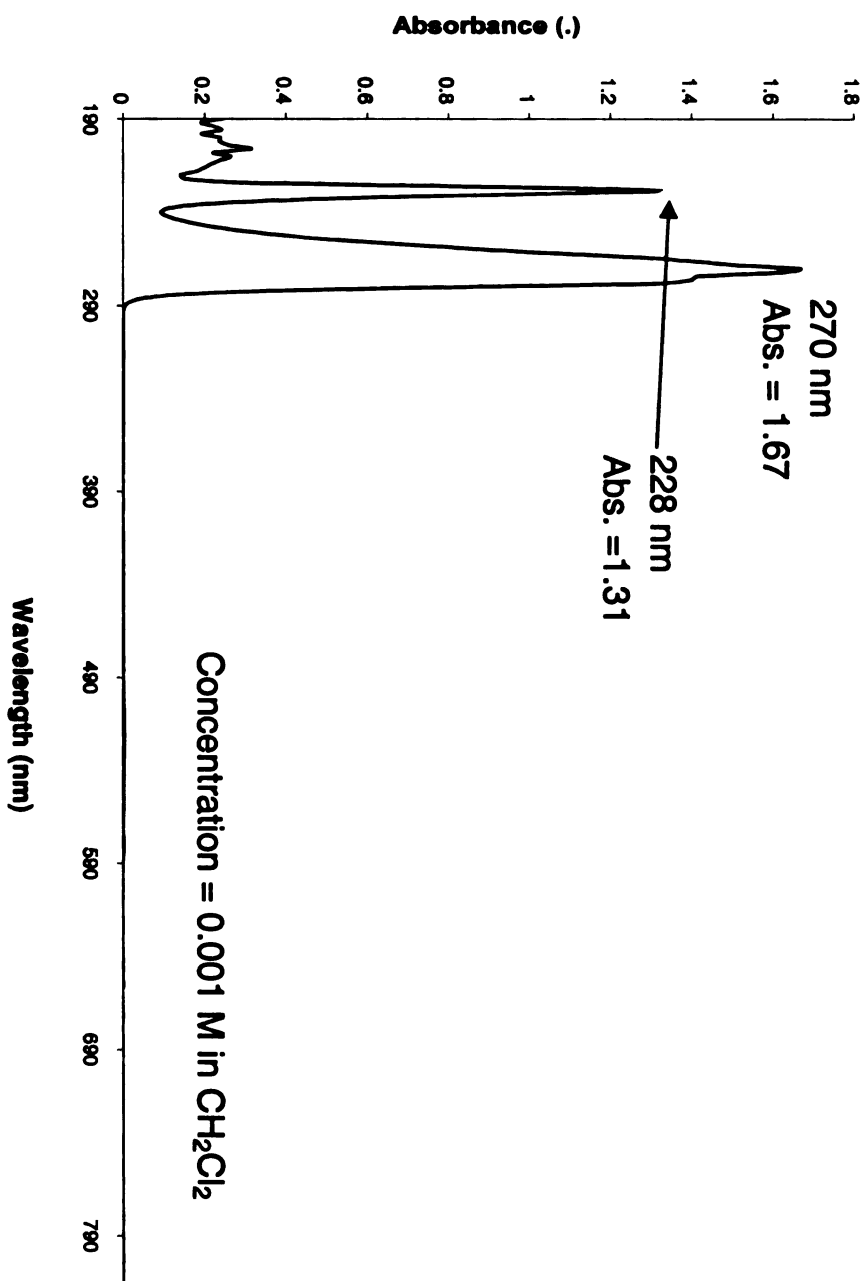
Figure 4.4. Absorption spectrum for the mono-epoxide monomer *phenyl glycidyl ether*
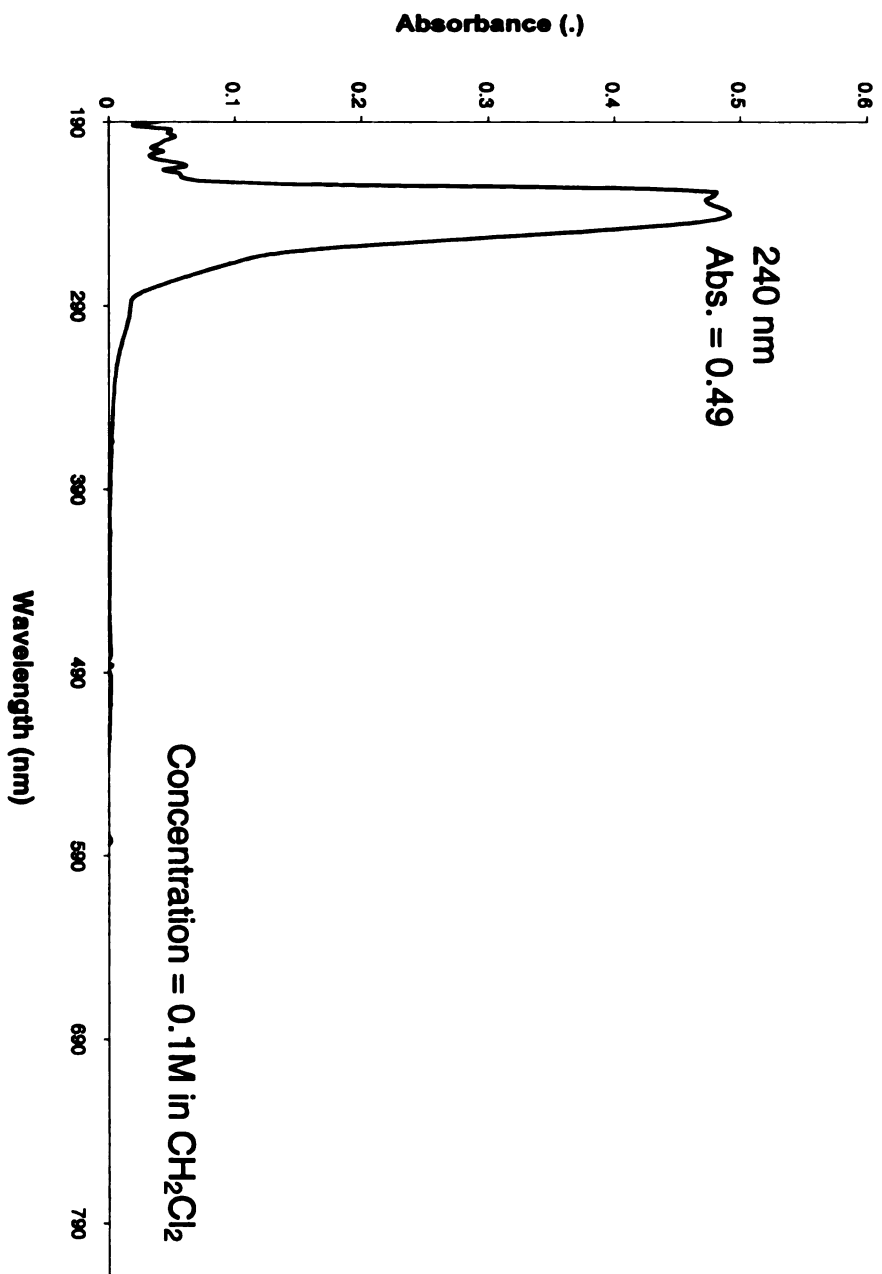
Figure 4.5. Absorption spectrum for the di-epoxide monomer *1,4-butanediol diglycidyl ether*

43
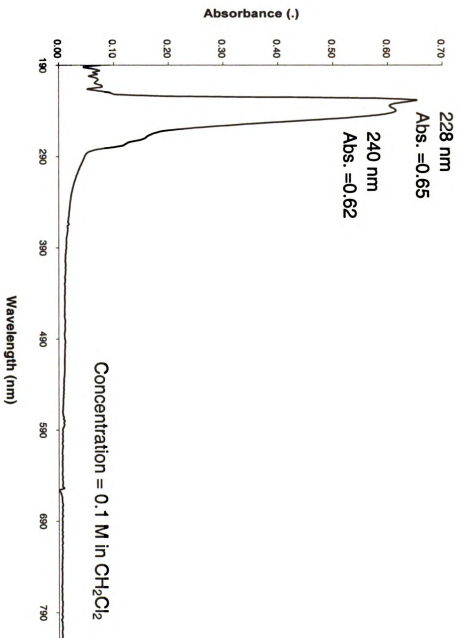
Figure 4.6. Absorption spectrum for the di-epoxide monomer *cyclohexane dimethanol diglycidyl ether*
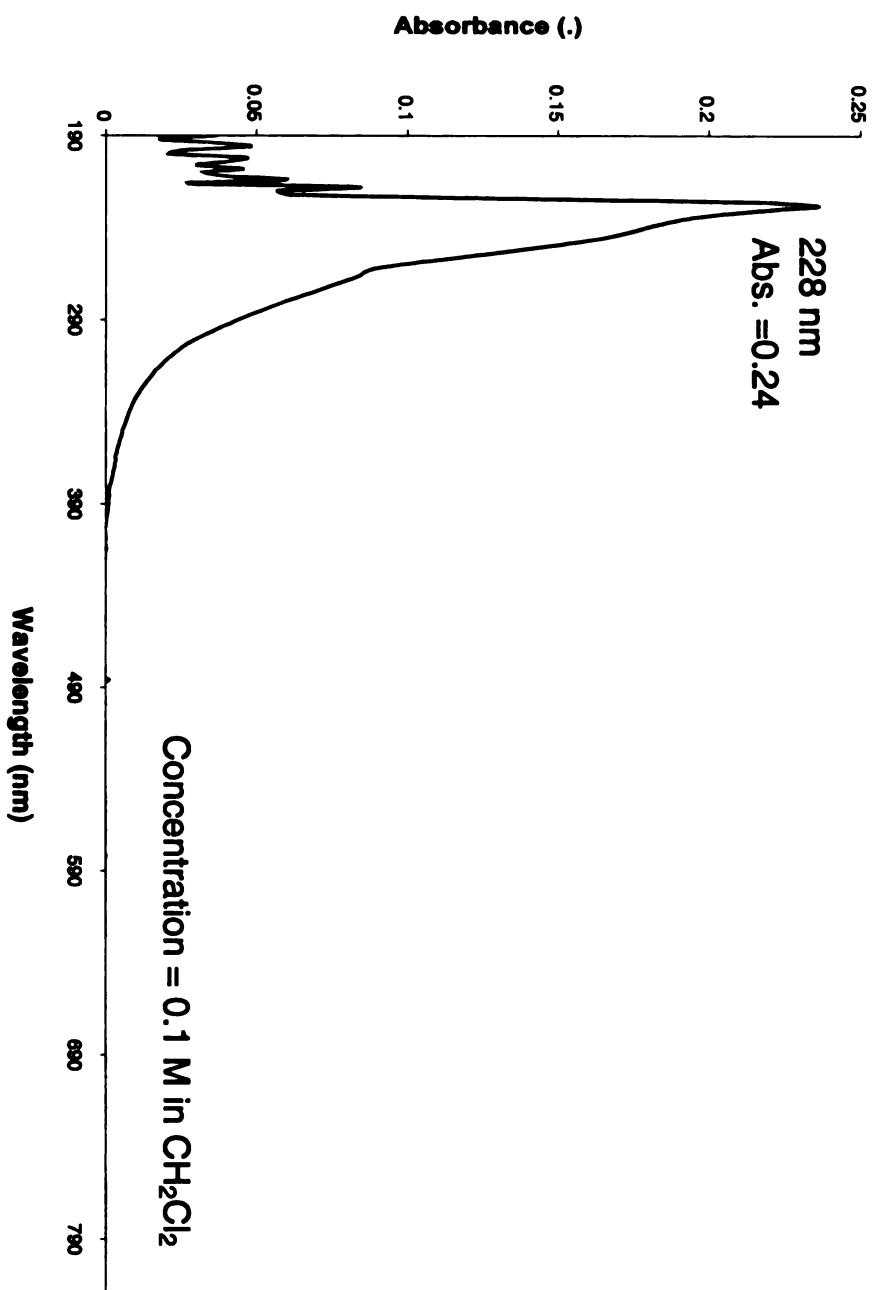
Figure 4.7. Absorption spectrum for the tri-epoxide monomer *trimethyol propane triglycidyl ether*
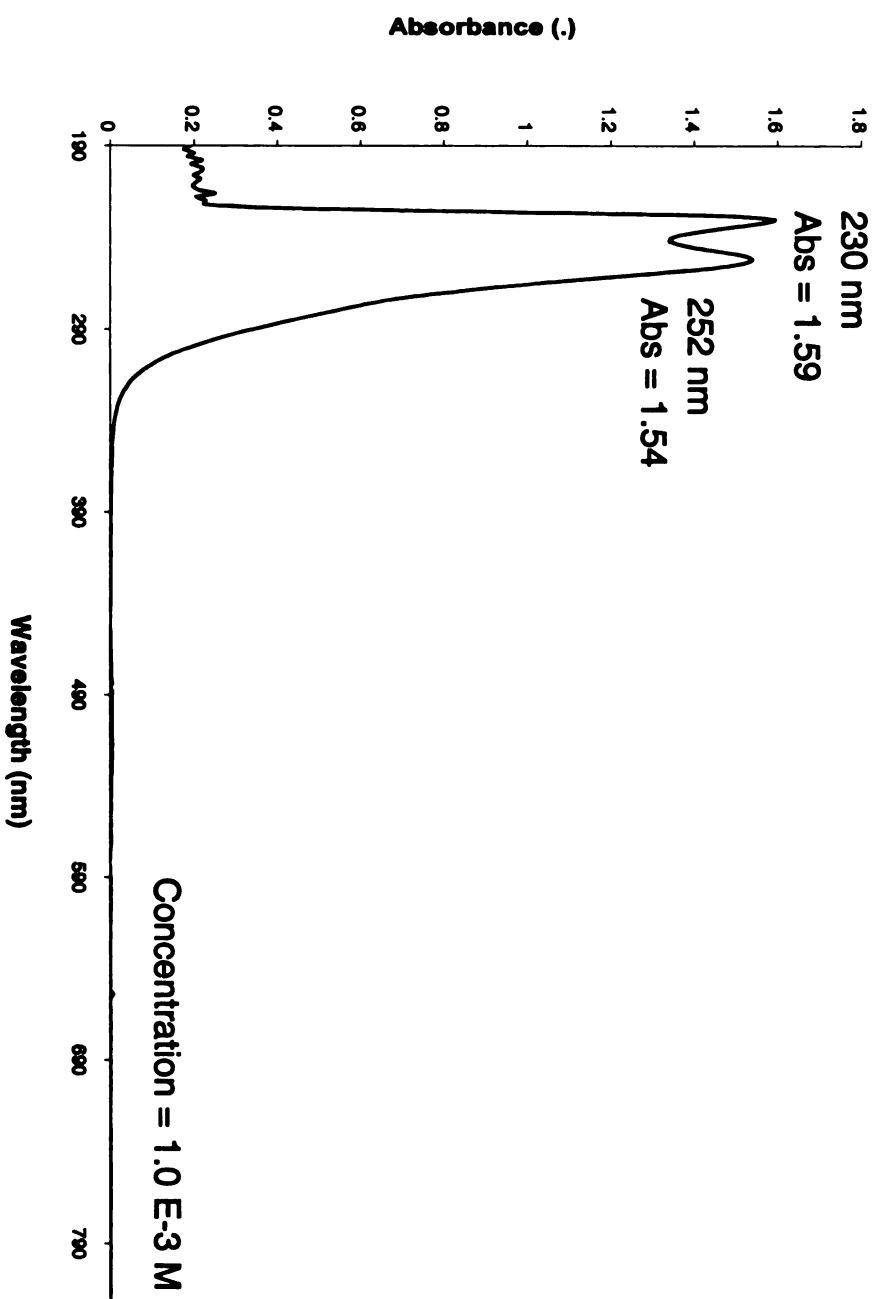
Figure 4.8. Absorption spectrum for the photoinitiator *tolycumyl iodonium tetrakis pentafluorophenyl borate*
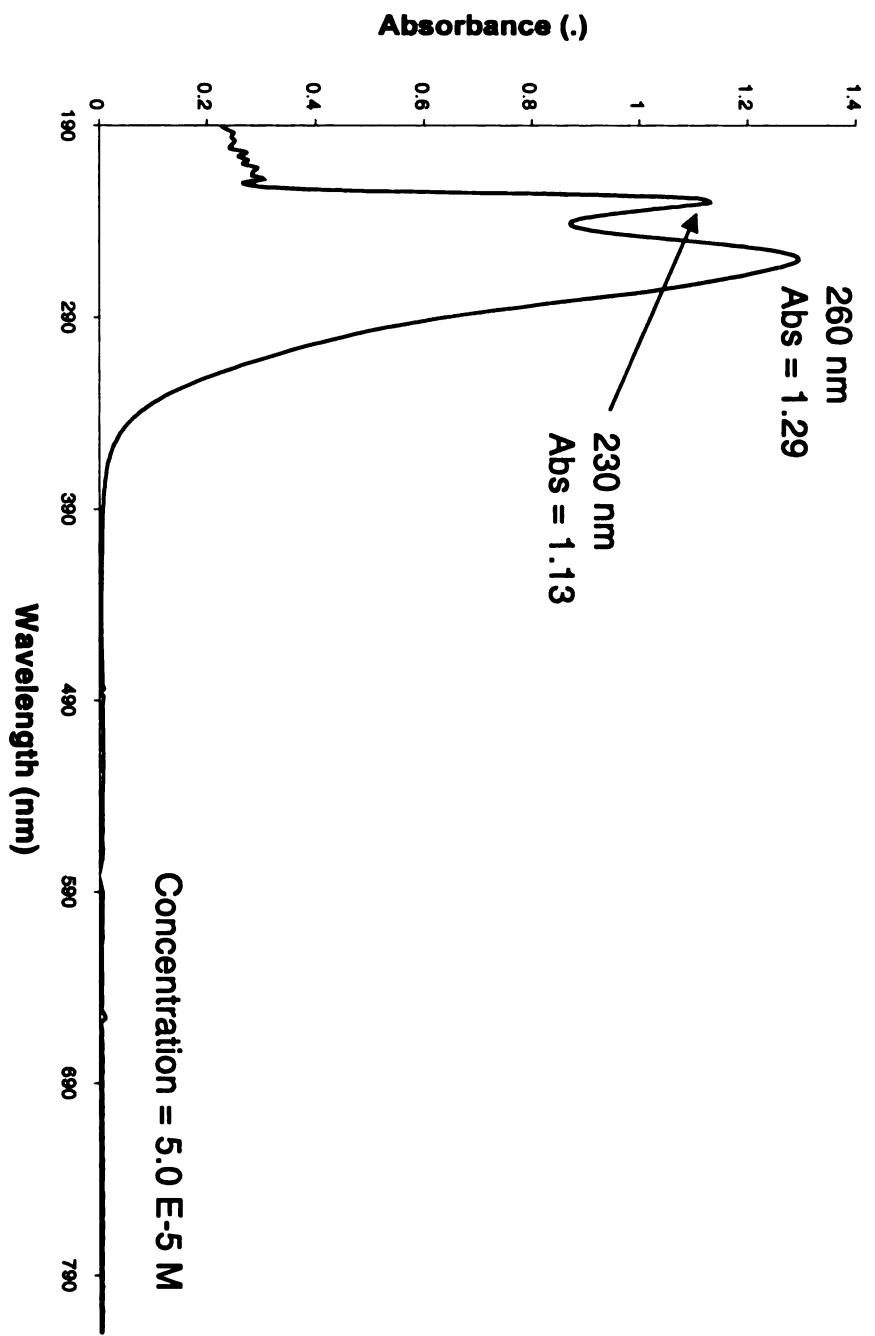
Figure 4.9. Absorption spectrum of the photoinitiator *diaryliodonium hexafluoroantimonate*

47
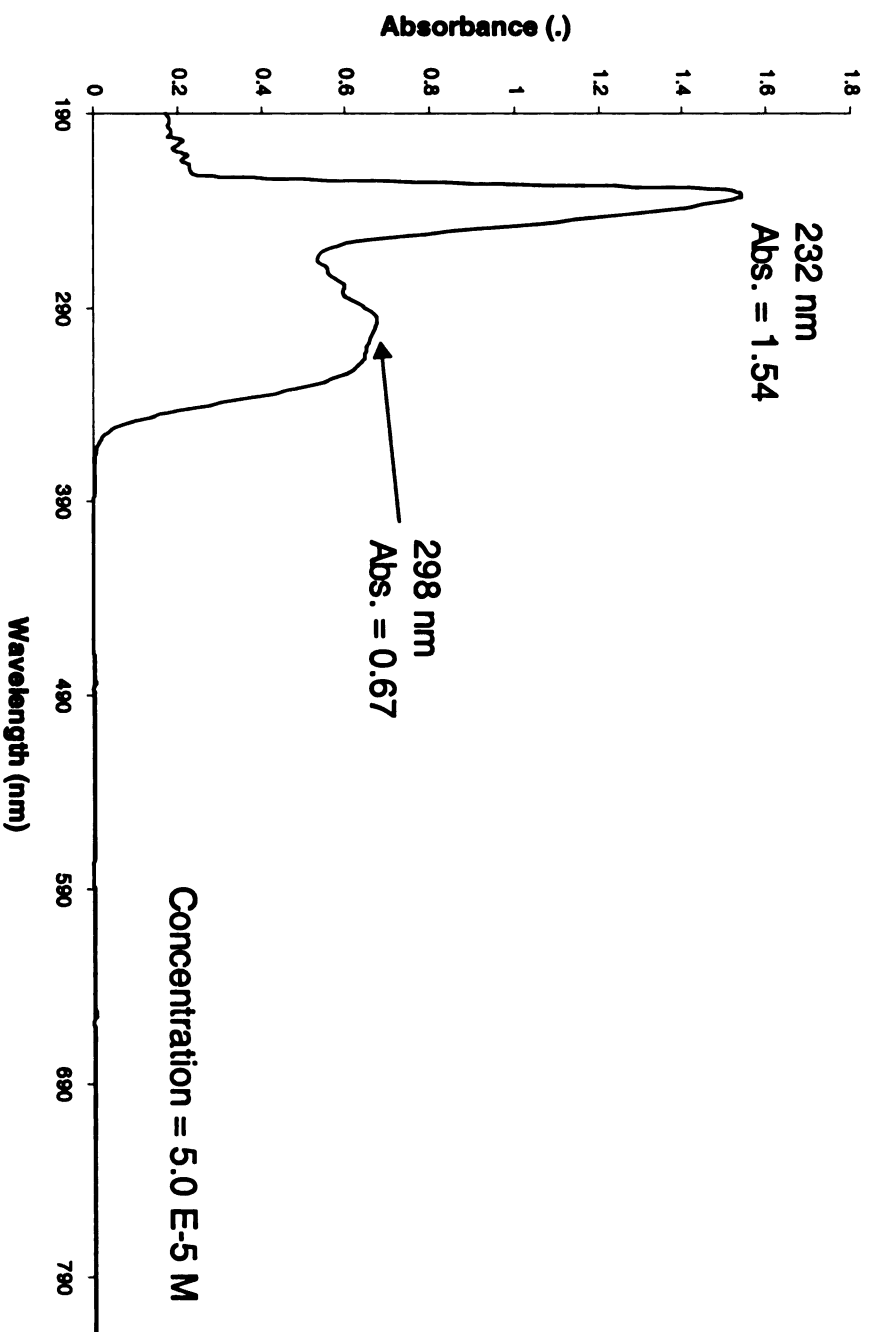
Figure 4.10. Absorption spectrum of the photoinitiator *triarylsulfonium hexafluorophosphate*
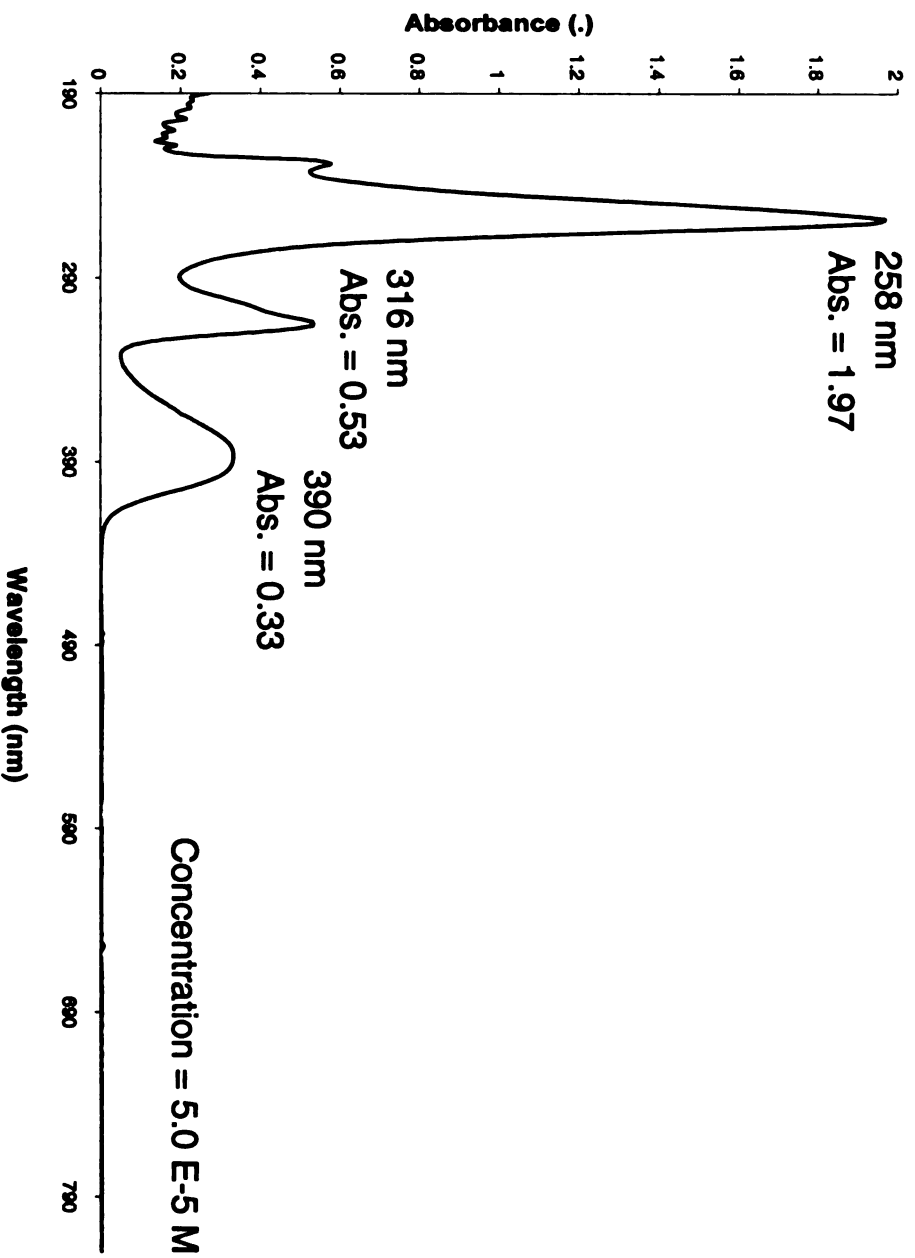
Figure 4.11. Absorption spectrum of the photosensitizer *1-chloro-4 propoxy 9-H thioxathen-9-one* (CPTX).
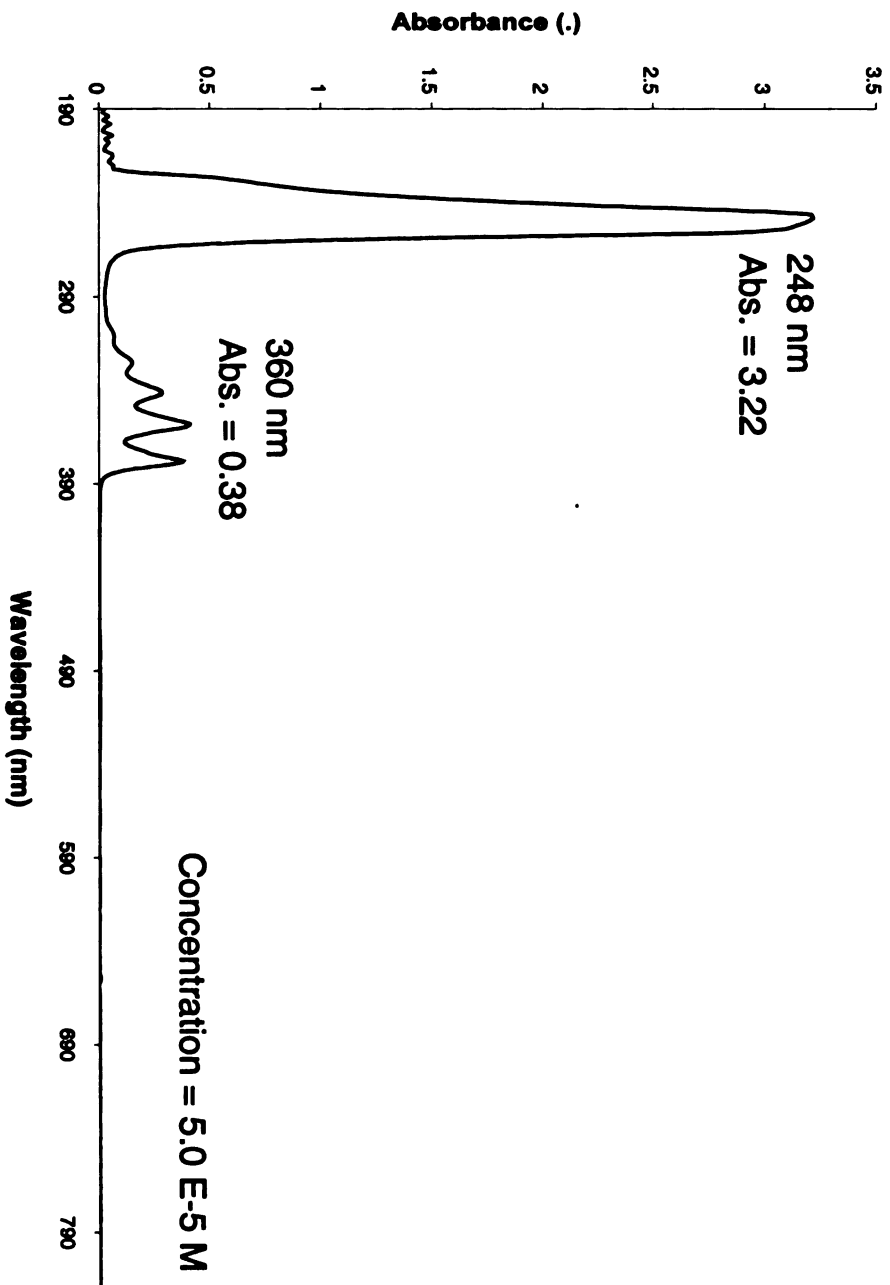
Figure 4.12. Absorption spectrum of the photosensitizer *anthracene*

4.2. Verification of Monomer Molecular Structures by NMR Spectroscopy

4.2.1. Introduction

It is imperative to know the exact weight per mole of epoxide groups present in each of the monomer molecules investigated in this research. The verification of the monomer molecular structures is performed using the technique of ^{1}H-NMR spectroscopy. NMR is based on the interactions between the nucleus of a particular atom with the applied magnetic field. The interacting atom is either a hydrogen (proton) or a carbon atom, thus giving the name PMR (proton magnetic resonance or ^{1}H-NMR) spectrum or CMR spectrum (based on ^{13}C nuclei). Further description of this technique is found in Chapter 2, section 2.5.3. The ^{1}H-NMR spectra were obtained for all epoxide monomers and are shown in Figures 4.13 through 4.18 in the following section.

Figure 4.13. 1H-NMR spectrum for octyl glycidyl ether
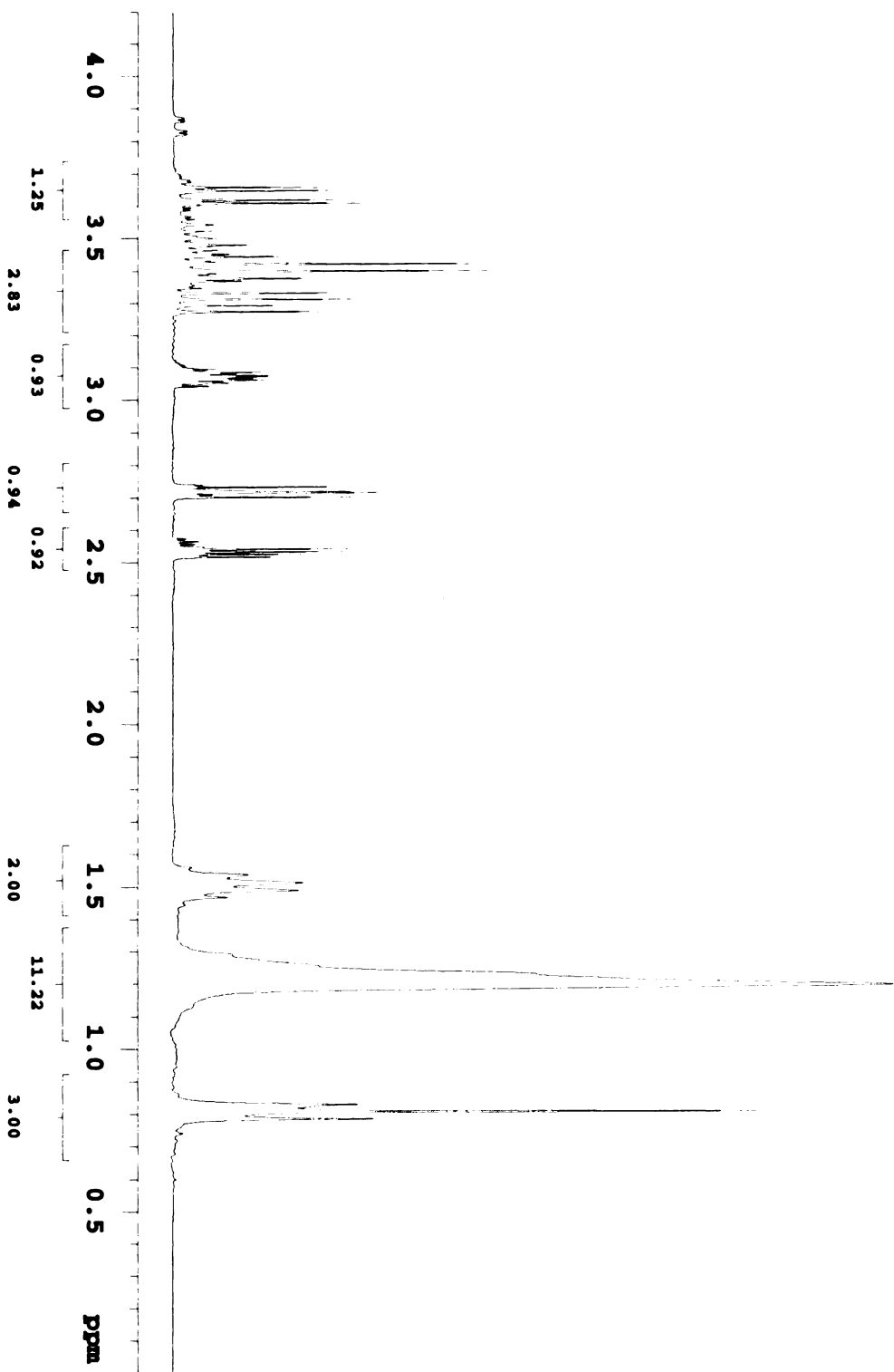
Figure 4.14. 1H-NMR spectrum for butyl glycidyl ether
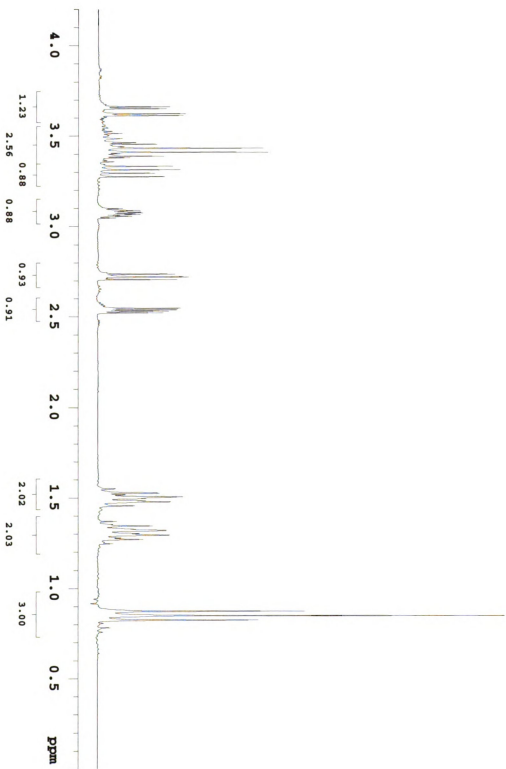
Figure 4.15. 1H-NMR spectrum for phenyl glycidyl ether
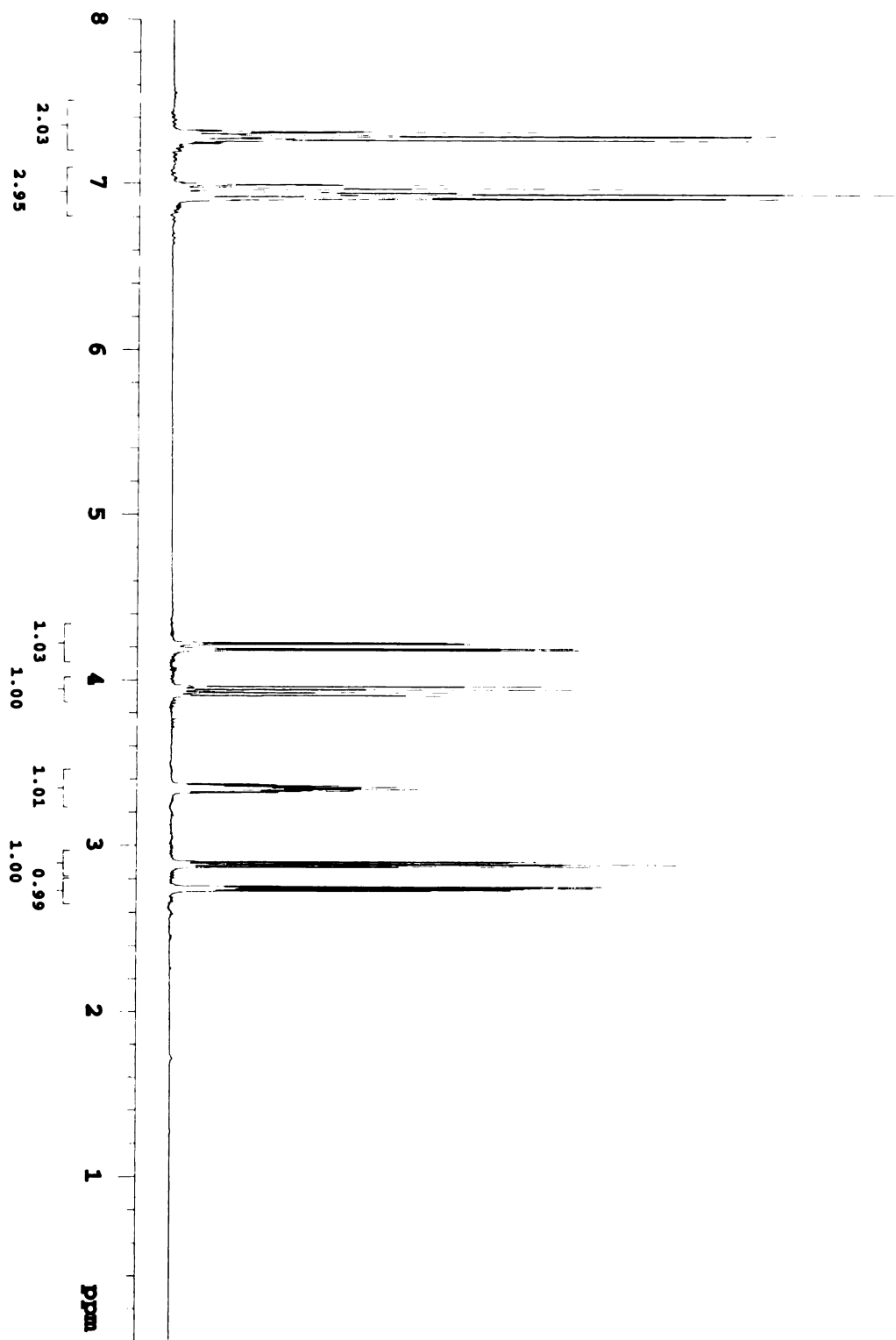
Figure 4.16. 1H-NMR spectrum for 1,4-butanediol diglycidyl ether
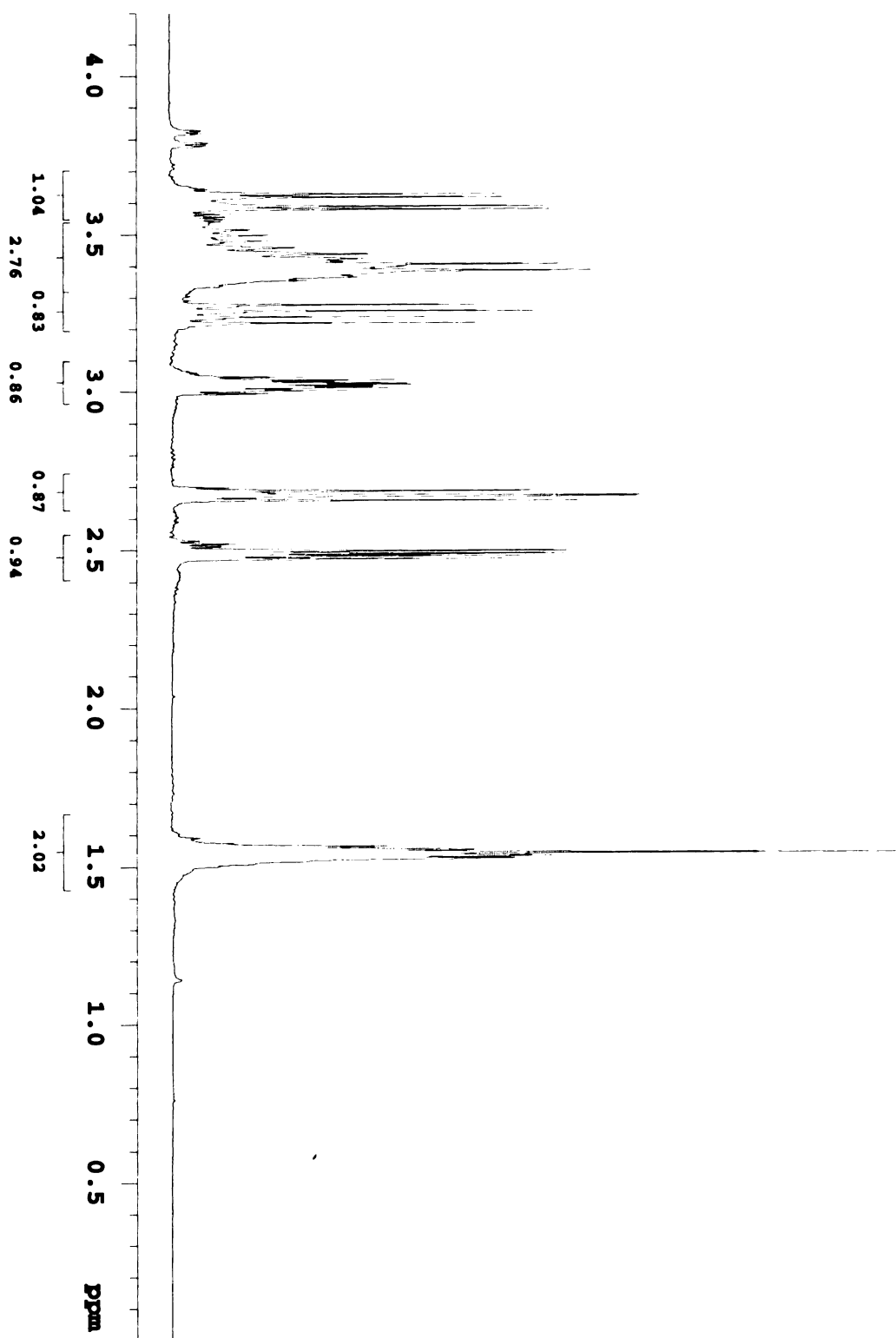
Figure 4.17. 1H-NMR spectrum for cyclohexane dimethanol diglycidyl ether
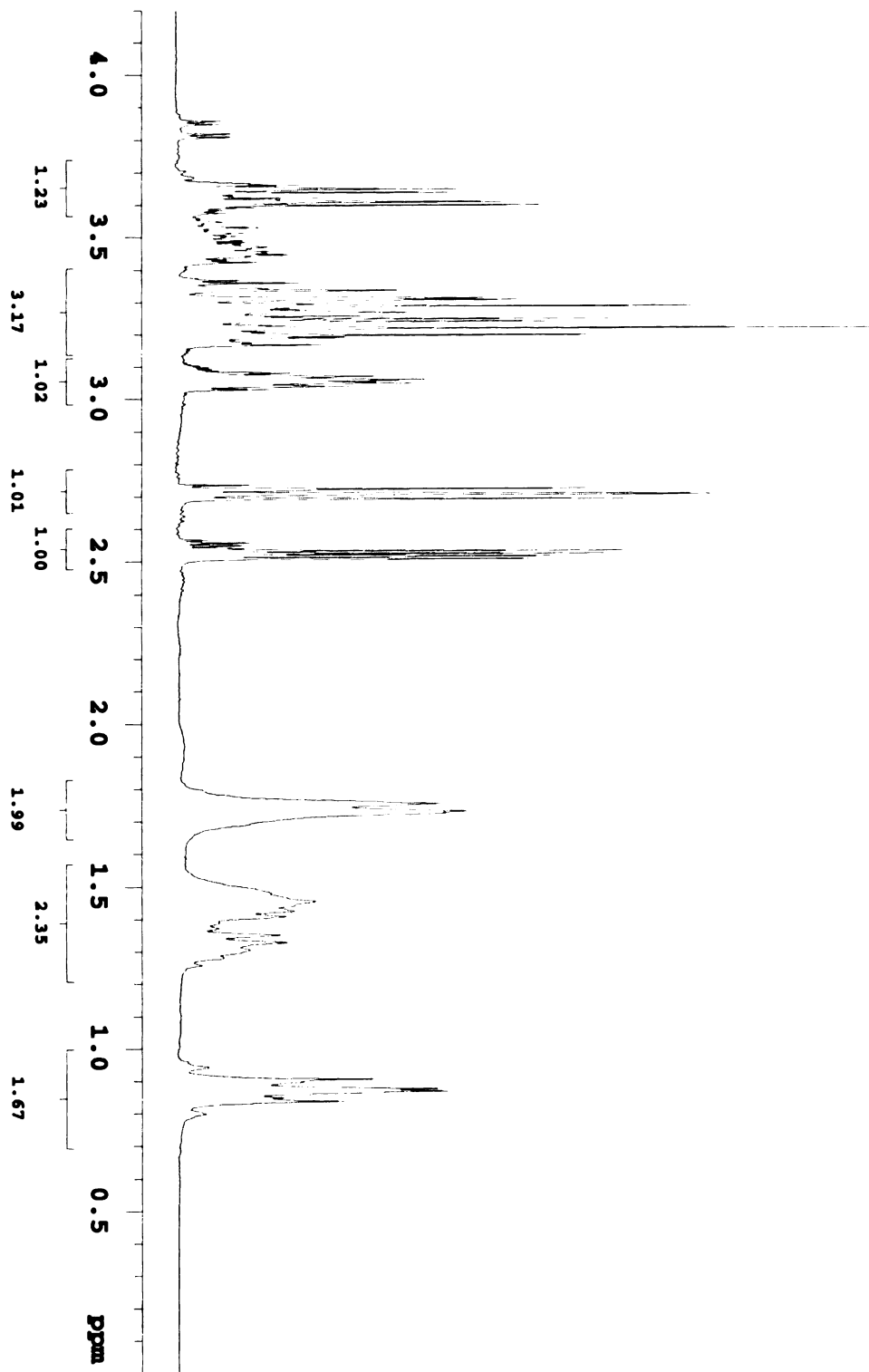
Figure 4.17. 1H-NMR spectrum for trimethylol propane diglycidyl ether
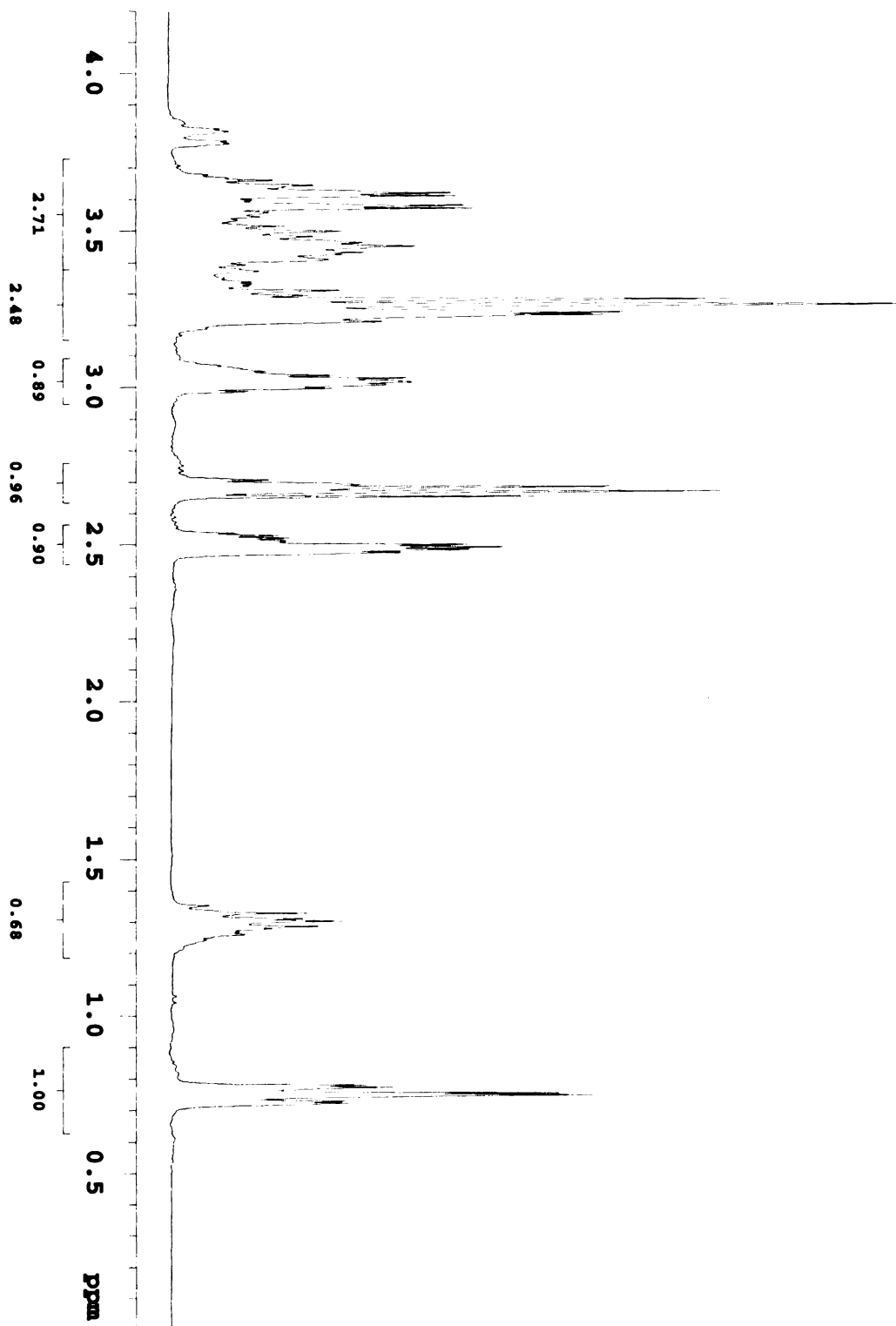
4.2.2. Analysis of ^{1}H-NMR Spectra

NMR spectroscopy was used to characterize and verify the molecular structures (including the molecular weights) of the epoxide molecules that are used in this research effort. All ^{1}H-NMR spectra were obtained using the NMR instrument VXR 300 by Varian using standard methods and standard values for the instrumental parameters such as the delay and the pulse width. For each spectrum, 32 free induction decays (FIDs) were signal averaged without apodization before Fourier transformation, and the resulting spectra exhibited signal-to-noise ratios of at least 200 to 1. All samples were dissolved in deuterated chloroform.

4.2.2.1 ^{1}H-NMR spectrum of mono-epoxide monomer octyl glycidyl ether

The NMR spectrum for the mono-epoxide monomer octyl glycidyl ether is shown in Figure 4.13. The proposed molecular structure with assignments for different or non-equivalent protons corresponding to the signals on the spectrum is as follows:
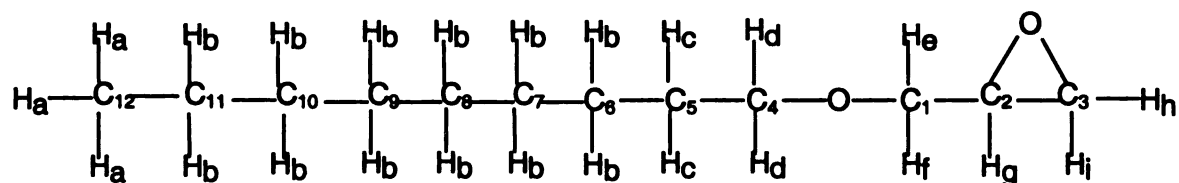
Figure 4.19. Molecular structure for the mono-epoxide monomer *octyl glycidyl ether*.

Based upon this structure, there are 24 total protons per molecule, and nine distinct electronic environments or nine different kinds of protons as assigned a, b, c, d, e, f, g,h and i for the molecule octyl glycidyl ether. They correspond to the nine different signals as seen on the NMR spectrum (Figure 5.13). The numbers beneath the ppm scale are values for the integrated area of the signals or signal intensity, which is directly

58

proportional to the number of protons giving rise to the signal. For example, the number three at about 0.8 ppm corresoponds to three protons H_a which form the methyl group. Likewise, the signal at about 1.25 ppm is for the twelve protons H_b. Each signal at about 3.1 ppm, 2.7 ppm and 2.5 ppm correspond to proton H_g, H_h and H_i. The remaining four protons: 2 H_d, 1 H_e and 1 H_f are the peaks found in the region of roughly 3.3 ppm to 3.7 ppm. Thus, the formula for octyl glycidyl ether is $C_9H_{19}O_2C_3H_5$ and the formular weight is 186.294 g/mole.

4.2.2.2. ^{1}H-NMR spectrum of mono-epoxide monomer butyl glycidyl ether

The analysis for this monomer is very similar to that for octyl glycidyl ether because the only difference here is the butyl group. The molecular structure is illustrated in Figure 4.20 below. As shown in Figure 4.14, the peak at about 0.85 ppm corresponds to the three protons H_a. The two signals at 1.3 ppm and 1.5 ppm are due the two protons H_b and two protons H_c respectively. Next, the three signals at 2.5 ppm, 2.7 ppm and 3.1 ppm belongs to each single proton of H_h, H_i and H_g. The two protons H_d, 1 proton H_e and 1 proton H_f are located in the region of 3.3 ppm to 3.7 ppm. Therefore, the formula of butyl glycidyl ether is $C_4H_9O_2C_3H_5$ with the formular weight of 130.186 g/mole.
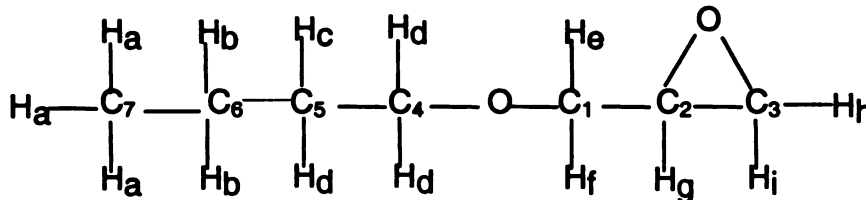
Figure 4.20. Molecular structure for the mono-epoxide monomer *butyl glycidyl ether*

4.2.2.3. ^{1}H-NMR spectrum for the mono-epoxide monomer phenyl glycidyl ether

Figure 4.21 shows that there are a total of 10 protons which can be determined

from seven different signals in the ^{1}H-NMR spectrum of phenyl glycidyl ether (Figure 4.15). The five aromatic protons H_a and H_b are shifted downfield as the two signals at
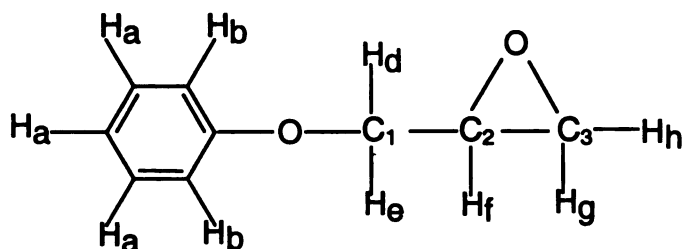
Figure 4.21. ^{1}H-NMR spectrum for the mono-epoxide monomer *phenyl glycidyl ether*.

about 7 ppm and 7.15 ppm respectively. Each of the proton H_d and H_e is due to a signal at about 4 ppm and 4.1 ppm. Finally, the three signals at approximately 2.85 ppm , 2.95 ppm and 3.2 ppm correspond to each proton of Hg, Hh and Hf. So the formula for phenyl glycidyl ether is $C_5H_5O_2C_3H_5$ with its formular weight of 150.177 g/mole.

4.2.2.4. ^{1}H-NMR spectrum for di-epoxide monomer 1,4-butanediol diglycidyl ether.

This molecule is symmetric with a perpendicular plane bisecting the $C_5\text{-}C_5$ bond. There are seven different kinds of protons, namely a, c, d, e, f, g, and h which correspond
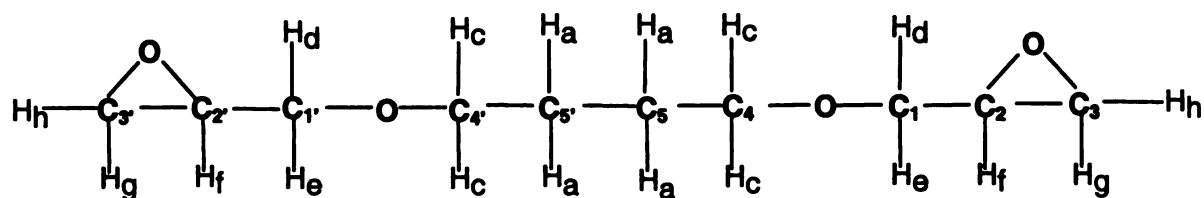
Figure 4.22. ^{1}H-NMR spectrum for di-epoxide monomer *1,4-butanediol diglycidyl ether*

to the seven signals as observed on the spectrum (Figure 4.16). Each half of the molecule has a total of 9 protons. The signal at 1.5 ppm is due to two protons H_a. Each proton H_h, H_g, and H_f corresponds to a signal at 2.5 ppm, 2.7 ppm and 3.0 ppm. The remaining four

protons (2 H_c, 1 H_d and 1 H_e) are found in the region of 3.2 ppm to 3.7 ppm. The formula

of phenyl glycidyl ether is determined to consist of two groups of $C_2H_4O_2C_3H_5$, each of

which contains an epoxide ring; thus the weight per mole of epoxide groups (or rings) for

1,4-butanediol diglycidyl ether is 101.23 g/mole.

4.2.2.5. ^{1}H-NMR spectrum for the di-epoxide monomer cyclohexane dimethanol diglycidyl ether.
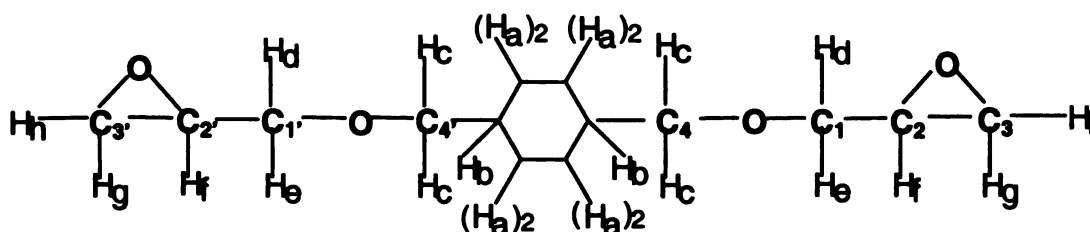
Figure 4.23. Molecular structure of di-epoxide *cyclohexane dimethanol diglycidyl ether*

This molecule is symmetric with respect to the vertical and perpendicular plane

bisecting the cyclohexane ring. There are a total of 12 protons, which derive from 8

different electronic environments, corresponding to 8 different kinds of protons. They

are: a, b, c, d, e, f, g, and h (Figure 4.23). Looking at the ^{1}H-NMR spectrum in Figure

4.17, each of the signal at roughly 2.5 ppm, 2.7 ppm and 3.05 ppm is due to each of the

proton H_h, H_g, and H_f accordingly. So each proton has an integrated value of about 0.60.

Based on this assignment, a peak at 1.75 ppm, a broad and split signal centered at about

1.4 ppm, and a signal 0.9 ppm correspond to the five protons H_a and H_b attached to the

cyclohexane. Thus a single molecule of cyclohexane dimethanol diglycidyl ether is made

up of two groups, each of which contains an epoxide ring. The weight per mole of

epoxide groups for the di-epoxide monomer cyclohexane dimethanol diglycidyl ether is

determined to be 128.17 g/mole.

4.2.2.6. ^{1}H-NMR spectrum of monomer trimethyol propane triglycidyl ether

As shown in Figure 4.24, a molecule of the monomer trimethyol propane triglycidyl ether has three epoxide groups. There are a total of 26 protons, which can be determined by 8 different signals from the ^{1}H-NMR spectrum (Figure 4.18). Specifically, the signal at about 0.75 ppm is due to three protons H_a. So each proton has an integrated value of about 0.33. Based on this designation, the signal at 1.3 ppm is due
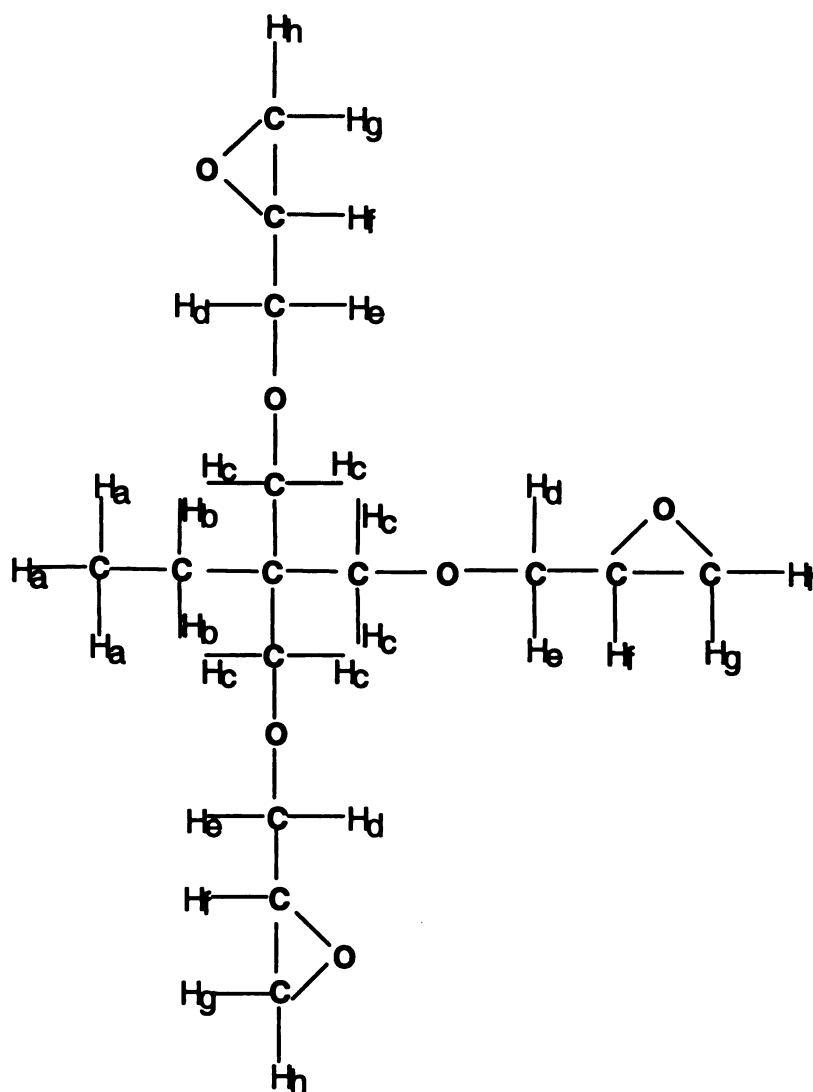
Figure 4.24. Molecular structure of the tri-epxide monomer *trimethyol propane triglycidyl ether.*

two protons H_b. Each signal at 2.5 ppm, 2.7 ppm and 3.0 ppm correspond to 3 protons H_h, 3 protons H_g, and 3 protons H_f of the three epoxide rings. The remaining 12 protons (6 H_c, 3 H_d and 3 H_e) are located in the region of 3.2 ppm to 3.7 ppm. So the average weight per mole of epoxide groups for the tri-epoxide monomer trimethyol propane triglycidyl ether is determined to be 100.79 g/mole. The results of ^{1}H-NMR analysis of molecular structure of the monomers and their weight per mole of epoxide groups in a molecule are presented in Table 4.4. In addition, Table 4.4 also presents the calculated density for each epoxide monomer. The method to obtain the calculated densities is described in the next chapter, section 5.1.2.1.

In summary, the molecular structures of all the epoxide monomers used in this research effort have been verified by analyzing their ^{1}H-NMR spectra. The results of this analysis provide an accurate account of the weight per mole of epoxide groups present in a single monomer moleclue for each monomer. The weight per mole of epoxide as well as the density are two important constants used in the calculation of the observed rates of polymerization and the degree of conversion based on the primary data obtained from the photodifferential scanning calorimetry (PDSC) studies. In addition, the NMR spectra for some of these epoxide monomers have already been published by Aldrich.[7] They were used for comparative purposes.

Table 4.4. Weight per mole of epoxide groups and densities of all epoxide monomers used in this research effort.

Monomer	Wt. per mole epoxide groups (g/mole)	Calc. Density (g/ml)
Octyl glycidyl ether	186.2936	0.9061 ± 0.0004
Butyl glycidyl ether	130.1864	0.9365 ± 0.0001
Phenyl glycidyl ether	150.1768	1.1074 ± 0.0001
1,4-butanediol diglycidyl ether	101.1249	1.1012 ± 0.0001
Cyclohexane dimethanol diglycidyl ether	128.1076	1.0928 ± 0.0001
Trimethyol propane triglycidyl ether	100.7889	1.1603 ± 0.0002

4.3. References

1. J. K. M. Sanders and B. K. Hunter, *Modern NMR Spectroscopy – A Guide for Chemists*, Oxford University Press, New York, 1987.

2. R. T. Morrison and R. N. Boyd, *Organic Chemistry*, 3rd ed., Allyn and Bacon, Inc., Boston, Massachusetts, 1973.

3. E. Breitmaier, *Structure Elucidation by NMR in Organic Chemistry – A Practical Guide*, John Wiley & Sons, New York, 1993.

4. R. Freeman and G. A. Morris, *Bull. Mag. Reson.*, 1, pp. 1 - 28, 1979.

5. R. T. Morrison and R. N. Boyd, *Organic Chemistry*, 3rd ed., Allyn and Bacon, Inc., Boston, Massachusetts, pp. 420 – 422 (1973).

6. E. Breitmaier, *Structure Elucidation by NMR in Organic Chemistry – A Practical Guide*, John Wiley & Sons, New York, pp. 178, (1993).

7. C. J. Pouchert, *The Aldrich Library of NMR Spectra*, ed. II, Vol. 1, Aldrich Chemical Company, Inc., Milwaukee, Wisconsin, pp. 173 – 214 (1983).

Chapter 5

Kinetic Studies for Cationic Photopolymerization of Epoxide Monomers

5.1. Photo-differential Scanning Calorimetry (PDSC) Studies

5.1.1. Introduction

Photo-differential scanning calorimetry (PDSC) is a convenient and reliable method that can be used to characterize the kinetics of photopolymerization reactions. Because the polymerizations are highly exothermic, the reaction rate may be measured by monitoring the rate at which heat is released from the polymerizing sample. The profiles of the heat of reaction versus time are obtained from PDSC and may be used to characterize the reaction kinetics, such as the rate of polymerization R_p, and to elucidate the behavior of the propagation rate constant k_p. Several authors have used PDSC to characterize free radical[1-5] and cationic[6-9] photopolymerizations. However, cationic polymerizations are highly exothermic, care must be taken in order to ensure the released heat of reaction does not exceed the time resolution of the instrument, which is in the order of 2-3 seconds. Therefore, appropriate incident light intensities and small sample sizes (about 15 mg) are used to allow the removal of heat evolved on the time scale of the equipment in order to maintain isothermal conditions.

In this thesis, PDSC experiments were performed to determine effects of the following parameters on reaction rate and limiting conversion of cationic photopolymerization of epoxides: temperature, type and concentration of photoinitiator, type and concentration of photosensitizer, monomer structure, and light intensity.

5.1.2. Experimental

5.1.2.1 Materials

Three classes of monomers were investigated in this study as listed in Table 4.1: 1) epoxides containing a single epoxide group, 2) epoxides containing two epoxide groups, and 3) epoxides containing three polymerizable epoxide groups. These classes will henceforth be denoted mono-epoxide, di-epoxide and tri-epoxide monomers, respectively. Three different mono-epoxide monomers were investigated: 1) octyl glycidyl ether, 2) butyl glycidyl ether, and 3) phenyl glycidyl ether. These mono-epoxide monomers were chosen to investigate the effect of the length and type of the pendant group attached to the epoxide ring. Two different di-epoxide monomers were used: 1) 1,4-butanediol diglycidyl ether, 2) cyclohexane dimenthanol diglycidyl. The comparison of the results from the mono-epoxide studies and the di-epoxide studies will allow the effect of crosslinking to be investigated, while comparison among the three di-epoxide monomers will allow the effects of the length and flexibility of the chain between the two reactive groups to be investigated. Finally, the tri-epoxide monomer trimethyol propane triglycidyl ether was investigated. All epoxide monomers were obtained from Shell Chemical Company.

The molecular weight and density are important constants used in the calculation of the rate of polymerization and the degree of conversion based on the primary data obtained from PDSC. The density was readily computed as a ratio of the sample's mass over its volume. For example, a 25-ml volumetric flask was filled up to the mark with the resin of butyl glycidyl ether. The mass of the resin was obtained via the 200 Metler scale, and the density was then calculated. The molecular weight was determined from

the molecular structures that were verified in the previous chapter. Table 4.4 provides a summary of the molecular weight and density at room temperature for all monomers.

As illustrated in Table 4.2, three different photoinitiators were used, including two iodonium salts and one sulfonium salt. The two iodonium salts were: 1) tolylcumyl iodonium tetrakis pentaflourophenyl borate, $(B^-[F_5]_4^-$ counterion) from Rhodia Inc; 2) diaryliodonium hexafluoro-antimonate, $([SbF_6]^-$ counterion) from Sartomer Company. The third photoinitiator was triarylsulfonium hexafluorophosphate $([PF_6]^-$ counterion) from Sartomer Company. Two photosensitizers from Aldrich Chemical Company, Inc. were used: 1) anthracene, and 2) CPTX (1-chloro-4-propoxy-9H-thioxanthen-9-one).

As detailed in the previous chapter, the structures of all the monomers were characterized using ^{1}H-NMR spectroscopy (section 4.2.2). Prior to their usage in the kinetic experiments, the monomers were dried over molecular sieves (4-8 mesh beads, from Aldrich Chemical Company, Inc.) to remove any dissolved water. This dehydration step was necessary because water molecules can participate in the nucleophilic attack of the propagating active centers, thereby terminating the polymerization reactions prematurely. The photoinitiators and photosensitizers were used as received. A typical reactive mixture's weight was about 15 milligrams, comprising of the monomer resin and other constituents. The concentrations of the photoinitiator and photosensitizer were calculated on molal basis (numbers of moles of photoinitiator or photosensitizer per kilogram resin), in order to maintain consistent concentrations among different initiating systems and to allow for their quantitative comparison. A representative formulation contained 8.0×10^{-3} moles / kg resin in photoinitiator with or without 8.0×10^{-4} moles / kg resin in photosensitizer. In all, 42 different formulations of monomer, photoinitator,

and photosensitizer were studied at a number of different temperatures and light intensities.

5.1.2.2. Methods for Photo-DSC Experiments

The PDSC experiments were conducted using a Perkin Elmer model DSC-DPA 7 differential scanning calorimeter. As shown in Figure 2.1, this instrument is equipped with a photocalorimetric accessory, including the transfer optics to produce full-beam ultraviolet (UV) light. The DSC chamber contains two cells, one for the reference and the other for the test sample. During the reaction, the test sample was held in an uncovered DSC aluminum pan and the reference pan was kept empty and also uncovered. However, the entire reaction chamber was covered with a fused silica window that allowed for full transmission of the light source and contained the heat generated from the reaction. A recirculating water bath, maintained at $10^{\circ}C$, was installed to filter out the IR emissions of the initiation light source, which was a 200-watt Hg/Xe arc lamp. The intensity of light striking the reference and the sample was controlled by varying the distance between the light source and sample and/or by placing appropriate neutral density filter (from Oriel Corp) in the beam path. In addition, the incident light intensity was measured by placing black graphite discs in the sample and reference cells and measuring the heat generated in the discs due to absorption of light. With the reference disc kept dark, light was shuttered on and illumination was allowed to proceed for about 2 minutes until a constant value of heat flow (mW) had been reached. All polymerization reactions were run isothermally at specified reaction temperatures and light intensities. All experiments were performed in triplicate and average results are reported. All images and figures are presented in color.

69

5.1.3. Data Analysis

5.1.3.1. Evaluation of Kinetics Parameters

5.1.3.1a. Rate of Photopolymerization

A profile for the rate of polymerization, R_p, can be calculated based on the PDSC profiles of the heat released by the reaction versus time. The rate of polymerization, R_p, is directly proportional to the rate of heat released from the polymerizing sample, and is thereby proportional to the height of the PDSC exotherm measured in W/g. The instantaneous rate of polymerization in units of moles (epoxide groups)/L•sec is calculated by the following relationship:

$$R_p = \frac{d[M]}{dt} = \frac{height\ of\ exotherm(W/g)_* \ \rho \ (g/cm^3)}{\Delta H_P} \tag{5.1}$$

where,

R_p in moles (epoxide groups)/L•sec,

ρ, density of the reaction mixture is taken as the density of the monomer resin because the amounts of photoinitiator and photosensitizer are so small and insignificant.

ΔH_p (J/moles) is the amount of heat evolved from one mole of epoxide groups and is a constant of 92,000 J/ mole (please see reference 10).

An example of the data analysis to obtain the rate of polymerization, R_p, is shown in Figures 5.1 and 5.2 below. As illustrated in Figure 5.1, immediately after illumination (which occurs at time zero) the PDSC exotherm curve increases sharply as active centers are photochemically produced and begin to propagate with the epoxide groups of the monomer. During this initial portion of the curve, rate of polymerization increases

70

largely because the concentration of active cationic centers is increasing. The plot of heat released soon reaches a maximum, and then declines as the monomer concentration is reduced by polymerization. Eventually the reaction rate goes to zero and the curve flattens out. It is important to note that the reaction rate may become zero even though both active centers and unreacted epoxide groups remain in the sample. The vitrification phenomenon occurs because the reactive groups do not have enough mobility to find and react with one another. The PDSC exotherm curve was mathematically converted to the rate of polymerization, R_p curve using Eq. 5.1 (Figure 5.2).
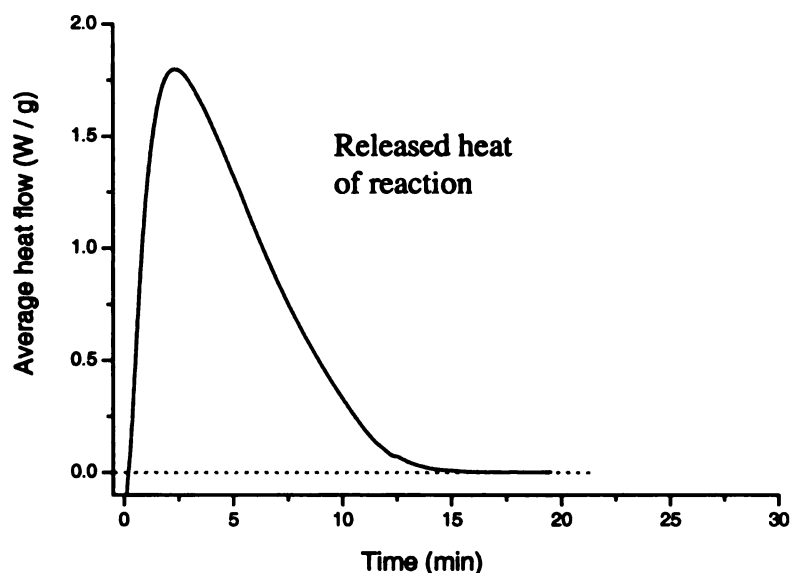
Figure 5.1. PDSC reaction exotherm for a reaction system containing di-epoxide monomer *1,4-butanediol diglycidyl ether* and 8.0 x 10^{-3} *molal* of photoinitiator *tolycumyl iodonium tetrakis (pentafluorophenyl) borate*, (B-$[F_5]_4^-$) at 50°C.
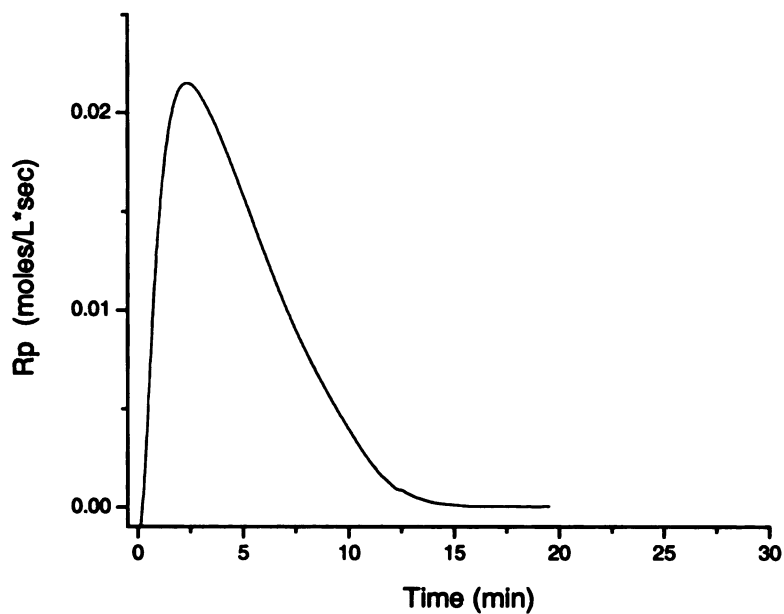
Figure 5.2. A profile of the rate of polymerization, R_p, for a reaction system containing di-epoxide monomer *1,4-butanediol diglycidyl ether* and 8.0 x 10^{-3} *molal* of photoinitiator *tolycumyl iodonium tetrakis (pentafluorophenyl) borate*, $(B^-[F_5]_4^-)$ at 50°C.

5.1.3.1b. Conversion by Photopolymerization

The concentration of epoxide groups at a given time, [M], and the epoxide conversion can be computed from the integral of the reaction rate as a function of time. Therefore, the instantaneous concentration of epoxide groups may be obtained from the PDSC profiles using the following equations:

$$[M] = [M_o] - \left(\frac{exotherm\ area(J/g) \cdot \rho}{\Delta H_p} \right) \tag{5.2}$$

$$Conversion = \left(\frac{exotherm\ area\,(J/g) \cdot \rho}{\Delta H_p \cdot [M_o]} \right) \tag{5.3}$$

where,

ΔH_p and ρ are the same as in Eq. 5.1

$$Conversion = \left(\frac{int\,egrated\ exotherm\ area \cdot Wt.}{\Delta H_p} \right) \tag{5.4}$$

where,

Wt. is weight per mole of epoxide groups, (Table 4.4)

A plot of the integrated heat of reaction is shown in Figure 5.3. A complete profile of the concentration of the epoxide groups or conversion may be calculated by determining the area under the PDSC exotherm as a function of time and applying Eq. (5.3) or Eq. (5.4). The baseline was drawn as in Figure.5.1 in order to obtain the accurate value of the total heat released from the reaction. The baseline was taken as the horizontal line that passes through the PDSC exotherm when it flattens out. Taking the integral of the exotherm curve in Figure 5.1, then dividing by the heat that would be released if all of the epoxide groups had reacted, provides a profile of the epoxide

conversion, as shown in Figure 5.4. In this figure note that the conversion reaches a flat

plateau value of the ultimate limiting conversion, and that the sample had achieved less

than 100% conversion when the reaction had stopped.
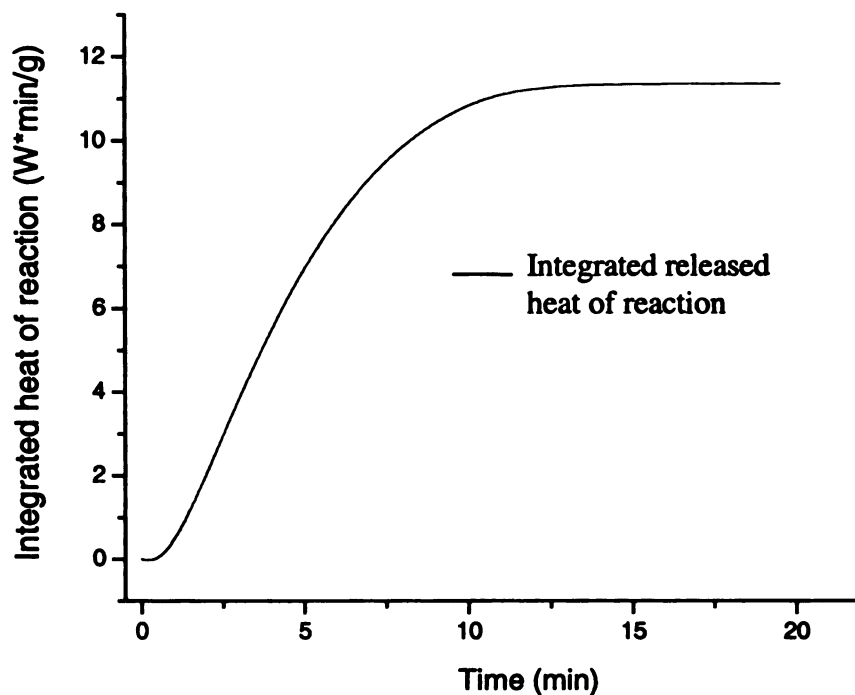
Figure 5.3. Integrated released heat of reaction for a reaction system containing di-epoxy *1,4-butanediol diglycidyl ether* and 8.0 x 10^{-3} *molal* of photoinitiator *tolycumyl iodonium tetrakis (pentafluorophenyl) borate*, $(B^-[F_5]_4^-)$ at $50^{\circ}C$.
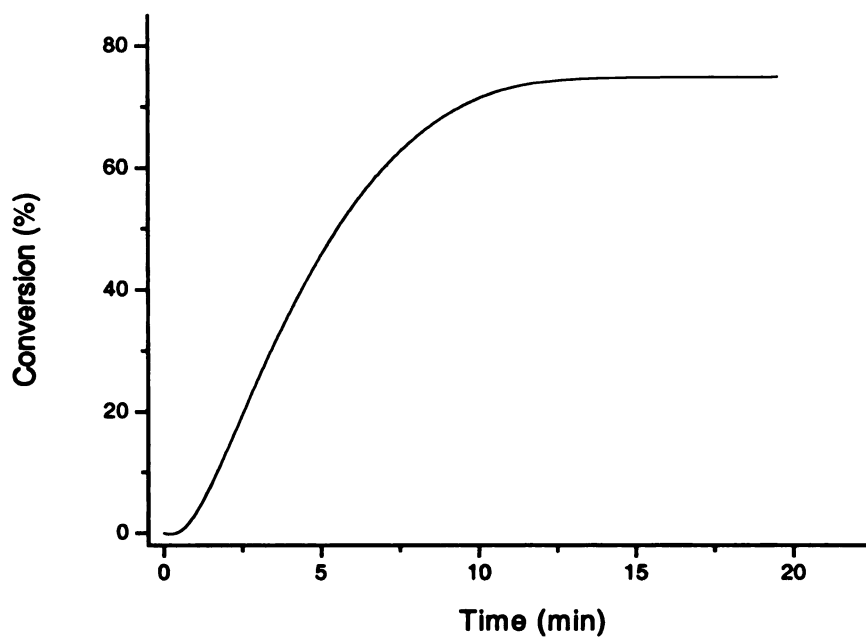
Figure 5.4. Conversion profile for the reaction system containing di-epoxy *1,4-butanediol diglycidyl ether* and 8.0 x 10^{-3} *molal* of photoinitiator *tolycumyl iodonium tetrakis pentafluorophenyl borate*, $(B^-[F_5]_4^-)$ at 50°C.

5.1.3.1c. Propagation Rate Constant

According to standard kinetic analysis, the rate of polymerization R_p is equal to the product of the propagation rate constant, k_p, multiplied by the concentration of the active centers, $[M^+]$, and concentration of the epoxide groups, $[M]$, as shown below:

$$R_p = \frac{d[M]}{dt} = k_p[M][M^+] \tag{5.5}$$

$$k_p[M^+] = \frac{R_p}{[M]} \tag{5.6}$$

Therefore, the quantity $k_p[M^+]$ can be calculated for each PDSC exotherm as shown in Figure 5.5 below. In this figure, $k_p[M^+]$ initially increases sharply and reaches a plateau value. It remains relatively constant and then begins to level off and finally decreases rapidly as the limiting conversion is reached. The shape of the profile of $k_p[M^+]$ is determined by two factors that may both be changing as the reaction proceeds: the concentration of active centers $[M^+]$ and the propagation rate constant k_p. One possible reason for a change in the effective propagation constant, k_p, for cationic photopolymerizations is a change in the reactivity of the active centers due to the proximity of the counterion. In the early stage of the reaction, polymerization leads to a large local increase in viscosity that causes reduction diffusional mobility. The active centers retains considerable mobility through propagation because they can effectively moves through the reaction mixture by reacting with new monomers. This type of mobility has been named "reaction diffusion" and may become the dominant mechanism for mobility of the active center in highly crosslinked polymerizations.[1-6] However, the bulky pentafluorophenyl borate counterion experiences a decrease in mobility as the viscosity increases. As a result, the counterion and the active center become separated,

and since separated ions are orders of magnitude more reactive than ion pairs,[17] this would lead to a large increase in the propagation rate constant, k_p. This type "reaction diffusion" is a prominent feature in the reaction kinetics of highly crosslinked free radical systems.[1-6]
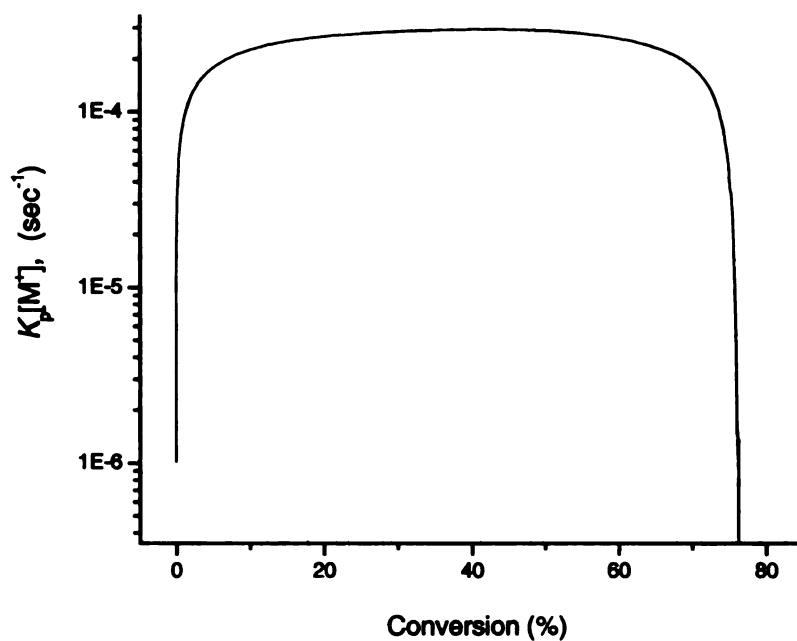
Figure 5.5. Profile of $k_p[M^+]$ for a reaction system containing di-epoxide monomer *1,4-butanediol diglycidyl ether* and 8.0 x 10^{-3} *molal* of photoinitiator *tolycumyl iodonium tetrakis pentafluorophenyl borate*, $(B^-[F_5]_4^-)$ and 8.0 x 10^{-4} *molal* photosenstizer CPTX at $50°C$.

5.1.4. Results and Discussion

5.1.4.1. Effect of Temperature on the Cationic Photopolymerization Kinetics for Systems with no Photosensitizers.

Reactions were carried out at a series of temperatures from 30, 40 to 50°C. The PDSC profiles of the rate of polymerization for cationic polymerization of mono-epoxide monomer octyl glycidyl ether, photoinitiated by 8.0×10^{-3} molal of tolycumyl iodonium tetrakis pentafluorophenyl borate, $B^-[F_5]_4^-$, are shown in Figure 5.6. The figure illustrates that, as expected, the rate of polymerization, R_p, and total conversion (Figures 5.6 and 5.7) increase with increasing temperature. This is evident from the fact that the exotherms reach the maximum rate in a shorter time and also exhibit a larger integrated heat value as the temperature is increased (recall that the integrated heat released by the reaction is directly proportional to the total conversion). Figures 5.8 and 5.9 illustrate the temperature effects of the same photoinitiator for di-epoxide monomer 1,4-butanediol diglycidyl ether, while the corresponding plots for this initiator in the tri-epoxide monomer trimethyol propane triglycidyl ether are shown in Figure 5.10 and 5.11. In each of these monomers, the same general trend for the effect of temperature is observed. As illustrated in Figures 5.12 and 5.13, the conversion value at the peak maximum of the rate of polymerization, R_p, is shifted to the right as the temperature is increased. This observation further confirms the significant effect of reaction temperature on the rate of polymerization, R_p, and the conversion of monomer. The temperature effects were also observed in reaction mixtures containing a photosensitizer as discussed in the section 5.1.4.5.
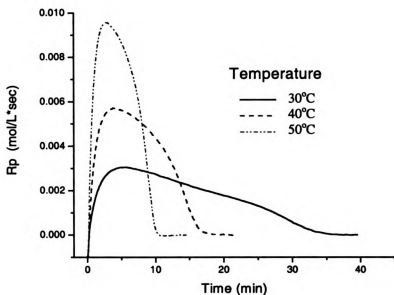
Figure 5.6. Reaction rates for cationic photopolymerization of monoepoxy *octyl glycidyl eter* and 8.0 x 10^{-3} *molal* of photoinitiator *tolycumyl iodoniumetrakis pentafluorophenyl borate*,($[F_5]_4^-$) at various temperatures.
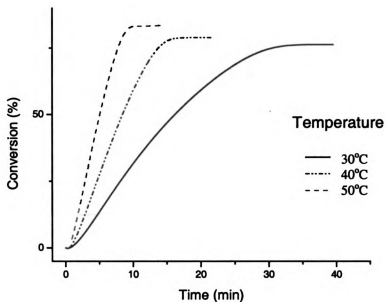
Figure 5.7. Effect of temperature on conversion for cationic photopolymerization of *octyl glycidyl ether* in the same reaction systems as *Figure 5.6*.
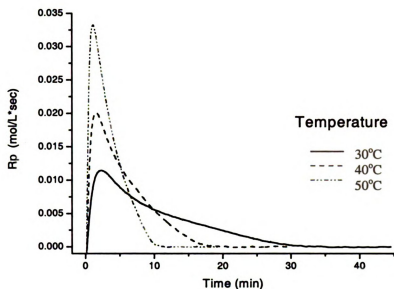
Figure 5.8. Reaction rates for cationic photopolymerization of *1,4-butanediol diglycidyl ether* and 8.0 x 10^{-3} *molal* of photoinitiator *tolycumyl iodonium tetrakis pentafluorophenyl borate,*---B$^-$[F$_5$]$_4^-$ at various temperatures.
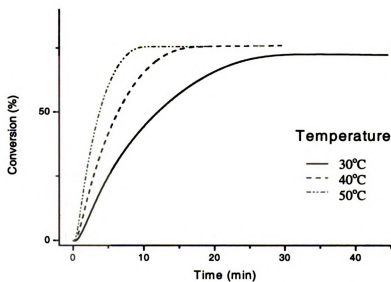

Figure 5.9. Effect of temperature on total conversion for cationic photopolymerization of *1,4-butanediol diglycidyl ether* in the same reaction systems as in *Figure 5.8.*
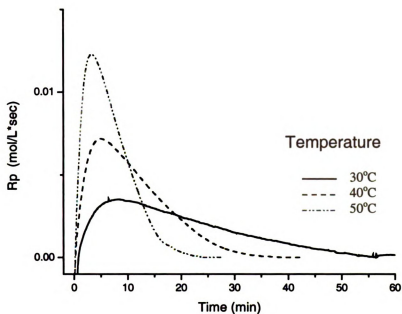
Figure 5.10. Rates of polymerization for cationic photopolymerization of tri-epoxide monomer *trimethyol propane triglycidyl ether* with 8.0 x 10^{-3} *molal* of *tolycumyl iodonium tetrakis pentafluorophenyl borate*,---B$^-$[F$_5$]$_4^-$ at various temperatures.
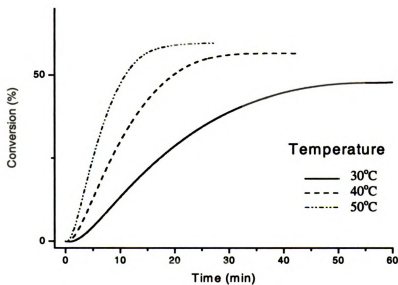
Figure 5.11. Effect of temperature on total conversion for cationic photopolymerization of the same reaction systems as in *Figure 5.10*.
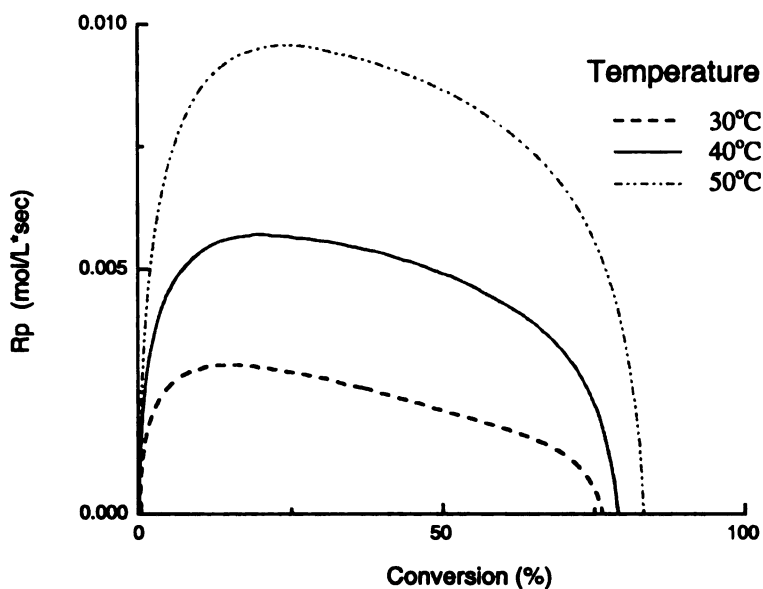
Figure 5.12. Profile of reaction rate vs. conversion for the reaction — of mono-epoxy *octyl glycidyl ether* and 8.0 x 10^{-3} *molal* of photoinitiator *tolycumyl iodonium tetrakis pentafluorophenyl borate* at various temperatures.
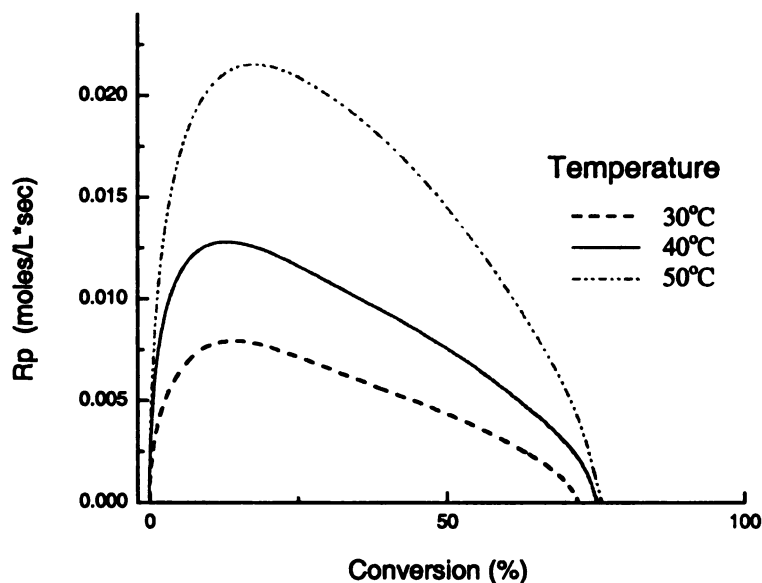
Figure 5.13. Profiles of reaction rate vs. conversion for the reaction systems of di-epoxy *1,4-butanediol glycidyl ether* and 8.0 x 10^{-3} *molal* of photoinitiator *tolycumyl iodonium tetrakis pentafluorophenyl borate* at various temperatures.

5.1.4.2. Effect of Light Intensity on the Cationic Photopolymerization Kinetics

PDSC experiments were also performed to elucidate the effect of the initiating light intensity on the photopolymerization kinetics. Figures 5.14–5.15 show the reaction rates and conversion profiles of octyl glycidyl ether photoinitiated by the photoinitiator diaryliodonium hexafluoroantimonate in an isothermal polymerization at temperature of 50°C with the light intensity varying from 35 mW/cm^2 to 90 mW/cm^2. A similar set of studies for the di-epoxide monomer 1,4-butanediol diglycidyl ether are shown in Figures 5.14–5.15. Based on the results observed from the two reaction systems, it is evident that as the light intensity is increased, the rate of polymerization is observed to increase. In addition, the total conversion was found to exhibit a small increase with increasing light intensity. It appeared that with the photoinitiator concentration at 8.0 x 10^{-3} molal and light intensity at 52 mW/cm^2, the total conversion of both mono-epoxide and di-epoxide monomers had closely reached its limiting point. Table 5.1 gives a result summary for these two reaction systems.

Table 5.1. Summary of the effects of incident light intensity on the rates of polymerization and conversions for two representative reaction systems. The photoinitiator was *diaryliodonium hexafluoroantimonate* at 8.0 x 10^{-3} *molal*.

Epoxide monomer	Light intensity (mW/ cm^2)	Peak time (min)	Peak rate of polymerization (mol/L*sec)	Total conversion (%)
Octyl glycidyl ether	35	2.26 ± 0.10	0.009 ± 0.001	80.01 ± 1.07
	52	1.37 ± 0.03	0.015 ± 0.001	82.60 ± 1.05
	90	0.78 ± 0.04	0.023 ± 0.001	82.94 ± 1.12
1,4-butanediol diglycidyl ether	50	1.31 ± 0.01	0.028 ± 0.002	74.95 ± 1.58
	74	0.82 ± 0.03	0.052 ± 0.001	76.60 ± 0.20
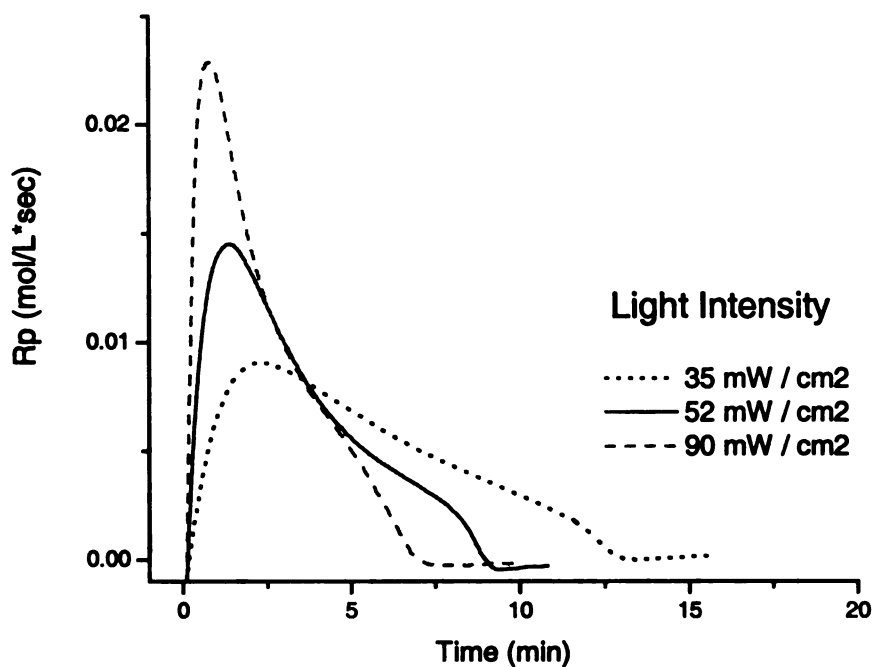
Figure 5.14. Effects of light intensity for cationic polymerization of *octyl glycidyl ether* photoinitiated by 8.0 x 10^{-3} *molal* of *diaryliodonium hexafluoroantimonate* at 50°C.
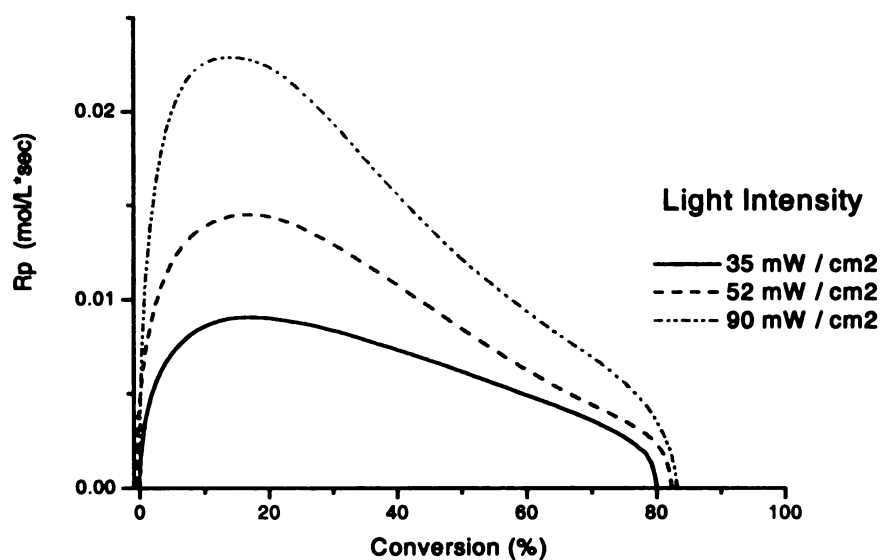
Figure 5.15. Effects of light intensity on both reaction rates and conversions for cationic photopolymerization of *octyl glycidyl ether* photoinitiated by 8.0 x 10^{-3} *molal* of *diaryliodonium hexafluoroantimonate* at 50°C.
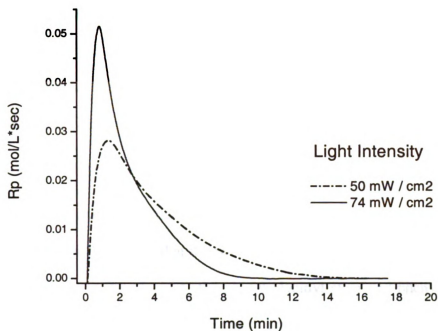
Figure 5.16. Rates of polymerization for cationic photopolymerization of *1,4-butanediol diglycidyl ether* at different initiation light intensities by 8.0 x 10^{-3} *molal* of photoinitiator *diaryliodonium hexafluoroantimonate* at 50°C.
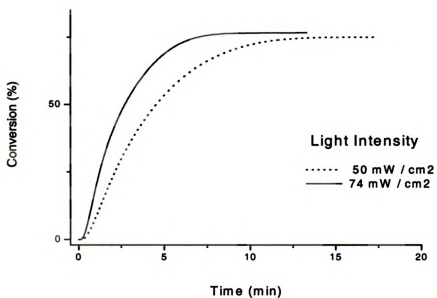
Figure 5.17. Effects of light intensity on conversion profiles for cationic photopolymerization of di-epoxide monomer *1,4-butanediol diglycidyl ether* by 8.0 x 10^{-3} *molal* of photoinitiator *diaryliodonium hexafluoroantimonate* at 50°C.

5.1.4.3. Effect of Different Photoinitiators on Cationic Photopolymerization Kinetics

To investigate the effect of the photoinitator on the photopolymerization kinetics, PDSC experiments were performed using three different photoinitiators. The two iodonium salts with different counterions were: 1) tolycumyl iodonium tetrakis pentafluorophenyl borate, $B^-[F_5]_4^-$; 2) diaryliodonium hexafluoroantimonate, $[SbF_6]^-$. The third photoinitiator was triarylsulfonium hexafluorophosphate, $[PF_6]^-$. Figures 5.18 through 5.23 show the effects that the two iodonium salts have on three different mono-epoxide monomers: octyl glycidyl ether, butyl glycidyl ether and phenyl glycidyl ether. Similar curves for the di-epoxide monomers are shown in Figures 5.24 through 5.27. These reactions were run isothermally at 50°C and constant light intensity of about 52 mW/cm². The effect of the photoinitiator on the polymerization kinetics were relatively subtle and small, however, in all three cases, the rate of polymerzation, R_p, with the diaryliodonium hexafluoroantimonate was a little faster than that with the tolycumyl iodonium tetrakis pentafluorophenyl borate.

Compared to the iodonium salts, the triarylsulfonium salt exhibited a considerable slower rate of polymerization and lower conversion. As illustrated by the data in Table 5.2, the triarylsulfonium hexafluorophosphate initiator exhibited low conversions and comparable polymerization rates even with relatively high initiator concentrations (16.0×10^{-3} molal) and high light intensity (90 mW/cm²).

Table 5.2. Effect of different photoinitiators on reaction rates (R_p) of cationic photopolymerization for various reaction systems at 50°C.

Photoinitiator & concentration	Light intensity	Phenyl glycidyl ether		1,4-butanediol diglycidyl ether		Trimethyol propane triglycidyl ether	
		Peak R_p	% Conv.	Peak R_p	% Conv.	Peak R_p	% Conv.
0.008 *molal* Initiator **A**	52 ± 0.2	0.024 ± 0.001	94.0 ± 0.8	0.022 ± 0.001	76.3 ± 1.1	0.012 ± 0.001	59.6 ± 1.2
0.008 *molal* Initiator **B**	53 ± 0.1	0.018 ± 0.001	98.4 ± 0.9	0.028 ± 0.002	74.6 ± 2.7	0.012 ± 0.001	59.4 ± 0.5
0.016 *molal* Initiator **C**	90 ± 0.1	0.041 ± 0.002	94.4 ± 1.9	0.137 ± 0.006	72.2 ± 0.8	0.040 ± 0.001	49.5 ± 0.6

Note: **A** = tolycumyl iodonium tetrakis pentafluorophenyl borate, B-$[F_5]_4^-$

B = diaryliodonium hexafluoroantimonate, $[SbF_6]^-$

C = triarylsulfonium hexafluorophosphate, $[PF_6]^-$
R_p in moles/L*sec
Light intensity in mW/cm^2
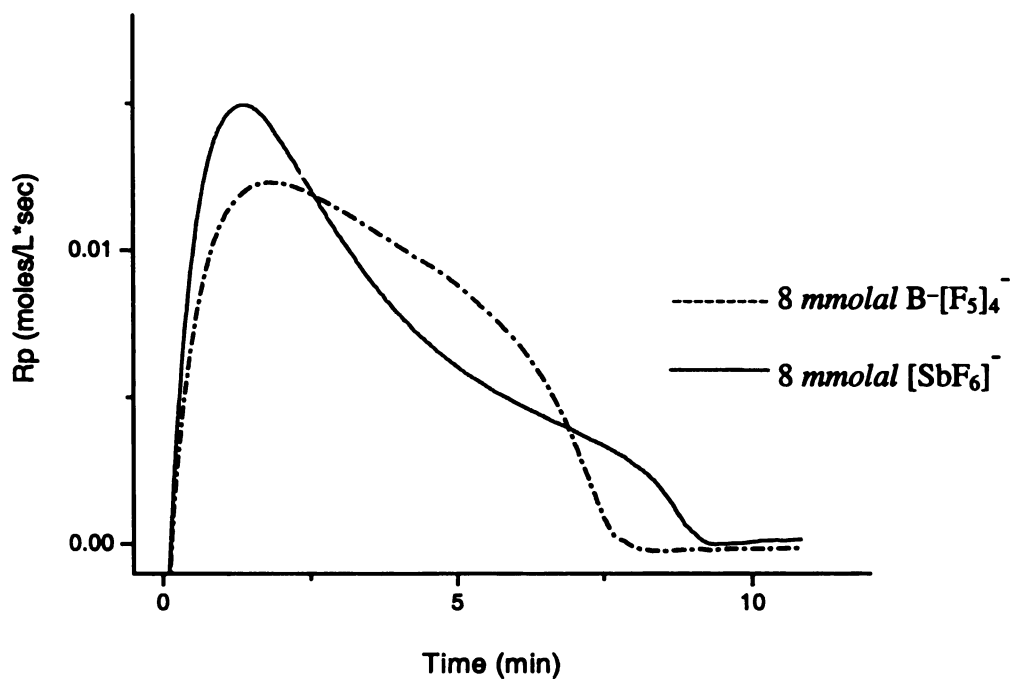
Figure 5.18. Effect of photoinitiators *tolylcumyl iodonium tetrakis pentafluorophenyl borate*, B-[F$_5$]$_4^-$; and *diaryliodonium hexafluoroantimonate*, [SbF$_6$]$^-$ for mono-epoxy *octyl glycidyl ether* at 50°C.
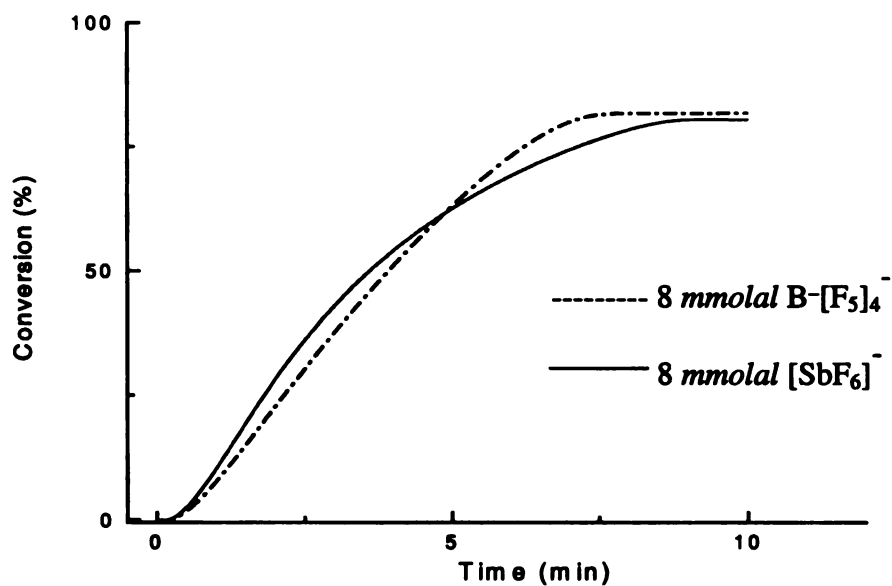
Figure 5.19. Effect of photoinitiators on conversion profiles in the same reaction systems as in *Figure 5.18*.
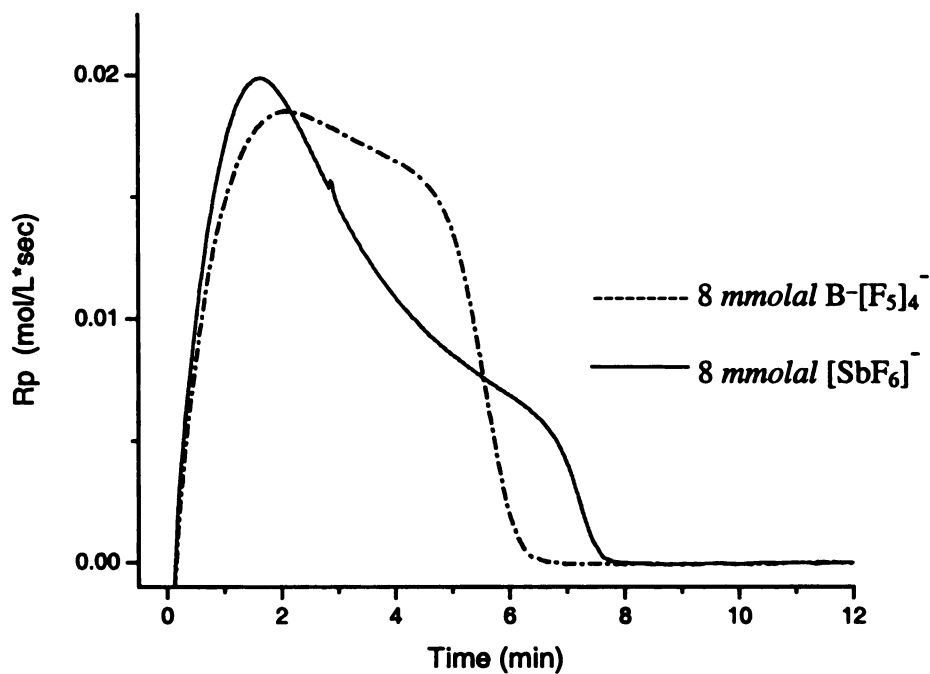
Figure 5.20. Effect of photoinitiators *tolylcumyl iodonium tetrakis pentafluorophenyl borate*, B-[F₅]₄⁻; and *diaryliodonium hexafluoroantimonate*, [SbF₆]⁻ for mono-epoxy *butyl glycidyl ether* at 50°C.
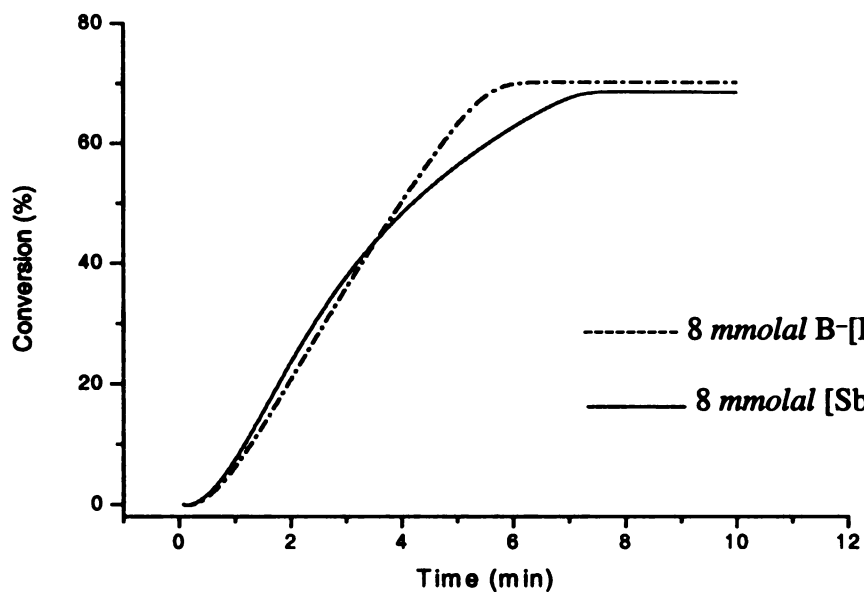
Figure 5.21. Effect of photoinitiators on conversion profiles in the same reaction systems as in *Figure 5.20*.
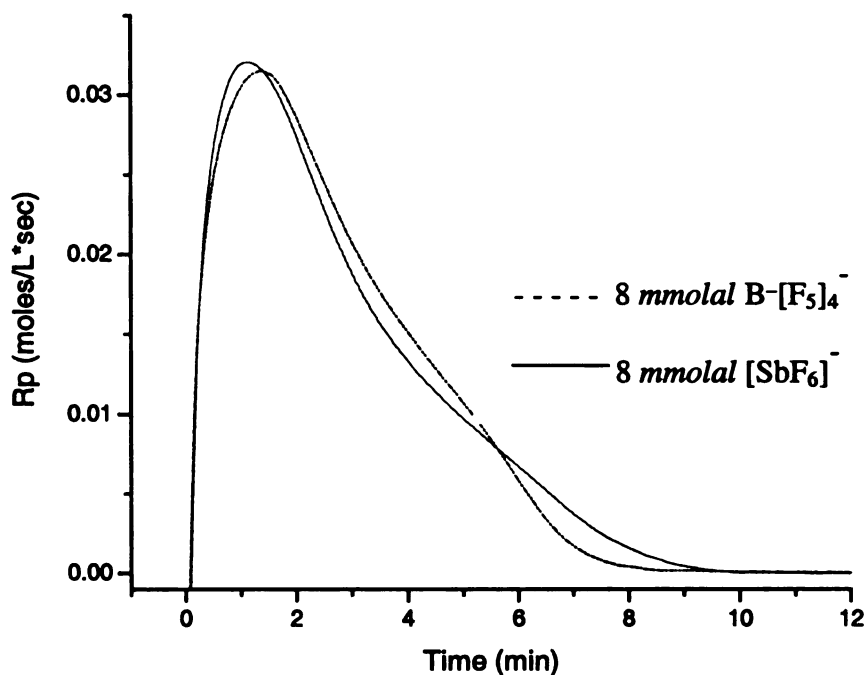
Figure 5.22. Effect of photoinitiators *tolylcumyl iodonium tetrakis pentafluorophenyl borate*, B-[F$_5$]$_4^-$; and *diaryliodonium hexafluoroantimonate*, [SbF$_6$]$^-$ for mono-epoxy *phenyl glycidyl ether* at 50°C.
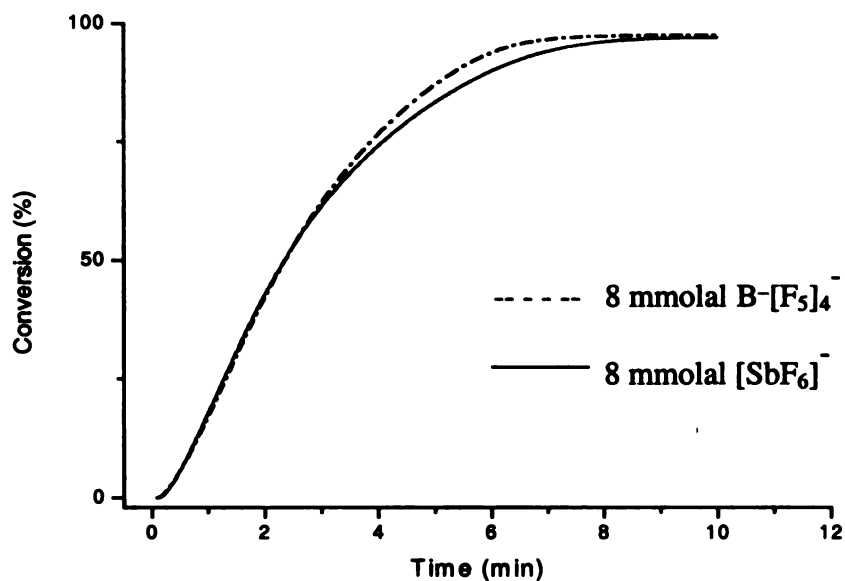
Figure 5.23. Effects of photoinitiators on conversion profiles in the same reaction systems as in *Figure 5.22*.
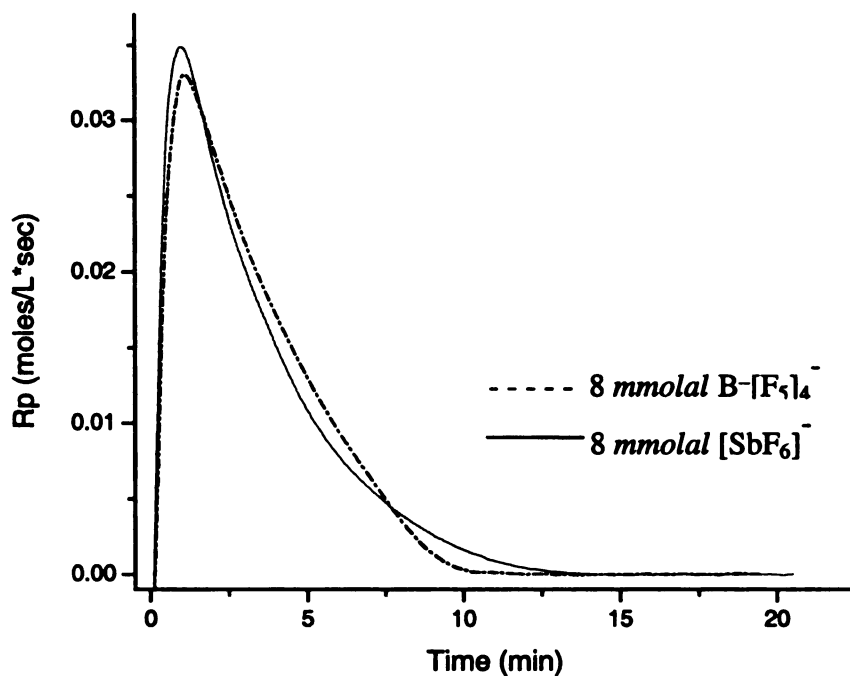
Figure 5.24. Effects of photoinitiators *tolylcumyl iodonium tetrakis (pentafluorophenyl) borate*, B-[F₅]₄⁻; and *diaryliodonium hexafluoroantimonate*, [SbF₆]⁻ for di-epoxide monomer *1,4-butanediol diglycidyl ether* at 50°C.
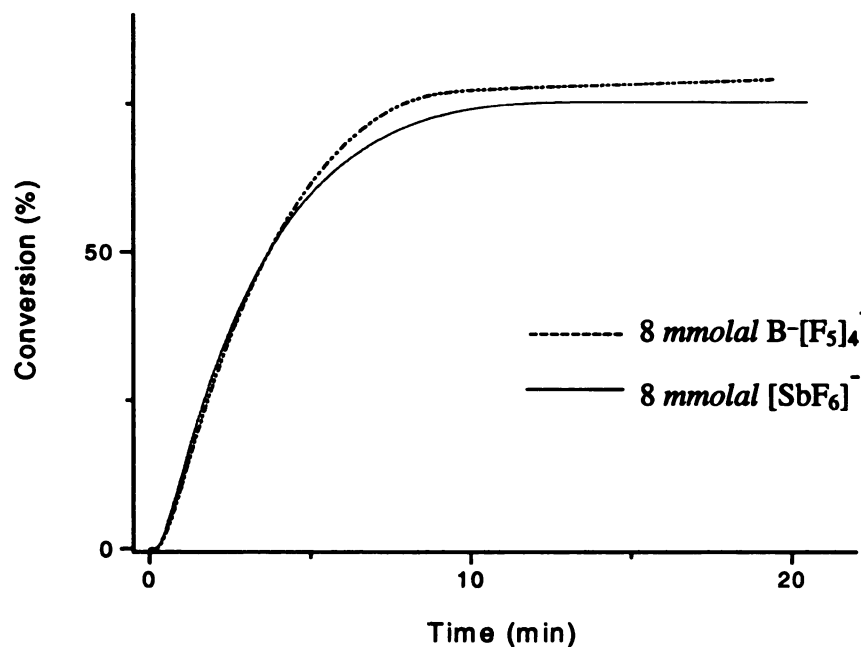
Figure 5.25. Effect of photoinitiators on conversion profiles in the same reaction systems as in *Figure 5.24*.
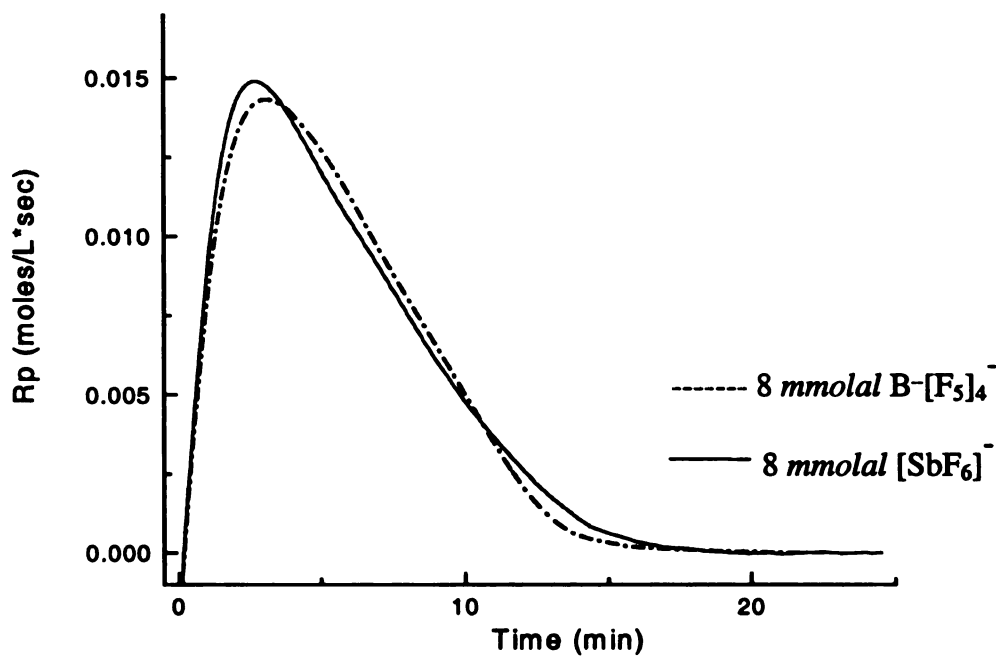
Figure 5.26. Effect of photoinitiators *tolylcumyl iodonium tetrakis (pentafluorophenyl) borate*, B-[F₅]₄⁻; and *diaryliodonium hexafluoroantimonate*, [SbF₆]⁻ for di-epoxide monomer *cyclohexane dimethanol diglycidyl ether* at 50°C.
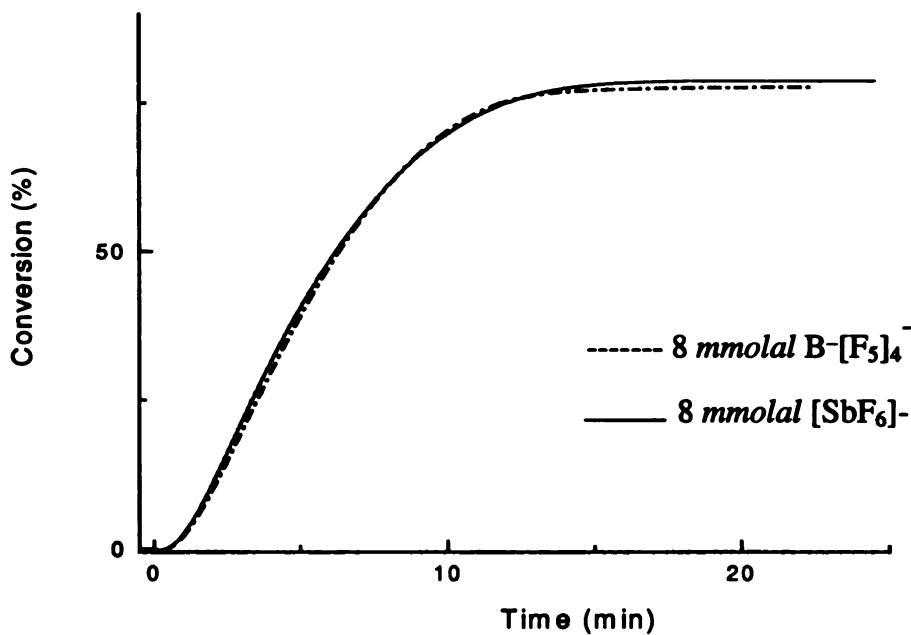
Figure 5.27. Effect of photoinitiators on conversion profiles in the same reaction systems as in *Figure 5.26*.

5.1.4.3. Effect of Photoinitiator Concentration on the Photopolymerization Kinetics

In addition to temperature, the effect of the photoinitiator concentration on the rate of polymerization was investigated. All the reactions were run under isothermal conditions at 50°C with various concentrations of the photoinitiator. Figures 5.28 through 5.32 illustrate the effects of the concentration of two different iodonium photoinitiators (tolycumyl iodonium tetrakis pentafluorophenyl borate and diaryliodonium hexafluoroantimonate) on the cationic polymerization kinetics for the mono-epoxide monomer butyl glycidyl ether. For both photoinitiators, the polymerization kinetics exhibit a large increase in reaction rate and conversion as the initiator concentration is increased from 2.0×10^{-3} to 4.0×10^{-3} and to 8.0×10^{-3} molal. Further increase of initiator concentration to 10.0×10^{-3}, 12.0×10^{-3} and 16.0×10^{-3} molal only produced a small increase in reaction rates and improved very little with respect to conversions. Similar effects were observed in the case with the di-epoxide monomer 1,4-butanediol diglycidyl ether using the same reaction conditions (Figures 5.34 to 5.39). Therefore, the photoinitiator concentration of 8.0×10^{-3} molal was chosen as the concentration to be used in other reaction systems. This choice would allow for the quantitative comparison among different reaction systems and would also prevent potential solubility problems. Tables 5.4 through 5.7 provide the result summary for the effects of photoinitiator concentration on the cationic photopolymerization kinetics.

Table 5.4. Concentration effects of photoinitiator *diaryliodonium hexafluoro-antimonate* on reaction rates and conversions of monoepoxy *butyl glycidyl ether* at 50°C

Concentration	Peak time (min)	Peak height (mol/L•sec)	% conversion
2.0×10^{-3}	2.05 ± 0.05	0.0074 ± 0.0003	48.2 ± 1.0
4.0×10^{-3}	1.72 ± 0.02	0.0144 ± 0.0004	62.3 ± 1.4

8.0×10^{-3}	1.63 ± 0.09	0.0224 ± 0.0005	71.1 ± 4.0
12.0×10^{-3}	1.62 ± 0.07	0.0235 ± 0.0007	70.7 ± 0.9
16.0×10^{-3}	1.62 ± 0.04	0.0253 ± 0.0006	72.0 ± 2.0

Table 5.5. Concentration effects of photoinitiator *tolycumyl iodonium tetrakis pentafluorophenyl borate* on reaction rates and conversions of mono-epoxy *butyl glycidyl ether* at 50°C.

Concentration	Peak time (min)	Peak height (mol/L•sec)	% conversion
2.0×10^{-3}	2.34 ± 0.13	0.0065 ± 0.0003	57.2 ± 3.4
4.0×10^{-3}	2.31 ± 0.14	0.0106 ± 0.0007	64.5 ± 1.9
8.0×10^{-3}	2.11 ± 0.01	0.0161 ± 0.0002	69.0 ± 0.2
12.0×10^{-3}	2.07 ± 0.08	0.0183 ± 0.0011	67.5 ± 3.1
16.0×10^{-3}	1.93 ± 0.07	0.0213 ± 0.0005	69.7 ± 1.1

Table 5.6. Concentration effects of photoinitiator *diaryliodonium hexafluoro-antimonate* on reaction rates and conversions of di-epoxy *1,4-butanediol diglycidyl ether* at 50°C.

Concentration	Peak time (min)	Peak height (mol/L•sec)	% conversion
2.0×10^{-3}	1.04 ± 0.08	0.026448 ± 0.0014	71.2 ± 2.9
4.0×10^{-3}	1.06 ± 0.06	0.033048 ± 0.0014	73.9 ± 1.3
8.0×10^{-3}	0.91 ± 0.04	0.040756 ± 0.0003	74.1 ± 1.2
12.0×10^{-3}	0.98 ± 0.14	0.038819 ± 0.0002	74.9 ± 0.1
16.0×10^{-3}	1.08 ± 0.02	0.039257 ± 0.0010	74.9 ± 1.1

Table 5.7. Concentration effects of photoinitiator *tolycumyl iodonium tetrakis pentafluorophenyl borate* on reaction rates and conversions of di-epoxy *1,4-butanediol diglycidyl ether* at 50°C.

Concentration	Peak time (min)	Peak height (mol/L•sec)	% conversion
2.0×10^{-3}	1.45 ± 0.05	0.0186 ± 0.0003	73.2 ± 0.4
4.0×10^{-3}	1.37 ± 0.02	0.0256 ± 0.0005	73.9 ± 0.7
8.0×10^{-3}	1.10 ± 0.02	0.0330 ± 0.0002	75.5 ± 0.3
12.0×10^{-3}	1.07 ± 0.04	0.0353 ± 0.0003	74.5 ± 0.3
16.0×10^{-3}	1.10 ± 0.02	0.0383 ± 0.0007	74.6 ± 0.3
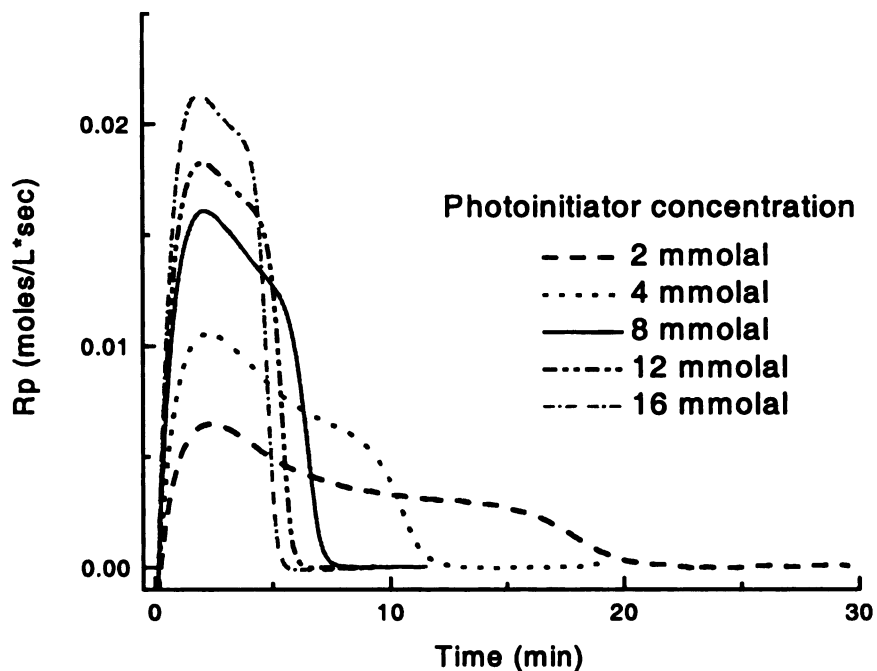
Figure 5.28. Concentration effect of photoinitiator *tolycumyl iodonium tetrakis (pentafluorophenyl) borate*, B-[F5]4⁻ on mono-epoxy *butyl glycidyl ether* at 50°C.
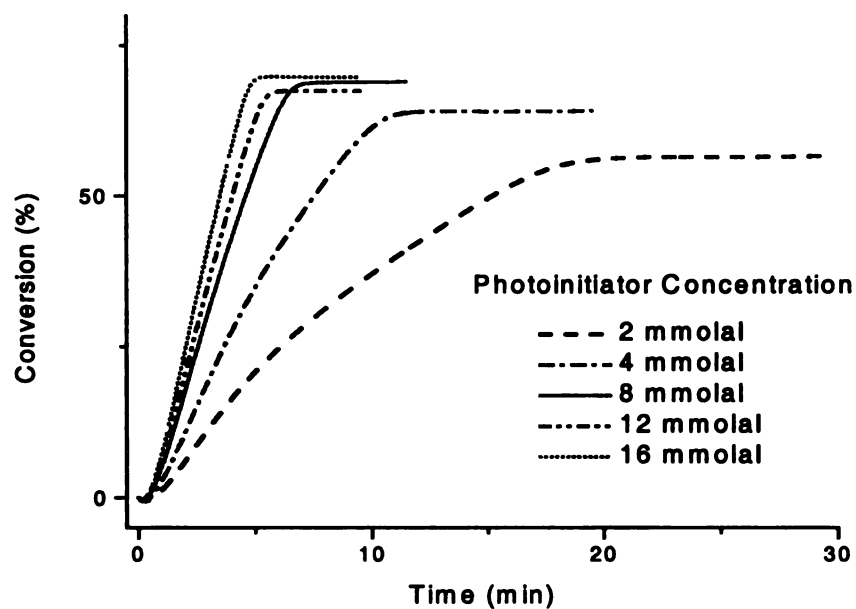
Figure 5.29. Effects of photoinitiator concentration on conversion in systems comprising of mono-epoxy *butyl glycidyl ether* and photoinitiator *tolycumyl iodonium tetrakis pentafluorophenyl borate*, B-[F5]4⁻ at 50°C.
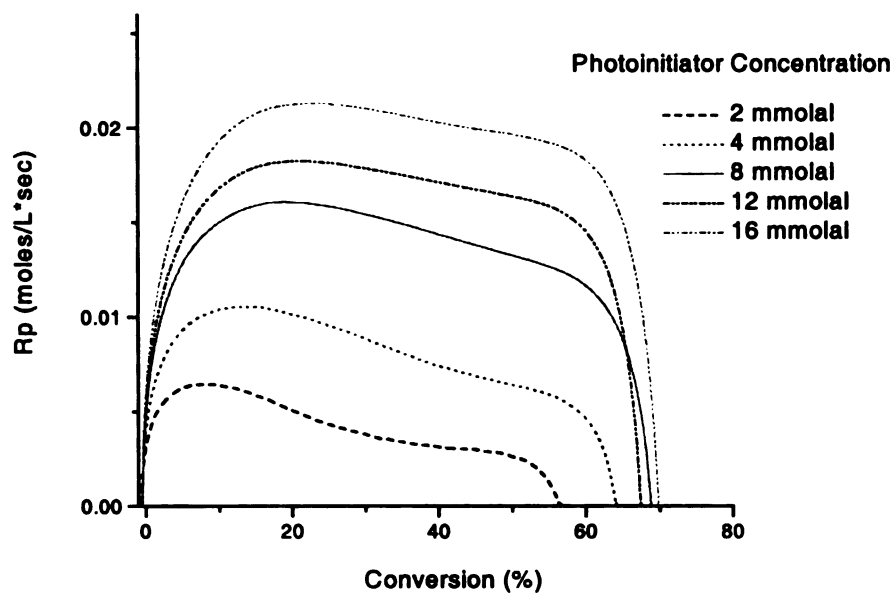
Figure 5.30. Profiles of the rate of polymerization, R_p, versus conversion for mono-epoxy *butyl glycidyl ether* with various concentrations of photoinitiator *tolycumyl iodonium tetrakis pentafluorophenyl borate*, B-[F_5]$_4^-$ at 50°C.
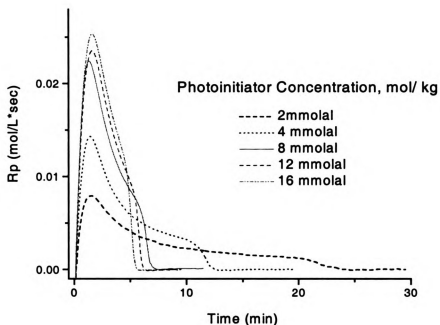
Figure 5.31. Concentration effects of photoinitiator *diaryliodonium hexafluoroantimonate*, [SbF$_6$]$^-$ on mono-epoxy *butyl glycidyl ether* at 50°C.
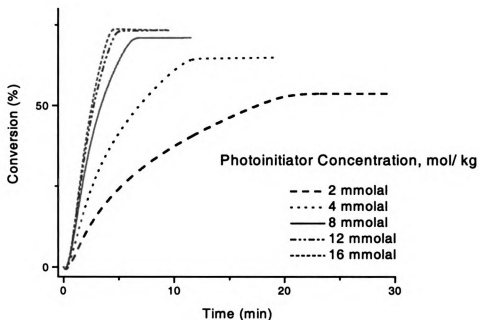
Figure 5.32. Effects of photoinitiator concentration on conversion in systems comprising of mono-epoxy *butyl glycidyl ether* and photoinitiator *diaryliodonium hexafluoro-antimonate*, [SbF$_6$]$^-$ at 50°C.
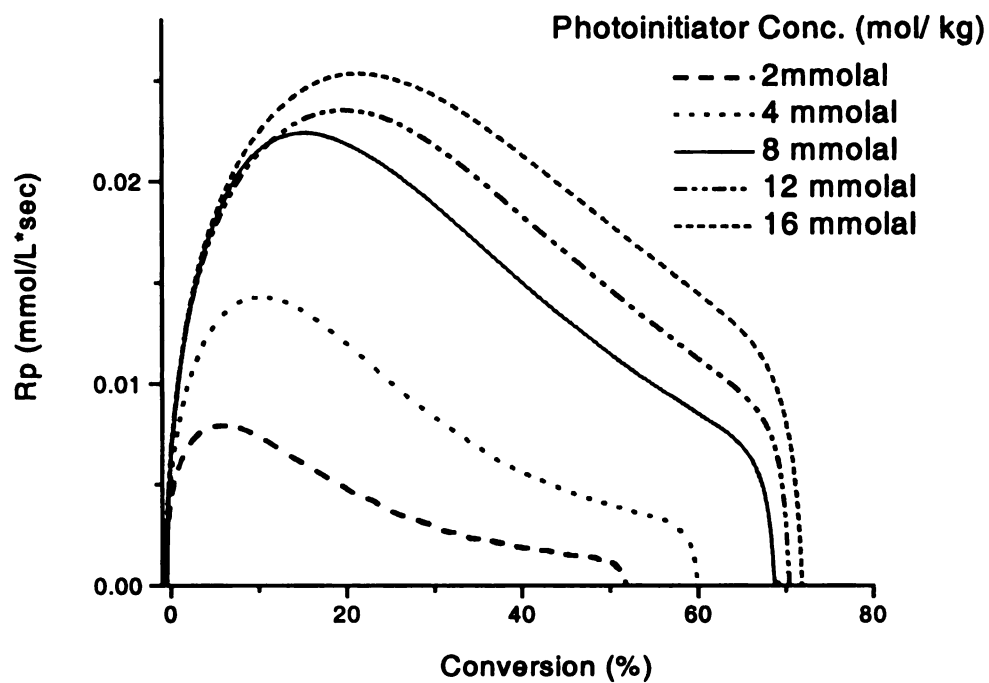
Figure 5.33. Profiles of the rate of polymerization versus conversion for mono-epoxy *butyl glycidyl ether* with various concentrations of photoinitiator *diaryliodonium hexafluoroantimonate*, [SbF₆]⁻ at 50°C.
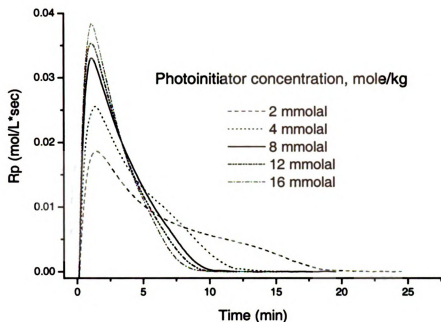
Figure 5.34. Concentration effects of photoinitiator *tolycumyl iodonium tetrakis pentafluorophenyl borate*, B⁻[F₅]₄⁻ on di-epoxy *1,4-butanediol diglycidyl ether* at 50°C.
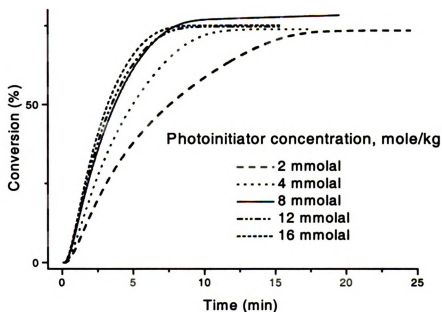
Figure 5.35. Effects of photoinitiator concentration on conversion in systems comprising of di-epoxy *1,4-butanediol diglycidyl ether* and photoinitiator *tolycumyl iodonium tetrakis pentafluorophenyl borate*, B⁻[F₅]₄⁻ at 50°C.
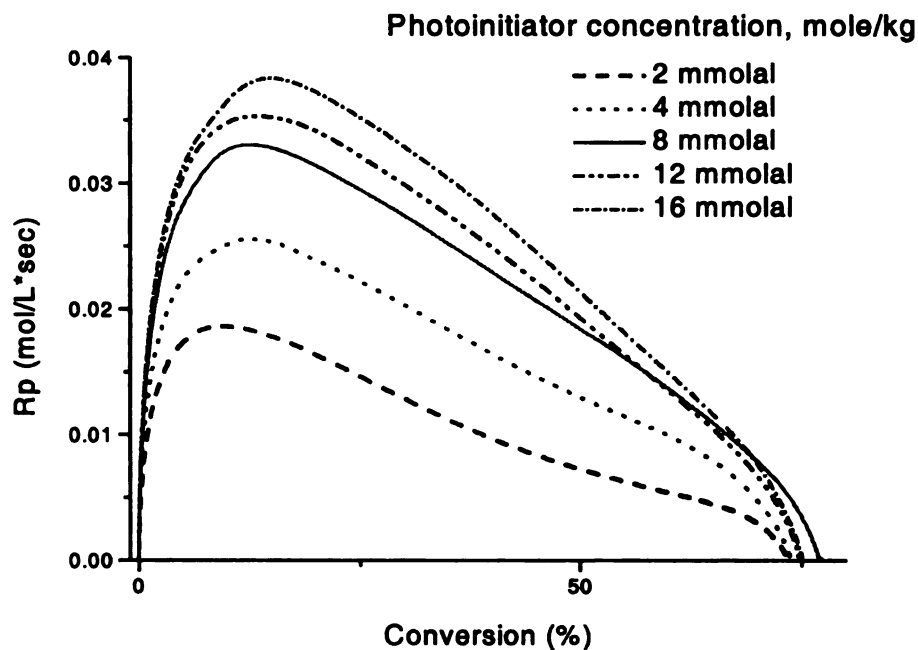
Figure 5.36. Profiles of the rate of polymerization versus conversion for di-epoxy *1,4-butanediol diglycidyl ether* with various concentrations of photoinitiator *tolycumyl iodonium tetrakis (pentafluorophenyl) borate*, B-$[F_5]_4^-$ at 50°C.

As illustrated in Figures 5.30, 5.33, 5.36 and 5.39, the rate of polymerization, R_p, and conversion increase with increasing concentration of the photoinitiator. Furthermore, the conversion value at the peak maximum is shifted to the right, which further confirms the significant effect of photoinitiator concentration on the rate of polymerization, R_p, and conversion. Since the photoinitiator is by the far the most expensive component in reactive system (typical cost is ~$40/pound), it is important to identify the optimum initiator concentration. Our studies indicate that concentrations above 8.0×10^{-3} molal provide little added benefit in terms of reaction rate and final conversion.
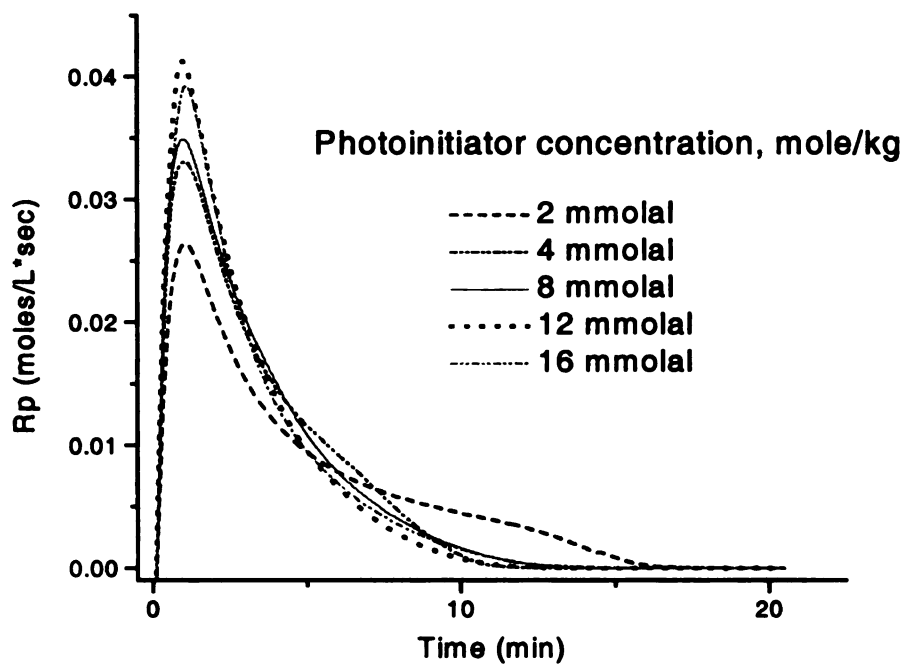
Figure 5.37. Concentration effects of photoinitiator *diaryliodonium hexaflouro-antimonate*, [SbF₆]⁻ on di-epoxy *1,4-butanediol diglycidyl ether* at 50°C.
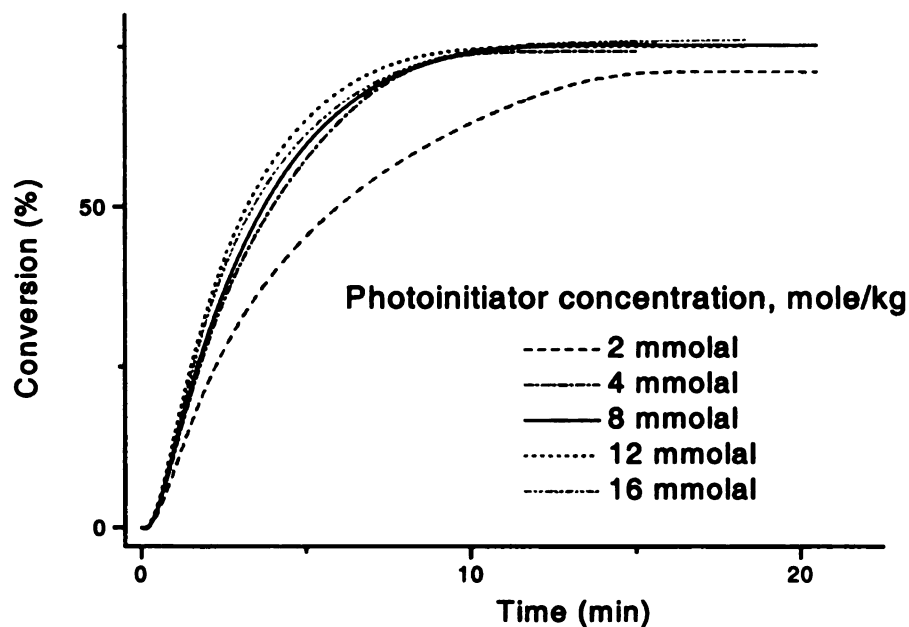
Figure 5.38. Effects of photoinitiator concentrations on conversion in reaction systems comprising of di-epoxy *1,4-butanediol diglycidyl ether* and photoinitiator *diaryliodonium hexafluoroantimonate*, [SbF₆]⁻ at 50°C.
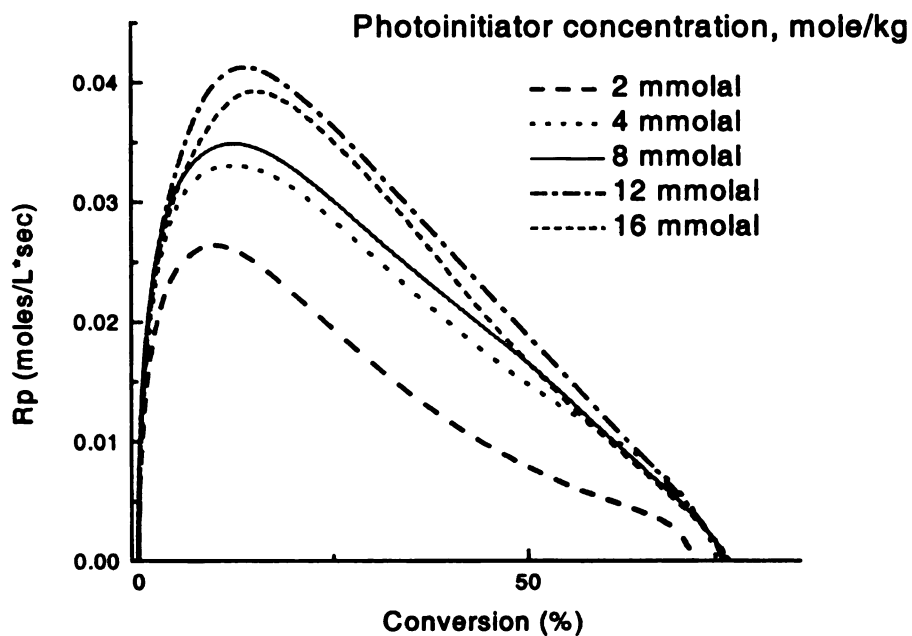
Figure 5.39. Profiles of the rate of polymerization versus conversion for di-epoxy *1,4-butanediol diglycidyl ether* with various concentrations of photoinitiator *diaryliodonium hexafluoroantimonate*, [SbF₆]⁻ at 50°C.

5.1.4.5. Effect of Photosensitizer on the Photopolymerization Kinetics

The absorption spectra of the photoinitiators (Figures 4.8-4.10) indicate their strong absorption in region below 300 nm. In order to increase their spectral sensitivity to the emission spectrum of the 200-Watt Hg/Xe arc lamp, two different photosensitizers were investigated: 1-chloro-4-propoxy-9H-thioxanthen-9-one (CPTX) and anthracene. These photosensitizers absorb strongly in the region of 310-380 nm, (Figures 4.11-4.12) and therefore may be used to shift the effective initiation wavelength to this near-UV region of the spectrum. The photosensitizers generally operate through an electron transfer mechanism in which an excited state photosensitizer molecule transfer an electron to the iodonium photoinitiator.[18,19] In this study two different photosensitizers were investigated: 1-chloro-4-propoxy-9H-thioxanthen-9-one (CPTX) and anthracene.

The addition of either photosensitizer to the reaction mixture significantly affected the rate of polymerization for the epoxide monomers, as shown in Figures 5.40 through 5.46. Specifically, Figures 5.40 and 5.41 show the temperature effect in reaction systems containing mono-epoxide octyl glycidyl ether with 8.0×10^{-4} molal of photosensitizer CPTX and 8.0×10^{-3} of photoinitiator diaryliodonium hexafluoroantimonate. In Figure 5.42 and 5.43, the photoinitiator was switched to tolycumyl iodonium tetrakis pentafluorophenyl borate. Then in Figures 5.44 and 5.47, The effects of different photosensitizers (CPTX and anthracene) were observed. In each case, the concentration of photosensitizer was 8.0×10^{-4} molal. The figures showed that the mono-epoxide octyl glycidyl ether was more reactive in the presence of CPTX than it was with anthracene, but that the addition of anthracene resulted in a higher polymerizaton rate than the photosensitizer-free system. The relatively large effect of

CPTX can be attributed to the stronger molecular absorption by the CPTX as compared to that by the anthracene (Figures 4-11 and 4-12). As a result, at the initial stage of the reaction, more CPTX molecules were photolyzed and became active to undergo electron transfer to the photoinitiator molecules, thereby setting off the initiation of the chain polymerization reactions. Although the reaction rate increases remarkably in the presence of a photosensitizer, the final limiting conversion does not increase by much (Figure 5.48). This phenomenon can be attributed to the fact that photosensitizer acts through the electron transfer process to increase the active centers available for polymerization while the final limiting conversion depends primarily on the glass transition temperature of the reacting mixture, which is determined by the molecular structure of the monomer. Tables 5.9, 5.10, 5.11 and 5.12 summarize the effects of the two photosensitizers CPTX and anthracene on polymerization rate and conversion for the three mono-epoxide monomers: butyl glycidyl ether, octyl glycidyl ether, and phenyl glycidyl ether with each photoinitiator (diaryliodonium hexafluoroantimonate or tolycumyl iodonium tetrakis pentafluorophenyl borate).

The same set of reaction conditions were then applied in the cases with the two di-epoxide monomers 1,4-butanediol diglycidyl ether and cyclohexane dimethanol diglycidyl ether, and the tri-epoxide monomer trimethyol propane. Similar results on the rate of polymerization and limiting conversion were observed. For the di-epoxide monomers, the effects on polymerization rate are illustrated in Figures 5.48 through 5.56 and the result summary for polymeization rate and conversion are presented in Tables 5.13 through 5.16. The same information for the tri-epoxide monomer trimethyol propane triglycidyl ether are found in Figures 5.57 through 5.64, and Tables 5.17 to 5.20.
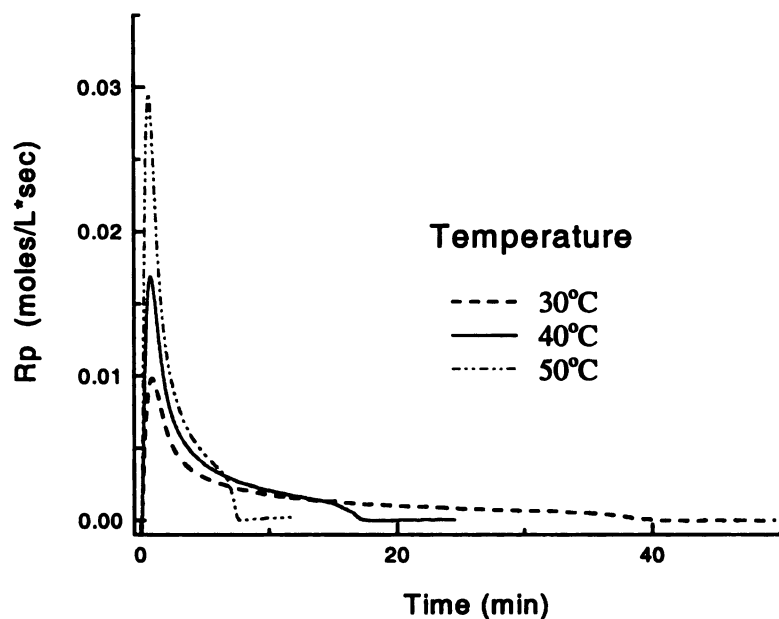
Figure 5.40. Temperature effects for reaction systems of mono-epoxy *octyl glycidyl ether* with 8.0 x 10^{-3} *molal* photoinitiator diaryliodonium hexafluoro-antimonate, [SbF$_6$]$^-$ and 8.0 x 10^{-4} *molal* photosensitizer CPTX.
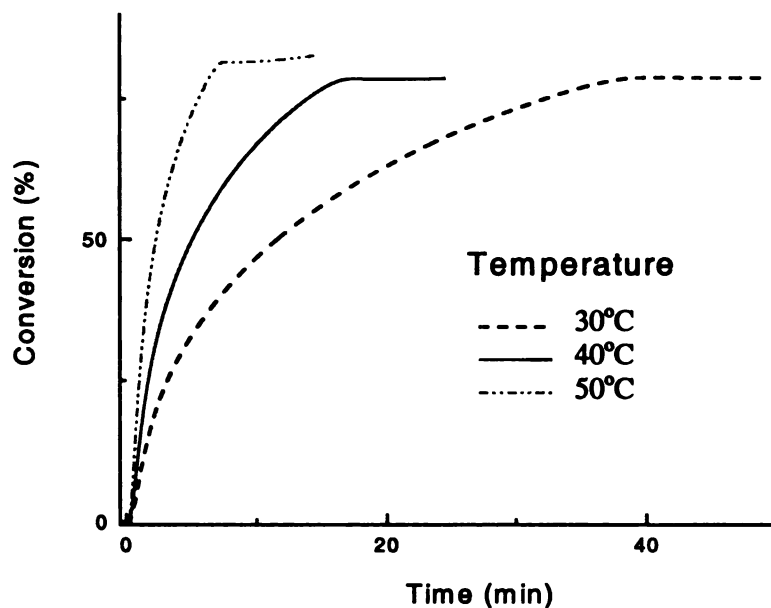
Figure 5.41. Effect of photosensitization on final conversion for the same reaction systems as in *Figure 5.40*.
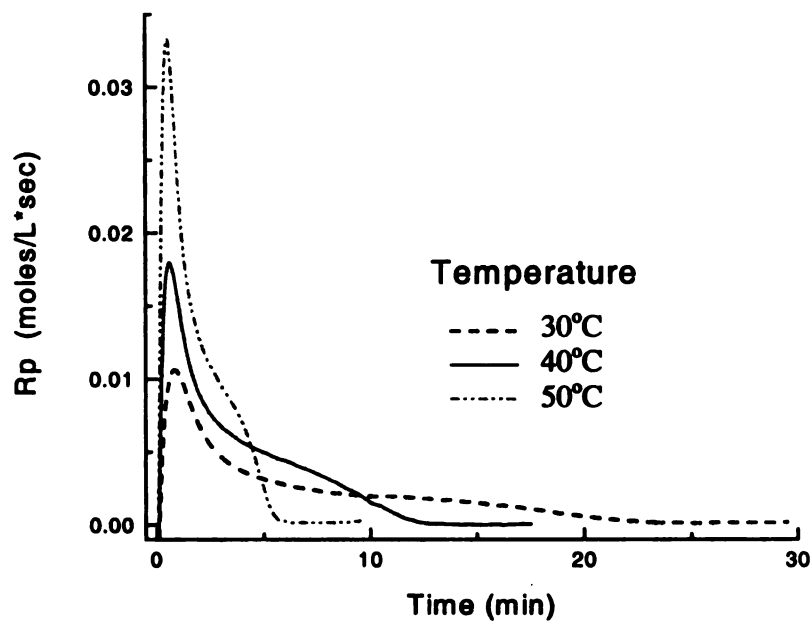
Figure 5.42. Temperature effects for reaction systems of monoepoxy *octyl glycidyl ether* with 8.0 x 10^{-3} *molal* photoinitiator *tolycumyl iodonium tetrakis pentafluorophenyl borate*, B-[F$_5$]$_4^-$ and 8.0 x 10^{-4} *molal* photosensitizer CPTX.
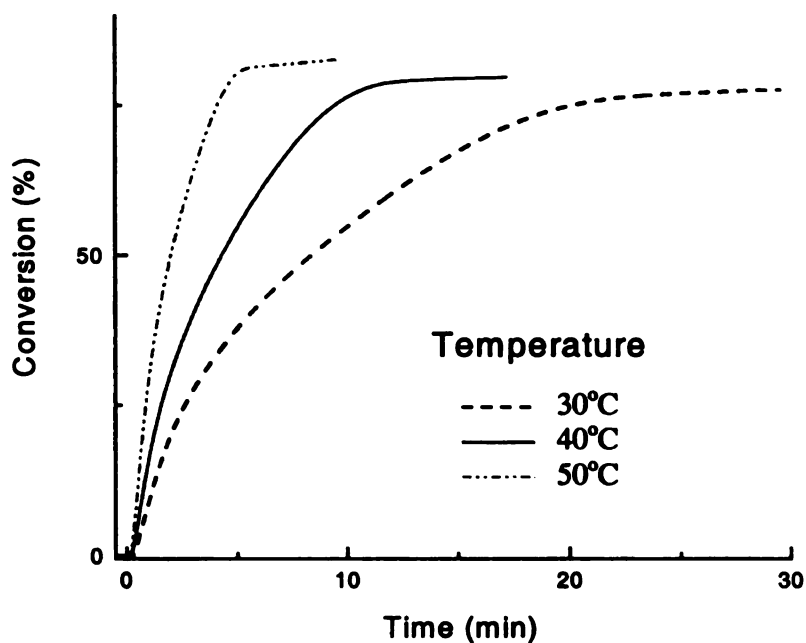
Figure 5.43. Effect of photosensitization on final conversion for the same reaction systems as in *Figure 5.42*.
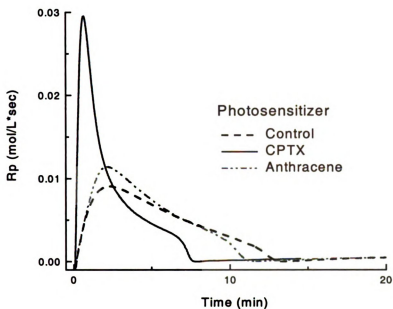
Figure 5.44. Photosensitizer effect for reaction systems of mono-epoxy *octyl glycidyl ether* with 8.0 x 10⁻³ *molal* of photoinitiator *diaryliodonium hexafluoroantimonate* and 8.0 x 10⁻⁴ *molal* of photosensitizer at 50°C.
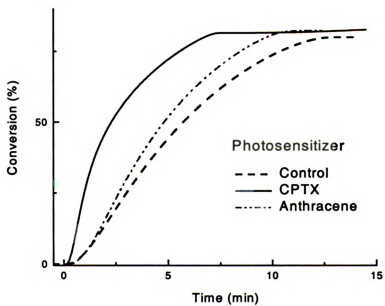
Figure 5.45. Photosensitizer effect on final conversion for the same reaction systems as in *Figure 5.44.*
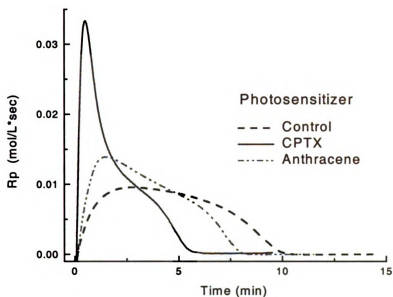
Figure 5.46. Photosensitizer effect for reaction system of mono-epoxy *octyl glycidyl ether* with 8.0 x 10⁻³ molal photoinitiator *tolycumyl iodonium tetrakis (pentafluorophenyl) borate*, B⁻[F₅]₄⁻ and 8.0 x 10⁻⁴ molal photosensitizer at 50°C.
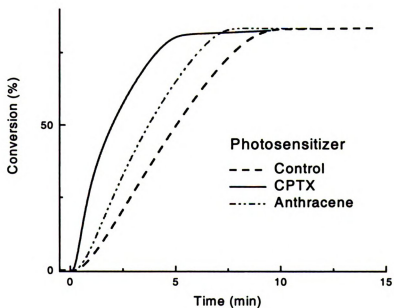
Figure 5.47. Photosensitizer effect on final conversion for the same reaction systems as in *Figure 5.46*.
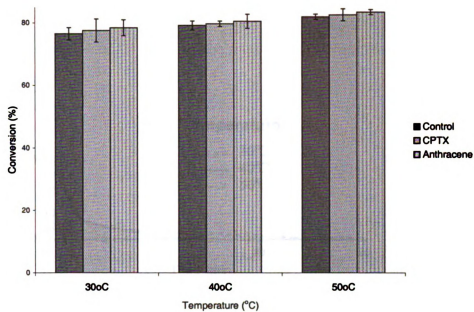
Figure 5.48. Photosensitizer effect on the conversion for reaction systems comprising of *octyl glycidyl ether* and 8.0 x 10^{-3} *molal* photoinitiator *tolycumyl iodonium tetrakis (pentafluorophenyl) borate*, B-$[F_5]_4^-$
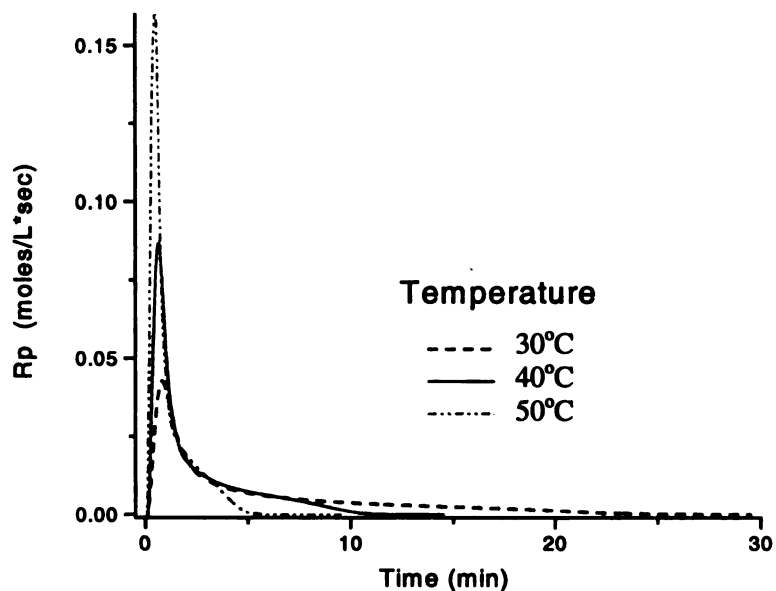
Figure 5.49. Temperature effects for reaction systems of di-epoxide monomer 1,4-butanediol diglycidyl ether with 8.0 x 10^{-3} molal of photoinitiator diaryliodonium hexafluoroantimonate, [SbF$_6$]$^-$ and 8.0 x 10^{-4} molal of photosensitizer CPTX.
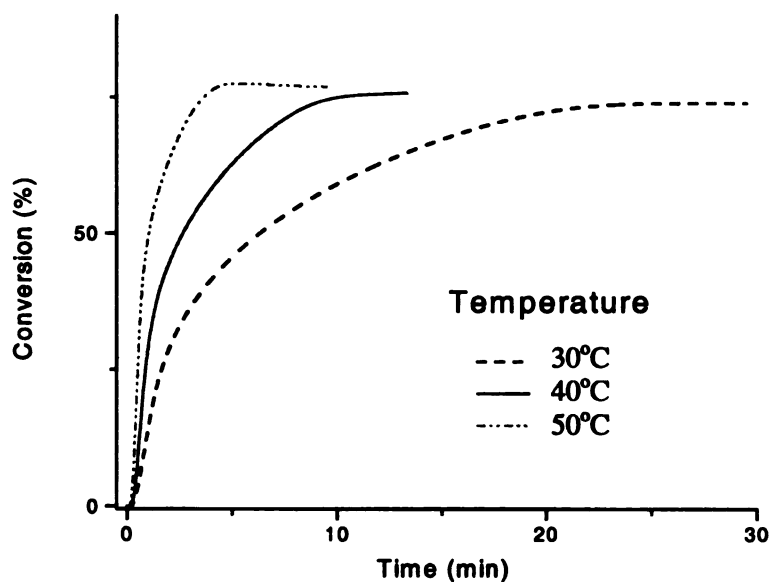
Figure 5.50. Photosensitizer effect on final conversion for the same reaction systems as in Figure 5.49.
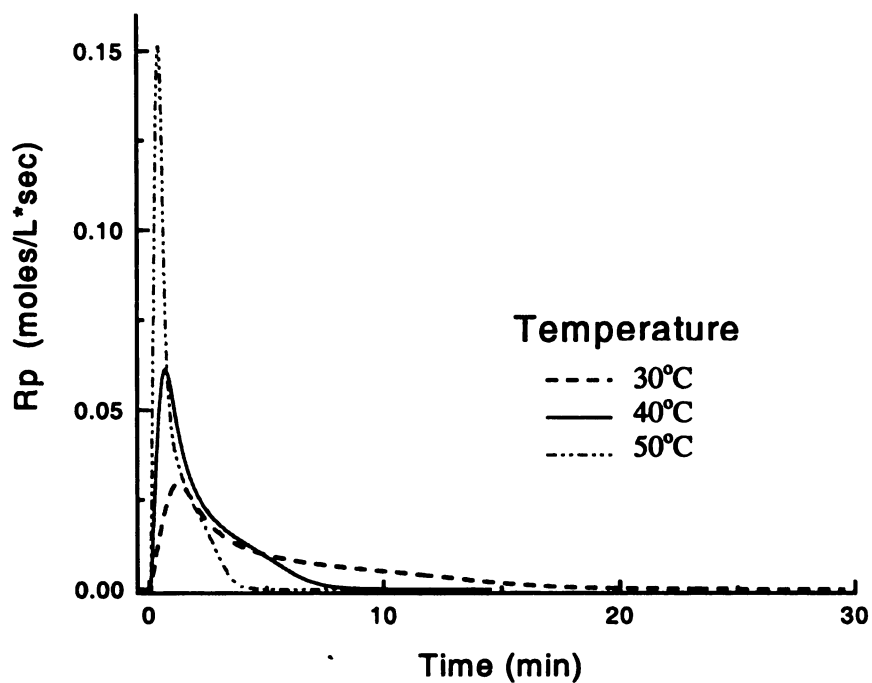
Figure 5.51. Temperature effects for reaction systems of di-epoxy *1,4-butanediol diglycidyl ether* with 8.0 x 10^{-3} *molal* of photoinitiator *Tolycumyl iodonium tetrakis (pentafluorophenyl) borate*, $B^-[F_5]_4^-$ and 8.0 x 10^{-4} *molal* of photosensitizer CPTX.
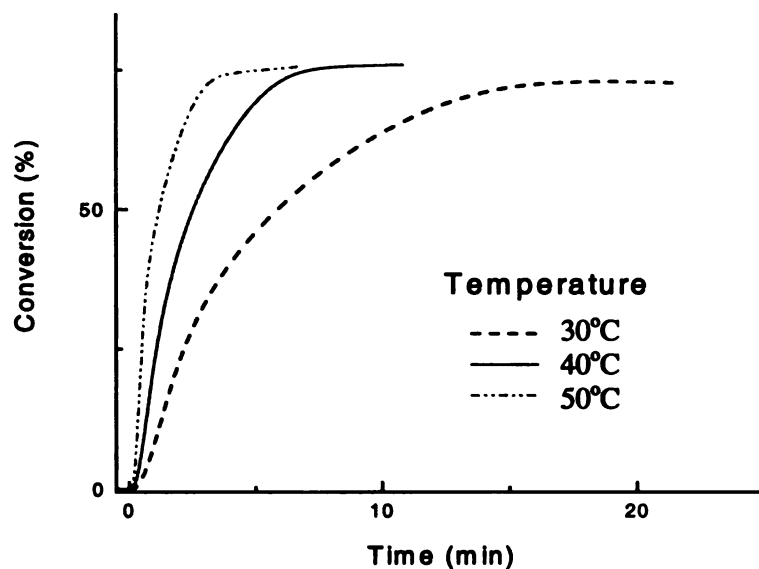
Figure 5.52. Photosensitizer effect on final conversion for the same reaction systems as in *Figure 5.51*.
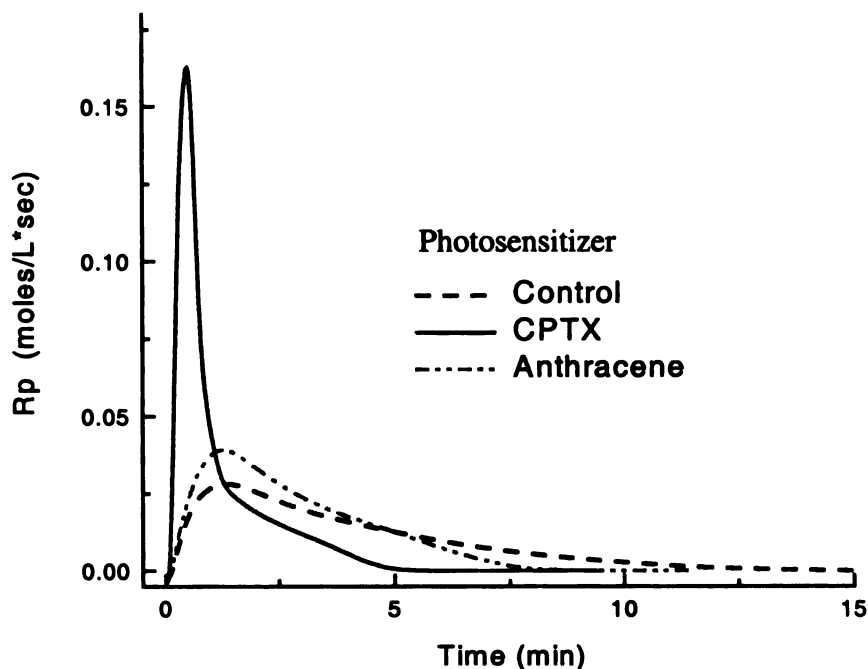
Figure 5.53. Photosensitizer effect for reaction system of di-epoxy *1,4-butanediol diglycidyl ether* with 8.0 x 10^{-3} *molal* of photoinitiator *diaryliodonium hexafluoroantimonate* and 8.0 x 10^{-4} *molal* of photosensitizer at 50°C.
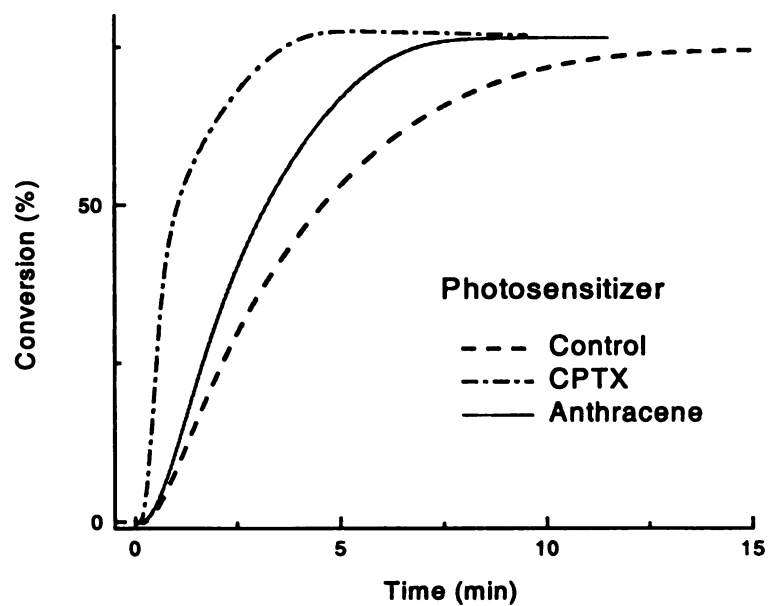
Figure 5.54. Photosensitizer effect on final conversion for the same reaction systems as in *Figure 5.53*.
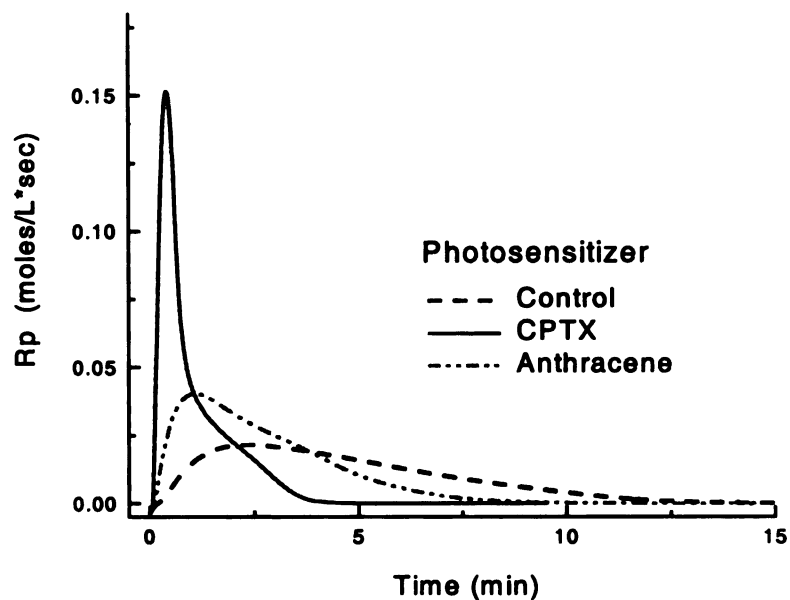
Figure 5.55. Photosensitizer effect for reaction system of di-epoxy *1,4-butandiol diglycidyl ether* with 8.0×10^{-3} *molal* of photoinitiator *tolycumyl iodonium tetrakis pentafluorophenyl borate*, $B^-[F_5]_4^-$ and 8.0×10^{-4} *molal* of photosensitizer at $50°C$.
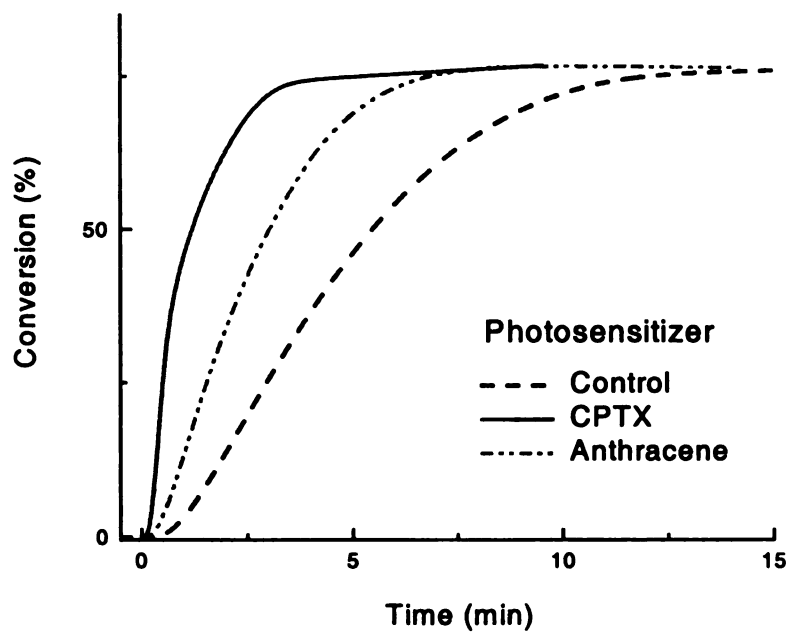
Figure 5.56. Photosensitizer effect on final conversion for the same reaction systems as in *Figure 5.55*.
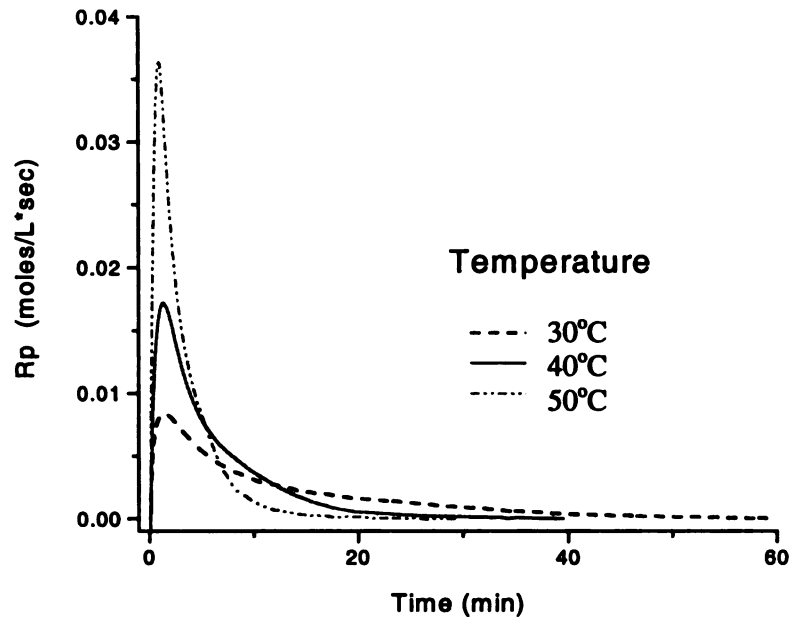
Figure 5.57. Temperature effects for reaction systems of tri-epoxy *trimethyol propane triglycidyl ether* with 8.0 x 10^{-3} *molal* of photoinitiator *diaryliodonium hexafluoroantimonate*, [SbF$_6$]⁻ and 8.0 x 10^{-4} *molal* of photosensitizer CPTX.
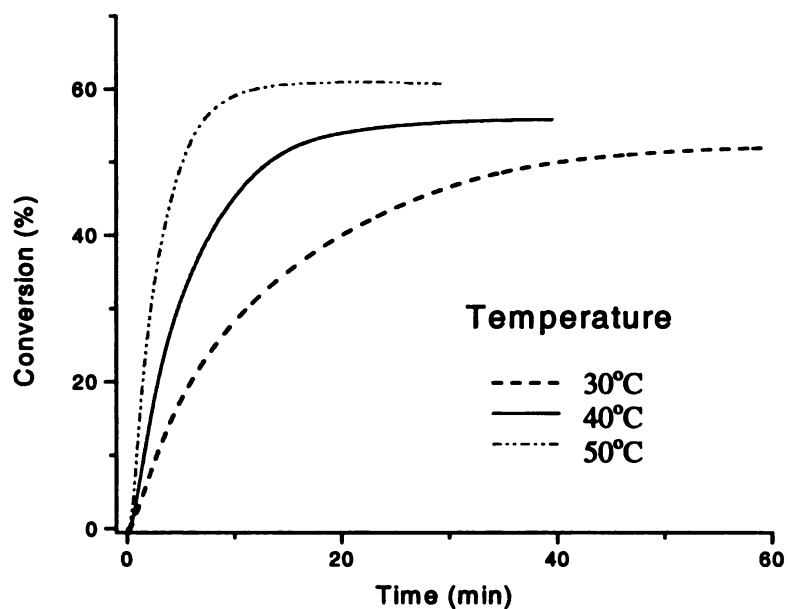
Figure 5.58. Photosensitizer effect on final conversion for the same reaction systems as in *Figure 5.57*.
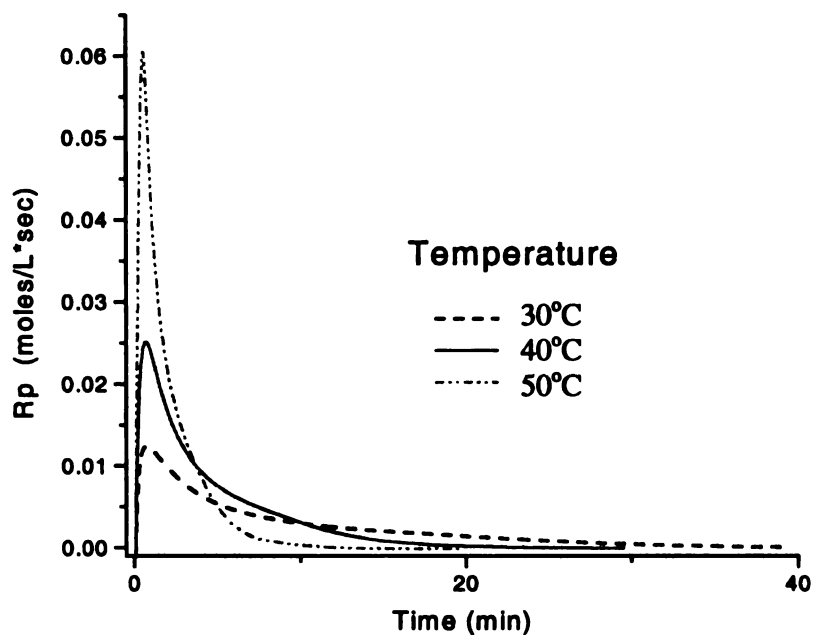
Figure 5.59. Temperature effects for reaction systems of tri-epoxide monomer *trimethyol propane triglycidyl ether* with 8.0 x 10^{-3} *molal* of *tolycumyl iodonium tetrakis pentafluorophenyl borate*, $B^-[F_5]_4^-$ and 8.0 x 10^{-4} *molal* of photosensitizer CPTX.
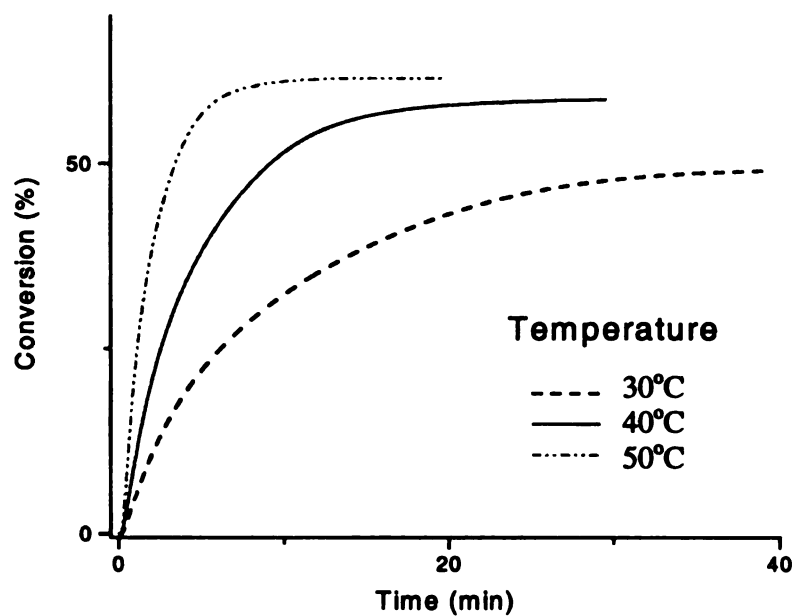
Figure 5.60. Photosensitizer effect on final conversion for the same reaction systems as in *Figure 5.59.*
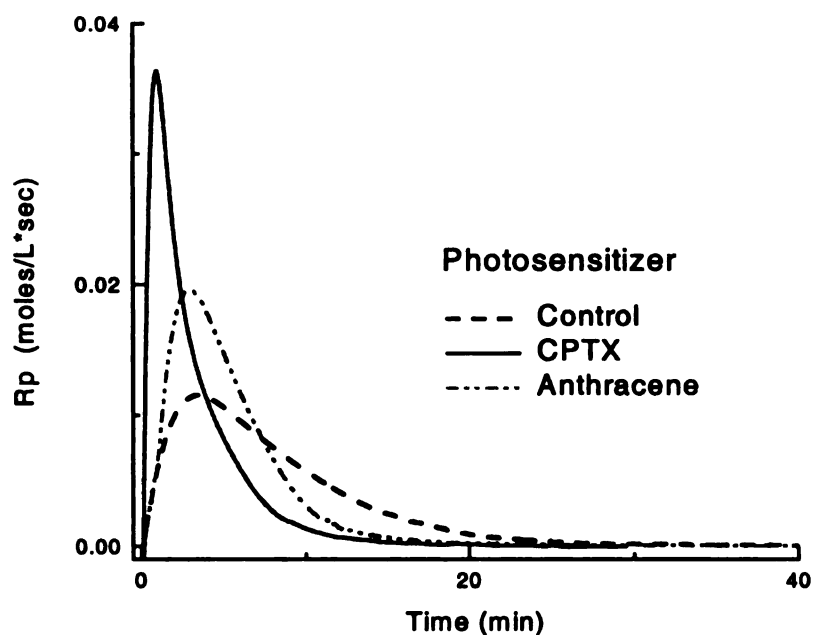
Figure 5.61. Photosensitizer effect for reaction system of tri-epoxide *trimethyol propane triglycidyl ether* with 8.0 x 10^{-3} *molal* of photoinitiator *diaryliodonium hexafluoroantimonate* and 8.0 x 10^{-4} *molal* of photosensitizer at 50°C.
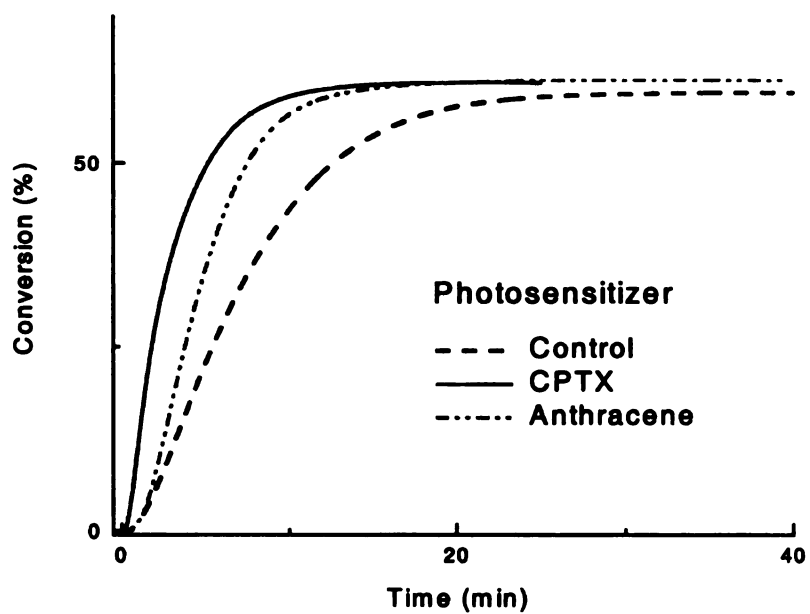
Figure 5.62. Photosensitizer effect on final conversion for the same reaction systems as in *Figure 5.61*.
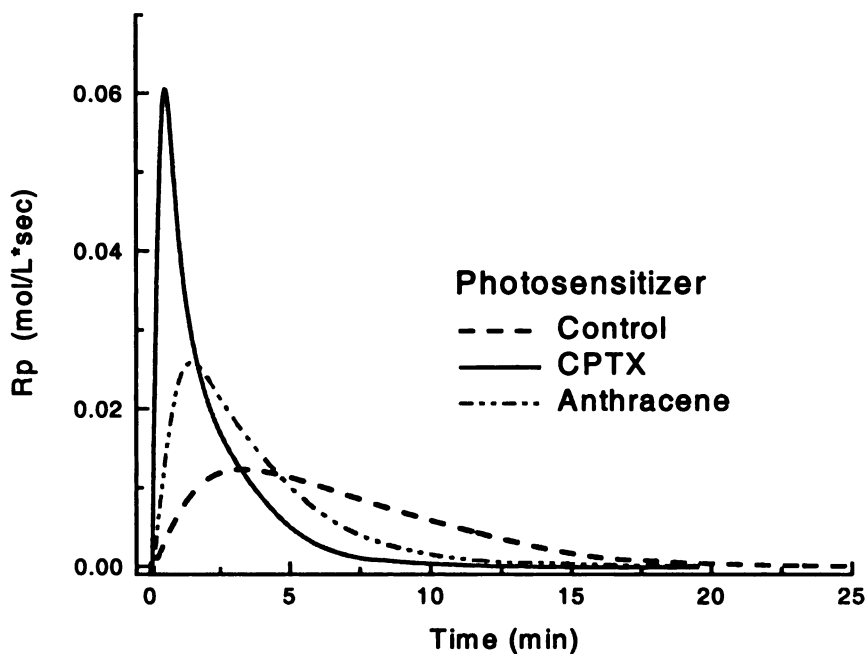
Figure 5.63. Photosensitizer effect for reaction system of tri-epoxy *trimethyol propane triglycidyl ether* with 8.0 x 10^{-3} *molal* of photoinitiator *tolycumyl iodonium tetrakis (pentafluorophenyl) borate*, $B^-[F_5]_4^-$ and 8.0x10^{-4} *molal* of photosensitizer at 50°C.
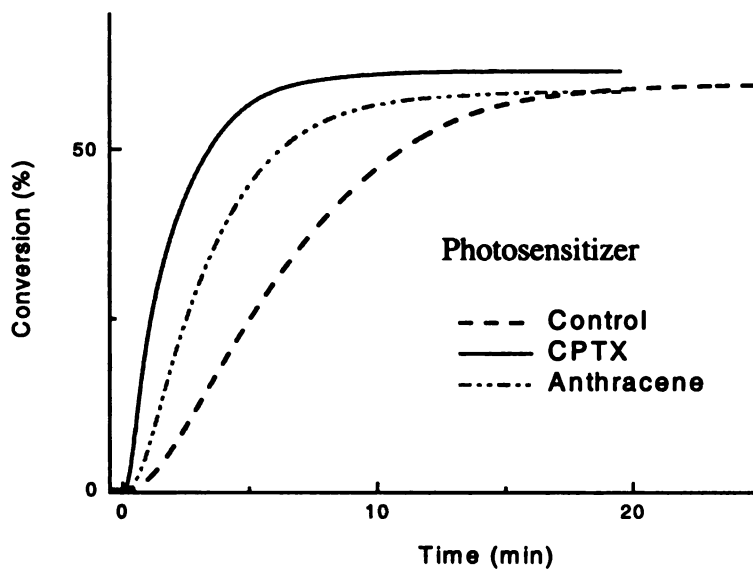
Figure 5.64. Photosensitizer effect on final conversion for the same reaction systems as in *Figure 5.63*.

As illustrated in Figure 5.57, the rate of polymerization increases sharply to exhibit the effect of both temperature and photosensitization. With just the photoinitiator alone, the reaction still occurs. Recall that the photosensitizer CPTX can absorb more strongly of the initiating light in the wavelength region above 300 nm than the sensitizer anthracene can. As a result, more energy is being transferred to the initiator by the electron transfer process, which in turn causes in an increase in the generation of the active cationic centers, which is manifested by the sharp increase in the rate of polymerization. The tri-epoxide monomer trimethyol propane triglycidyl ether has three epoxide rings in the molecule, which consequently gives rise to the highest local concentration of epoxide rings available for reaction. Theoretically, the rate of polymerization should be faster than that of the di-epoxide and mono-epoxide monomers. The actual observed rate of polymerization is higher than that of the mono-epoxide but is lower than that of the di-epoxide monomer. One possible explanation lies in the time when vitrification sets in. Because vitrification occurs much faster than that in the case with tri-epoxide, the mobility of the active centers is severely handicapped. As a result, the rate of polymerizztion is reduced. Figure 5.58 shows that the ultimate limiting conversion is more affected by increasing reaction temperature than that observed in the di- and mono-epoxide monomers. The difference can be explained by the same principle, conversion depends strongly on the glass transition temperature of the polymer, which is primarily dependent on the structure of the monomer. Higher temperature translates into higher kinetic energy of the active polymer chains, and may result in higher rate of effective collisions or reaction has just occurred. The same trends are observed in the case with the photoinitiator tolycumyl iodonium tetrakis pentafluorphenyl borate.

Table 5.9. Effects on the polymerization rate, R_p, for a reaction system containing 8.0×10^{-3} *molal* of photoinitiator *tolycumyl iodonium tetrakis (pentafluorophenyl) borate*, $B^-[F_5]_4^-$ and 8.0×10^{-4} *molal* of photosensitizer and a *mono-epoxide* monomer at various temperatures.

Photosensitizer	Temp. (°C)	Butyl glycidyl ether		Octyl glycidyl ether		Phenyl glycidyl ether	
		Peak time (min)	Peak height (mole/L*sec)	Peak time (min)	Peak height (mole/L*sec)	Peak time (min)	Peak height (mole/L*sec)
No sensitizer	30°C	5.38 ± 0.07	0.0044 ± 0.0001	5.37 ± 0.05	0.0030 ± 0.0001	2.46 ± 0.37	0.0072 ± 0.0001
	40°C	4.34 ± 0.49	0.0078 ± 0.0004	3.98 ± 0.24	0.0057 ± 0.0001	2.24 ± 0.15	0.0128 ± 0.0003
	50°C	2.95 ± 0.06	0.0136 ± 0.0004	2.88 ± 0.15	0.0096 ± 0.0002	1.73 ± 0.08	0.0244 ± 0.0007
CPTX	30°C	0.63 ± 0.03	0.0138 ± 0.0004	0.84 ± 0.08	0.0107 ± 0.0005	0.46 ± 0.05	0.0333 ± 0.0004
	40°C	0.55 ± 0.02	0.0299 ± 0.0004	0.60 ± 0.03	0.0179 ± 0.0007	0.43 ± 0.02	0.0410 ± 0.0041
	50°C	0.46 ± 0.03	0.0551 ± 0.0020	0.50 ± 0.02	0.0333 ± 0.0008	0.42 ± 0.06	0.0655 ± 0.0025
Anthracene	30°C	2.93 ± 0.35	0.0051 ± 0.0001	2.78 ± 0.30	0.0041 ± 0.0001	1.52 ± 0.08	0.0092 ± 0.0003
	40°C	2.28 ± 0.02	0.0095 ± 0.0002	1.96 ± 0.17	0.0078 ± 0.0002	1.47 ± 0.12	0.0154 ± 0.0008
	50°C	1.50 ± 0.07	0.0177 ± 0.0001	1.44 ± 0.20	0.0140 ± 0.0001	1.29 ± 0.04	0.0291 ± 0.0003

Table 5.10. Effects on the polymerization rate, R_p, for a reaction system containing 8.0×10^{-3} *molal* of photoinitiator *diaryliodonium hexafluoroantimonate*, [SbF$_6$]$^-$ and 8.0×10^{-4} *molal* of photosensitizer and a *mono-epoxide* monomer at various temperatures.

Photosensitizer	Temp. (°C)	Butyl glycidyl ether		Octyl glycidyl ether		Phenyl glycidyl ether	
		Peak time (min)	Peak height (mole/L*sec)	Peak time (min)	Peak height (mole/L*sec)	Peak time (min)	Peak height (mole/L*sec)
No sensitizer	30°C	6.92 ± 0.20	0.0067 ± 0.0001	4.35 ± 0.23	0.0033 ± 0.0001	3.65 ± 0.36	0.0068 ± 0.0001
	40°C	4.64 ± 0.16	0.0108 ± 0.0001	3.22 ± 0.03	0.0055 ± 0.0001	3.38 ± 0.34	0.0101 ± 0.0001
	50°C	3.59 ± 0.24	0.0183 ± 0.0002	2.26 ± 0.15	0.0091 ± 0.0002	2.99 ± 0.08	0.0183 ± 0.0002
CPTX	30°C	1.77 ± 0.06	0.0193 ± 0.0005	0.89 ± 0.03	0.0098 ± 0.0003	0.57 ± 0.05	0.0333 ± 0.0014
	40°C	1.12 ± 0.01	0.0270 ± 0.0003	0.74 ± 0.03	0.0170 ± 0.0005	0.62 ± 0.03	0.0410 ± 0.0023
	50°C	0.94 ± 0.01	0.0434 ± 0.0006	0.64 ± 0.02	0.0297 ± 0.0003	0.60 ± 0.01	0.0655 ± 0.0024
Anthracene	30°C	6.82 ± 0.33	0.0082 ± 0.0001	3.63 ± 0.10	0.0039 ± 0.0002	3.09 ± 0.06	0.0092 ± 0.0003
	40°C	4.52 ± 0.49	0.0139 ± 0.0003	2.71 ± 0.20	0.0066 ± 0.0002	2.91 ± 0.03	0.0154 ± 0.0005
	50°C	2.92 ± 0.26	0.0255 ± 0.0007	2.17 ± 0.36	0.0116 ± 0.0007	2.51 ± 0.08	0.0291 ± 0.0002

Table 5.11. Photosensitizer effects on the limiting conversion for a reaction system containing 8.0×10^{-3} *molal* of photoinitiator *tolycumyl iodonium tetrakis pentafluorophenyl borate*, $B-[F_5]_4^-$ and 8.0×10^{-4} *molal* of photosensitizer and a *mono-epoxide* monomer at various temperatures.

Photosensitizer	Temp. (°C)	Butyl glycidyl ether % conversion	Octyl glycidyl ether % conversion	Phenyl glycidyl ether % conversion
No sensitizer	30°C	70.5 ± 5.3	76.5 ± 2.0	92.2 ± 5.5
	40°C	70.7 ± 2.4	79.2 ± 1.4	93.9 ± 3.8
	50°C	72.2 ± 0.1	82.0 ± 0.8	93.9 ± 0.8
CPTX	30°C	71.5 ± 3.5	77.6 ± 3.7	89.6 ± 5.6
	40°C	73.6 ± 2.1	79.7 ± 0.9	96.5 ± 2.0
	50°C	74.5 ± 0.5	82.6 ± 1.9	98.6 ± 1.6
Anthracene	30°C	72.9 ± 0.6	78.4 ± 2.6	93.0 ± 4.8
	40°C	73.2 ± 1.2	80.6 ± 2.3	95.2 ± 3.9
	50°C	74.1 ± 1.0	83.5 ± 0.8	97.4 ± 1.3

121

Table 5.12. Photosensitizer effects on the limiting conversion for a reaction system containing 8.0×10^{-3} *molal* of photoinitiator *diaryliodonium hexafluoroantimonate*, [SbF$_6$]$^-$ and 8.0×10^{-4} *molal* of photosensitizer and a *mono-epoxide* monomer at various temperatures.

Photosensitizer	Temp. (°C)	Butyl glycidyl ether % conversion	Octyl glycidyl ether % conversion	Phenyl glycidyl ether % conversion
No sensitizer	30°C	67.0 ± 0.6	67.0 ± 0.6	92.7 ± 1.6
	40°C	68.3 ± 2.8	68.3 ± 2.8	97.0 ± 2.0
	50°C	69.1 ± 2.0	69.1 ± 1.9	98.3 ± 0.9
CPTX	30°C	71.4 ± 1.5	71.4 ± 1.5	94.7 ± 2.6
	40°C	74.1 ± 1.5	74.1 ± 1.5	96.9 ± 1.4
	50°C	74.9 ± 0.8	74.9 ± 0.8	99.3 ± 0.2
Anthracene	30°C	66.8 ± 1.7	66.8 ± 1.7	94.0 ± 2.5
	40°C	74.3 ± 0.8	74.3 ± 0.8	96.4 ± 1.1
	50°C	74.6 ± 0.7	74.6 ± 0.7	98.6 ± 0.3

Table 5.13. Effects on the polymerization rate, R_p, for a reaction system containing 8.0×10^{-3} *molal* of photoinitiator *Tolycumyl iodonium tetrakis (pentafluorophenyl) borate*, B-[F5]4$^-$ and 8.0×10^{-4} *molal* of photosensitizer and a *di-epoxide* monomer at various temperatures.

Photosensitizer	Temp. (°C)	1,4-butanediol diglycidyl ether		Cyclohexane dimethanol diglycidyl ether	
		Peak time (min)	Peak height (mole/L*sec)	Peak time (min)	Peak height (mole/L*sec)
No sensitizer	30°C	5.00 ± 0.80	0.0079 ± 0.0003	7.08 ± 0.42	0.0042 ± 0.0001
	40°C	2.71 ± 0.23	0.0128 ± 0.0001	4.47 ± 0.34	0.0086 ± 0.0004
	50°C	2.29 ± 0.23	0.0216 ± 0.0001	3.08 ± 0.07	0.0143 ± 0.0001
CPTX	30°C	1.24 ± 0.08	0.0296 ± 0.0013	1.63 ± 0.19	0.0081 ± 0.0007
	40°C	0.69 ± 0.08	0.0618 ± 0.0007	1.19 ± 0.13	0.0191 ± 0.0003
	50°C	0.40 ± 0.06	0.1559 ± 0.0414	0.69 ± 0.01	0.0450 ± 0.0017
Anthracene	30°C	3.21 ± 0.03	0.0128 ± 0.0001	4.03 ± 0.13	0.0059 ± 0.0006
	40°C	2.10 ± 0.08	0.0225 ± 0.0001	2.79 ± 0.06	0.0122 ± 0.0002
	50°C	1.09 ± 0.05	0.0402 ± 0.0004	1.73 ± 0.09	0.0282 ± 0.0022

Table 5.14. Effects on the polymerization rate, R_p, for a reaction system containing 8.0×10^{-3} *molal* of photoinitiator *diaryliodonium hexafluoroantimonate*, $[SbF_6]^-$ and 8.0×10^{-4} *molal* of photosensitizer and a *di-epoxide* monomer at various temperatures.

Photosensitizer	Temp. (°C)	1,4-butanediol diglycidyl ether		Cyclohexane dimethanol diglycidyl ether	
		Peak time (min)	Peak height (mole/L*sec)	Peak time (min)	Peak height (mole/L*sec)
No sensitizer	30°C	3.09 ± 0.42	0.0097 ± 0.0009	7.37 ± 0.19	0.0032 ± 0.0001
	40°C	1.98 ± 0.08	0.0170 ± 0.0001	5.26 ± 0.04	0.0065 ± 0.0001
	50°C	1.34 ± 0.03	0.0282 ± 0.0016	2.72 ± 0.13	0.0149 ± 0.0007
CPTX	30°C	0.83 ± 0.01	0.0427 ± 0.0013	1.87 ± 0.27	0.0068 ± 0.0006
	40°C	0.63 ± 0.02	0.0867 ± 0.0016	1.18 ± 0.02	0.0195 ± 0.0032
	50°C	0.48 ± 0.04	0.1620 ± 0.0047	0.87 ± 0.02	0.0523 ± 0.0135
Anthracene	30°C	2.68 ± 0.03	0.0122 ± 0.0006	4.12 ± 0.44	0.0048 ± 0.0006
	40°C	2.05 ± 0.22	0.0212 ± 0.0007	3.21 ± 0.10	0.0116 ± 0.0002
	50°C	1.26 ± 0.03	0.0392 ± 0.0033	2.02 ± 0.04	0.0236 ± 0.0002

Table 5.15. Photosensitizer effects on the limiting conversion for a reaction system containing 8.0 x 10^{-3} molal of photoinitiator *tolycumyl iodonium tetrakis pentafluorophenyl borate, B-[F$_5$]$_4^-$ and 8.0 x 10^{-4} molal of photosensitizer and a di-epoxide monomer at various temperatures.*

Photosensitizer	Temp. (°C)	1,4-butanediol diglycidyl ether % conversion	Cyclohexane dimethanol diglycidyl ether % conversion
No sensitizer	30°C	71.8 ± 1.4	69.8 ± 1.8
	40°C	75.0 ± 1.3	75.0 ± 4.1
	50°C	76.2 ± 1.1	76.8 ± 0.3
CPTX	30°C	72.6 ± 1.6	73.1 ± 0.8
	40°C	76.2 ± 0.8	75.3 ± 0.3
	50°C	76.6 ± 0.9	78.8 ± 1.4
Anthracene	30°C	74.4 ± 1.0	74.1 ± 4.2
	40°C	75.6 ± 0.6	74.6 ± 1.3
	50°C	76.3 ± 0.4	78.8 ± 4.2

Table 5.16. Photosensitizer effects on the limiting conversion for a reaction system containing 8.0 x 10^{-3} *molal* of photoinitiator *diaryliodonium hexafluoroantimonate*, [SbF$_6$]$^-$ and 8.0 x 10^{-4} *molal* of photosensitizer and a *di-epoxide* monomer at various temperatures.

Photosensitizer	Temp. (°C)	1,4-butanediol diglycidyl ether % conversion	Cyclohexane dimethanol diglycidyl ether % conversion
No sensitizer	30°C	70.3 ± 3.8	33.7 ± 1.8
	40°C	74.4 ± 0.7	47.8 ± 1.3
	50°C	74.5 ± 2.7	76.1 ± 3.0
CPTX	30°C	73.8 ± 2.2	47.3 ± 2.7
	40°C	75.9 ± 1.6	77.0 ± 4.1
	50°C	76.8 ± 4.2	77.6 ± 3.6
Anthracene	30°C	75.2 ± 1.4	41.3 ± 2.0
	40°C	75.9 ± 2.1	76.1 ± 0.7
	50°C	76.4 ± 2.5	77.6 ± 1.0

126

Table 5.17. Photosensitizer effects on the polymerization rate, R_p, for a reaction system containing 8.0 x 10^{-3} *molal* of photoinitiator *tolycumyl iodonium tetrakis (pentafluorophenyl) borate*, $B^-[F_5]_4^-$ and 8.0 x 10^{-4} *molal* of photosensitizer and a *tri-epoxide* monomer at various temperatures.

Photosensitizer	Temp. (°C)	Trimethyol propane triglycidyl ether	
		Peak time (min)	Peak height (mole/L*sec)
No sensitizer	30°C	7.24 ± 1.15	0.0037 ± 0.0004
	40°C	5.02 ± 0.11	0.0072 ± 0.0005
	50°C	3.28 ± 0.10	0.0123 ± 0.0006
CPTX	30°C	0.74 ± 0.06	0.0124 ± 0.0003
	40°C	0.68 ± 0.01	0.0251 ± 0.0013
	50°C	0.54 ± 0.01	0.0605 ± 0.0012
Anthracene	30°C	3.64 ± 0.15	0.0055 ± 0.0001
	40°C	2.34 ± 0.06	0.0120 ± 0.0001
	50°C	1.48 ± 0.06	0.0259 ± 0.0003

Table 5.18. Photosensitizer effects on the polymerization rate, R_p, for a reaction system containing 8.0 x 10^{-3} *molal* of photoinitiator *diaryliodonium hexafluoroantimonate*, $[SbF_6]^-$ and 8.0 x 10^{-4} *molal* of photosensitizer and a *tri-epoxide* monomer at various temperatures.

Photosensitizer	Temp. (°C)	Trimethyol propane triglycidyl ether	
		Peak time (min)	Peak height (mole/L*sec)
No sensitizer	30°C	7.38 ± 0.24	0.0035 ± 0.0003
	40°C	4.96 ± 0.17	0.0065 ± 0.0003
	50°C	3.48 ± 0.11	0.0116 ± 0.0002
CPTX	30°C	1.41 ± 0.06	0.0084 ± 0.0004
	40°C	1.32 ± 0.03	0.0171 ± 0.0004
	50°C	0.93 ± 0.01	0.0363 ± 0.0007
Anthracene	30°C	4.74 ± 0.34	0.0050 ± 0.0001
	40°C	3.17 ± 0.07	0.0107 ± 0.0001
	50°C	2.97 ± 0.05	0.0196 ± 0.0002

Table 5.19. Photosensitizer effects on conversion for a reaction system containing 8.0 x 10^{-3} *molal* of photoinitiator *tolycumyl iodonium tetrakis pentafluorophenyl borate*, $B^-[F_5]_4^-$ and 8.0 x 10^{-4} *molal* of photosensitizer and a tri-epoxide monomer at various temperatures.

Photosensitizer	Temp. (°C)	Trimethyol propane triglycidyl ether
		% conversion
No sensitizer	30°C	47.9 ± 1.0
	40°C	56.4 ± 2.2
	50°C	59.6 ± 1.2
CPTX	30°C	48.5 ± 1.2
	40°C	58.6 ± 0.8
	50°C	60.2 ± 0.3
Anthracene	30°C	50.7 ± 0.3
	40°C	59.1 ± .02
	50°C	59.2 ± 0.6

Table 5.20. Photosensitizer effects on conversion for a reaction system containing 8.0 x 10^{-3} *molal* of photoinitiator *diaryliodonium hexafluoroantimonate*, $[SbF_6]^-$ and 8.0 x 10^{-4} *molal* of photosensitizer and a *tri-epoxide* monomer at various temperatures.

Photosensitizer	Temp. (°C)	Trimethyol propane triglycidyl ether
		% conversion
No sensitizer	30°C	50.1 ± 0.7
	40°C	55.2 ± 1.6
	50°C	59.3 ± 0.5
CPTX	30°C	52.1 ± 0.8
	40°C	55.9 ± 0.6
	50°C	60.7 ± 0.8
Anthracene	30°C	50.1 ± 0.9
	40°C	54.0 ± 0.7
	50°C	61.2 ± 0.9

5.1.4.6. Effect of Photosensitizer Concentration on Photopolymerization Kinetics

Recall that the addition of photosensitizer to the reaction mixtures increased the spectral sensitivity of the photoinitiator, and the photosensitizer CPTX was shown in *Section 5.1.3.5* to be more efficient than anthracene. In this section, the efficiency of the photosensitizer CPTX was further studied by varying its concentration in a series of reaction systems containing 8.0×10^{-3} molal photoinitiator diaryliodonium hexafluoroantimonate, $[SbF_6]^-$ and mono-epoxide butyl glycidyl ether. Figures 5.65-5.66 show the significant effects of photosensitizer on the overall reaction rate, R_p, and the total conversion. The figures illustrate that the most dramatic enhancement in the rate of photopolymerization is observed as the photosensitizer concentration is increased from 0 to 0.8 millimolal. As the concentration is increased another order of magnitude to 8.0 millimolal, the reaction rate continues to increase, but in a much less dramatic manner. These trends are illustrated by the values for the peak polymerization rate. As the photosensitizer concentration is increased from 0 to 0.8 mmolal, the peak polymerization rate more than doubles (from 0.0249 mol/L sec to 0.0527 mol/L sec); however, the further increase in initiator concentration to 8 mmolal (a ten fold increase in concentration) the peak rate increases only another 22% to a value of 0.0646 mol/L sec. Increases in the photosensitizser concentration had an even smaller effect on the limiting conversion. The final limiting conversion increases slightly from ~72% to ~75% as the photosensitizer concentration was increased from 0.8 to 8 mmolal. This relatively modest effect on the final limiting conversion is not surprising since the photosensitizer increases the active center concentration, and the limiting conversion is not highly dependent on the active center concentration. The limiting conversion is primarily

determined by the glass transition temperature of the polymer, and this is primarily determined by the structure of the polymer chain (which is determined by the monomer structure). This effect will be illustrated more clearly in section 5.1.4.7. The results on the effect of the photosensitizer are presented in Table 5.21 below.

Table 5.21. Concentration effects of photosensitizer CPTX on reaction systems containing 8.0 x 10^{-3} *molal* of photoinitiator *diaryliodonium hexafluoroantimonate* and monomer mono-epoxy *butyl glycidyl ether*.

Concentration	Peak time (min)	Peak height (mol/L•sec)	% conversion
No sensitizer	1.23 ± 0.08	0.0249 ± 0.0005	71.3 ± 4.0
8.0 x 10^{-4}	0.41 ± 0.05	0.0527 ± 0.0039	72.5 ± 5.2
2.0 x 10^{-3}	0.40 ±.0.01	0.0530 ± 0.0006	73.7 ± 0.6
4.0 x 10^{-3}	0.34 ± 0.03	0.0650 ± 0.0035	75.1 ± 1.0
6.0 x 10^{-3}	0.36 ± 0.01	0.0566 ± 0.0004	73.8 ± 1.2
8.0 x 10^{-3}	0.33 ± 0.02	0.0646 ± 0.0021	74.5 ± 0.3
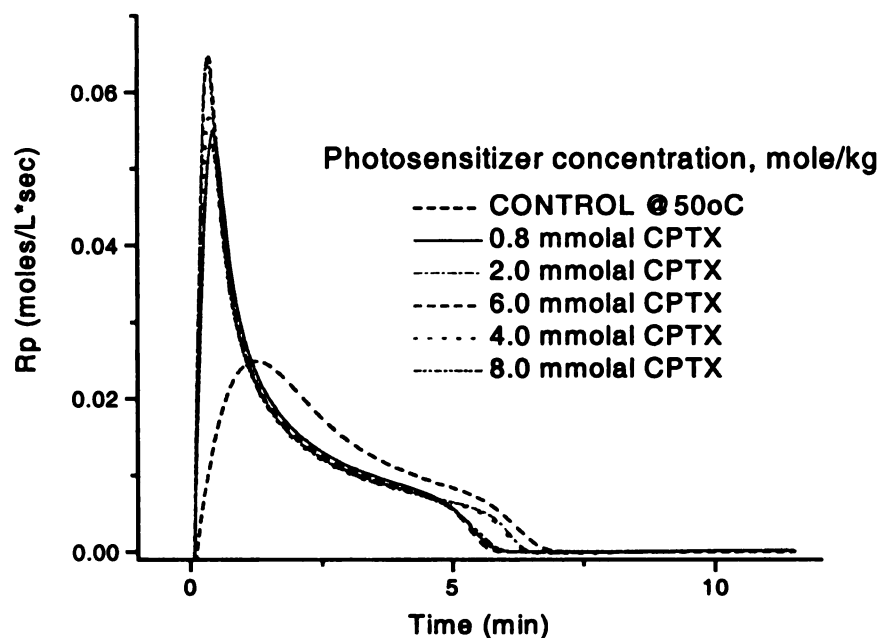
Figure 5.65. Effects of photosensitizer concentration for reaction systems containing mono-epoxy *butyl glycidyl ether* and 8.0 x 10^{-3} *molal* of photoinitiator *diaryliodonium hexafluoroantimonate*, $[SbF_6]^-$ at 50°C.
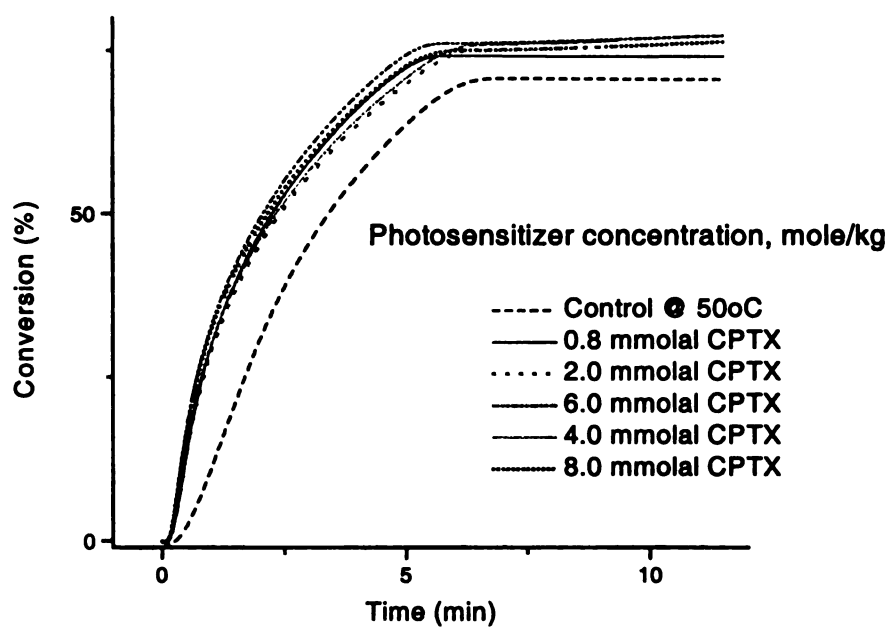
Figure 5.66. Effects of photosensitizer concentrations on final conversion of the same reaction systems in *Figure 5.65*.

5.1.4.7. Effect of Monomer's Structure and Functionality on the Cationic Photopolymerization Kinetics

The purpose of these studies was to determine the effect of the monomer structure and functionality on the cationic photopolymerization kinetics and on the ultimate limiting conversion. For the purposes of this thesis, the functionality of a monomer is defined as to the number of epoxide groups in a single monomer molecule. In this research, the three mono-epoxide monomers were: butyl glycidyl ether, octyl glycidyl ether, and phenyl glycidyl ether. The two di-epoxide monomers were: 1,4-butanediol diglycidyl ether, cyclohexane dimethanol diglycidyl ether. Finally, the tri-epoxide monomer was trimethyol propane triglycidyl ether.

First we will examine the effect of the monomer structure on the photopolymerization kinetics and limiting conversion of the three mono-epoxide monomers. These results are illustrated in Figure 5.67 and 5.68. Figure 5.67 illustrates that the phenyl glycidyl ether exhibits the highest polymerization rate, following by butyl glycidyl ether, and that the octyl glycidal ether exhibits the lowest polymerization rate. This result can be explained by considering the size and geometry of the monomer molecules. The highest polymerization rates will be exhibited by monomers that have a high probability of colliding with the active cationic centers in an orientation that will allow reaction. The octyl glycidyl ether possesses a relatively long pendant hydrocarbon chain that can preclude collisions of the proper orientation, and therefore exhibits the slowest polymerization rate. Similarly, the phenyl glycidyl ether has the most compact molecular structure and exhibits the highest polymerization rate. It is interesting that the octyl glycidyl ether exhibits a lower polymerization rate than the butyl glycidyl ether, but achieves a higher final limiting conversion. This may be attributed to the fact that the

133

smaller pendant butyl group allows the polymer to form a glass more readily, and therefore the system vitrifies and loses mobility at a lower conversion for the butyl glycidyl ether than for the octyl glycidyl ether.

The functionality of the monomer had a significant effect on the reaction rate and conversion as shown in Figures 5.69-5.70. Figure 5.69 illustrates that the di-epoxide monomer 1,4-butanediol diglycidyl ether exhibits a higher polymerization rate than the mono-epoxide monomer *phenyl glycidyl ether* (which was the most reactive mono-epoxide monomer). This higher polymerization rate can be attributed to the relative high local epoxide concentration in the vicinity of the active center. Figure 5.70 illustrates that the limiting conversion is significantly lower for the di-epoxide monomer. This is due the fact that the crosslinking reaction that occurs in the di-epoxide case restricts the mobility of the polymer chains and facilitates vitrification. In addition, the crosslinking reaction can produce pendant epoxide groups that are buried within the crosslinked structure and are not accessible to the cationic active centers. Not surprisingly, the tri-epoxide monomer exhibit the lowest limiting conversion of all, as illustrated by the values in Table 5.22. In this case there is a high probability of producing pendant epoxide groups that are not accessible to the cationic active centers.
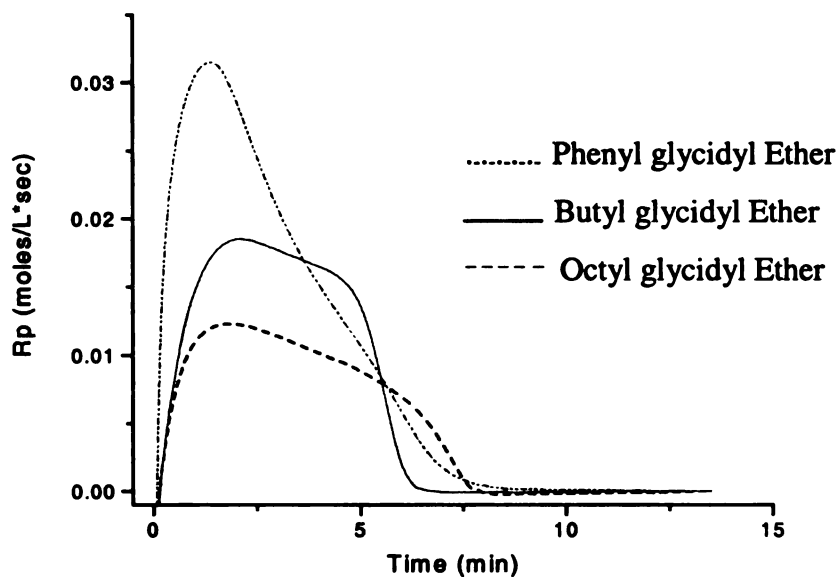
Figure 5.67. Rates of polmerization for various mono-epoxide monomers photoinitiated by 8.0×10^{-3} molal of *tolycumyl iodonium tetrakis pentafluorophenyl borate*, B-[F$_5$]$_4^-$ at 50°C.
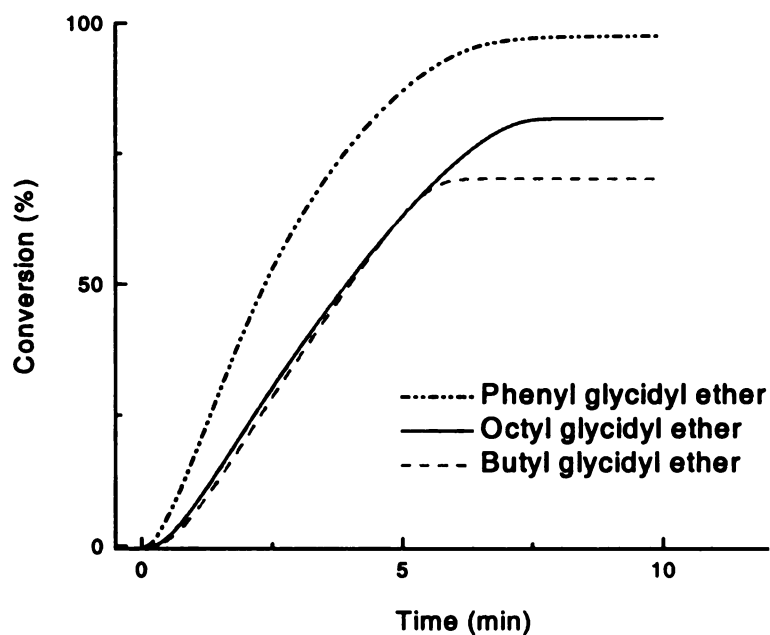
Figure 5.68. Conversion profiles of various mono-epoxide monomers photoinitiated by 8.0×10^{-3} molal of *tolycumyl iodonium tetrakis pentafluorophenyl borate*, B-[F$_5$]$_4^-$ at 50°C.
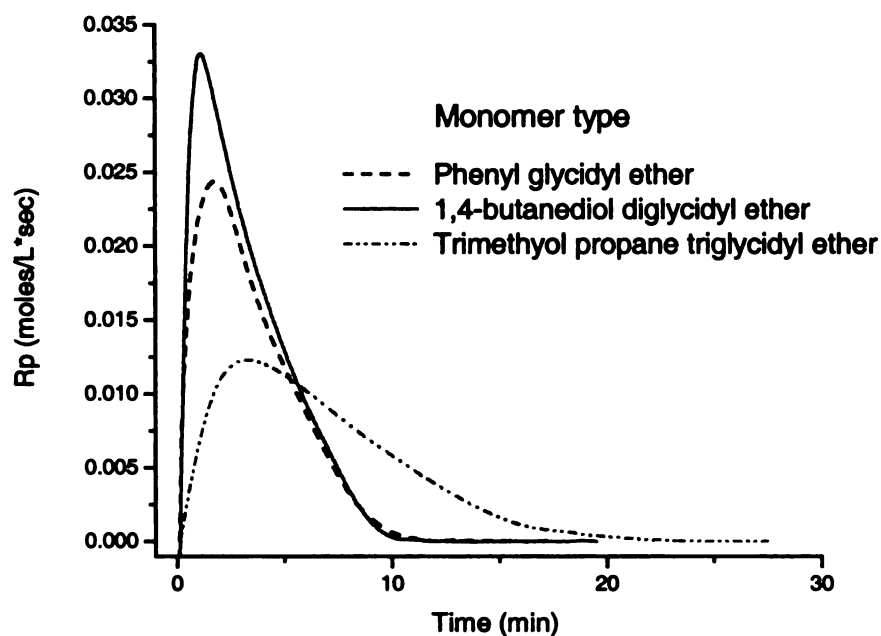
Figure 5.69. Effect of monomer's functionality on reaction rates for reaction systems with 8.0 x10^{-3} molal of photoinitiator *tolycumyl iodonium tetrakis pentafluorophenyl borate*, B-[F$_5$]$_4^-$ at temperature of 50°C.
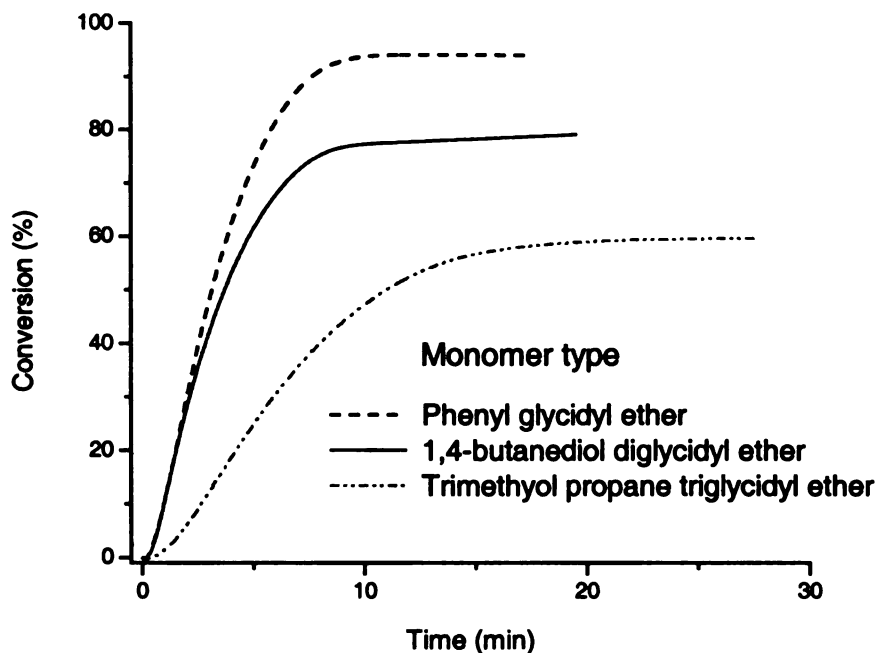
Figure 5.70. Effect of monomer's functionality on conversion for reaction systems with 8.0 x 10^{-3} molal photoinitiator *tolycumyl iodonium tetrakis pentafluorophenyl borate*, B-[F$_5$]$_4^-$ at temperature of 50°C.

Table 5.22. Effect of monomer structure and functionality on the conversion of reaction mixtures comprising of 8.0 x 10^{-3} *molal* photoinitiator *tolycumyl iodonium tetrakis pentafluorophenyl borate*, $B^-[F_5]_4^-$ and different epoxide monomer at 50°C.

Monomer functionality	Monomer structure	Light intensity (mW/cm^2)	% Conversion
Mono-epoxide	butyl glycidyl ether	~ 52	79.2 ± 0.7
	octyl glycidyl ether	~ 52	82.0 ± 0.8
	phenyl glycidyl ether	~ 52	93.9 ± 0.8
Di-epoxide	1,4-butanediol diglycidyl ether	~ 52	76.2 ± 1.1
	cyclohexane dimethanol diglycidyl ether	~ 52	76.8 ± 0.3
Tri-epoxide	trimethyol propane triglycidyl ether	~ 36	59.6 ± 1.2

5.1.5. Conclusions

PDSC experiments were performed to study the reaction kinetics of cationic photopolymerization of epoxides. This method was indeed useful in studying various parameters that can affect the rate of polymerization, R_p, and final conversion. The chemical compounds used in this research effort were seven different epoxide monomers, three photoinitiators, and two photosensitizers. This gave a total of 40 different possible combinations of individual reaction systems. After the data analysis was done, there was undoubtedly some variability among the reaction systems. However, there were four general trends that had been established. First of all, the reaction rate increased with increasing temperature (as supported by the behavior of the propagation rate constant k_p). The conversion also increased by a small amount going from 30, 40 to 50°C. Second, the photoinitiator tolycumyl iodonium tetrakis pentafluorophenyl borate, $B^-[F_5]_4^-$ was proven to be as effective (if not better in some cases) as the photoinitiator diaryliodonium hexafluoroantimonate, $[SbF_6]^-$. The photoinitiator triarylsulfonium hexafluorophosphate, $[PF_6]^-$ was the least effective one of the three photoinitiators. The concentration of the photoinitiator also influenced the reaction rate, R_p and final conversion; however, this effect became less significant above 8.0×10^{-3} molal. Third, with respect to photosensitization to increase spectral sensitivity of the photoinitiators to the initiating light source, the photosensitizer CPTX (1-chloro-4-propoxy-9H-thioxanthen-9-one) was more efficient than anthracene was. This was mainly due to the ability of CPTX to absorb more strongly in the region of 320-390 nm. The study of concentration effect of photosensitizer indicated that concentration above the molality of 8.0×10^{-4} still enhanced the reaction rate R_p by a small amount, but did not improve the final conversion

by much. Lastly, the structure and functionality of the monomer also had an effect. For reactivity: di-epoxide > tri-epoxide > mono-epoxide; and for conversion: mono-epoxide > di-epoxide > tri-epoxide.

5.2. Conversion by Fourier Transform Infrared Spectroscopy (FTIR)

5.2.1. Introduction

The method of Fourier Transform Infrared Spectroscopy (FTIR) has also been applied by many researchers[11-15] to study the reaction kinetics of cationic photopolymerization. The basic operating principle for FTIR is that when infrared red light is passed through a sample, certain frequencies are absorbed while others are transmitted, resulting in an absorption (or transmittance) spectrum that is dependent upon the molecular vibrational frequencies of that sample. For the epoxide compounds used in this research effort, the absorption band corresponding to the C—H bond should lie in the region of $740 - 920$ cm^{-1}, depending on the molecular structure of the particular epoxide molecule. By monitoring the change of this absorption band, the degree of conversion can be obtained.

5.2.2. Experimental

The FTIR experiments were conducted using the Nicolet IR/42 spectrometer by Nicolet Instruments, Inc.. The formulation was applied onto the polyethylene membrane of an IR card (# 61 by 3M). The absorption spectrum of the sample was taken before the UV irradiation. The light source was a 12-watt UV lamp that can produce a light beam at wavelength of 365 nm. The sample was irradiated for a specified amount of time to allow the polymerization reaction to proceed at room temperature and in the open. Next, the sample was scanned in the FTIR spectrometer to obtain the absorption spectrum, from

which the change of the absorption band in the region of 740-920 cm^{-1} would be used to determine the degree of conversion as a result of the UV irradiation. Because of the experimental set-up, this was not an *in situ* process.

5.2.3. Results and Discussion

Each epoxide monomer has a characteristic absorption band corresponding to the C—H bond. As shown in Figure 5.71, the absorption peak is at 914 cm^{-1} for mono-epoxy *octyl glycidyl ether*.[16] The conversion was calculated by the following relationship:

$$\text{Conversion} = \frac{C_t - C_{to}}{C_{to}} \cdot 100 \tag{5.8}$$

where,

C_{to} is the absorption peak before UV irradiation
C_t is the absorption peak for a time t of UV irradiation

Figure 5.72 shows the FTIR spectra for the cationic photopolymerization of di-epoxide monomer 1,4-butanediol diglycidyl ether by 8.0 x 10^{-3} molal of Tolycumyl iodonium tetrakis pentafluorophenyl borate, B$^-$[F$_5$]$_4^-$ and 8.0 x 10^{-4} molal of photosensitizer CPTX. The characteristic absorption peak[16] occurred at 912 cm^{-1}. Additional FTIR experiments were done by the same procedure for other epoxide monomers with different photoinitiators and photosenstizers. The results in terms of percent conversion were tabulated and reported in Table 5.23.
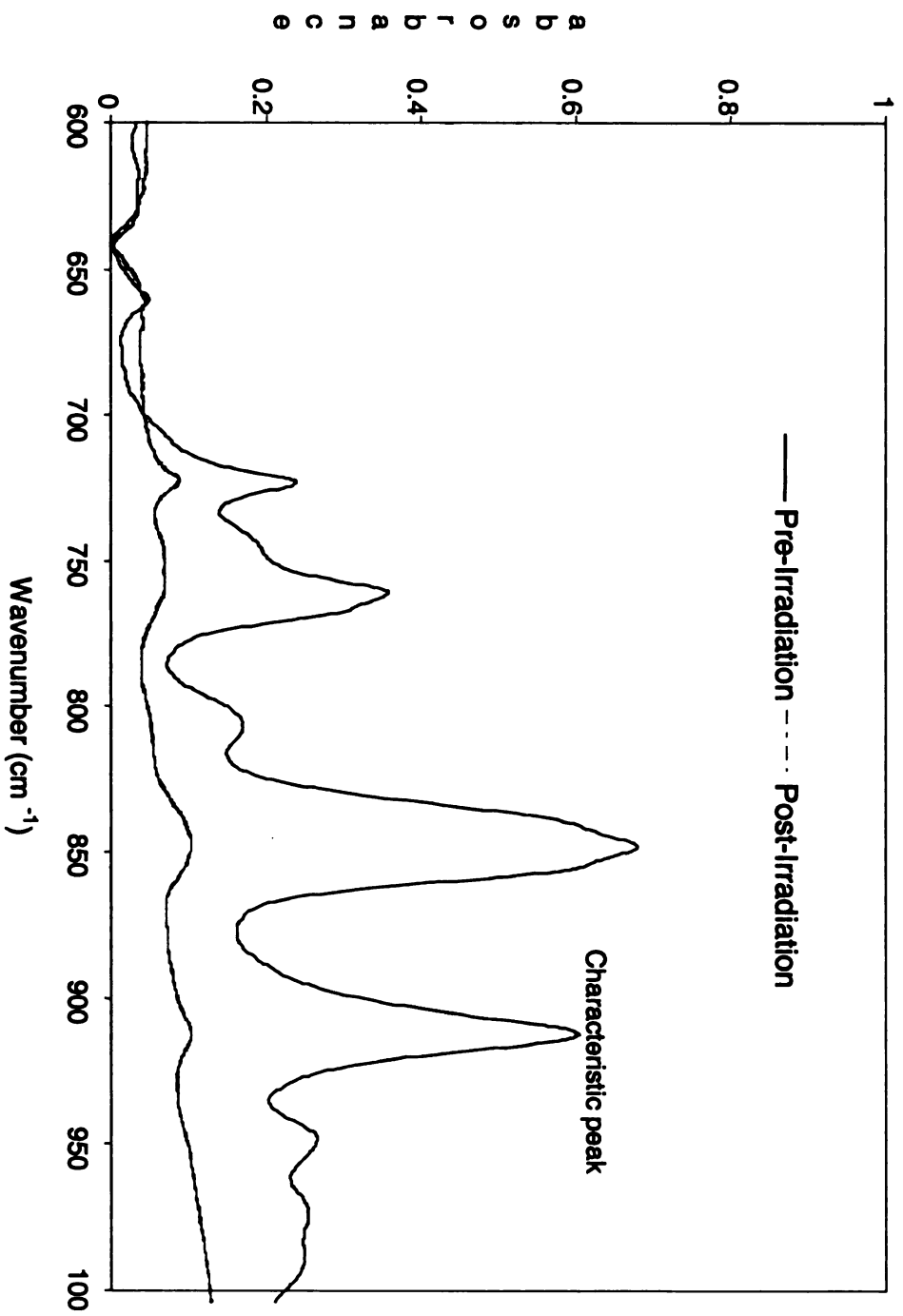
Figure 5.71. FTIR spectra for cationic photopolymerization of mono-epoxy *octyl glycidyl ether* initiated by 8.0 x 10⁻³ *molal* of tolycumyl iodonium tetrakis pentafluorophenyl borate and 8.0 x 10⁻⁴ *molal* CPTX.

Figure 5.72. FTIR spectra for cationic photopolymerization of di-epoxy *1,4-butanediol diglycidyl ether* initiated by 8.0×10^{-3} *molal* of tolycumyl iodonium tetrakis pentafluorophenyl borate and 8.0×10^{-4} *molal* CPTX.

Table 5.23. Percent conversion for various reaction systems using the method of FTIR.

Photoinitiator	Photosensitizer	Monomer	% conversion
Tolycumyl iodonium tetrakis pentafluourophenyl borate	CPTX (1-chloro-4-propoxy-9H-thioxanthen-9-one)	Octyl glycidyl ether	85
		Butyl glycidyl ether	90
		Phenyl glycidyl ether	98
		1,4-butanediol diglycidyl ether	62
		Cyclohexane dimethanol diglycidyl ether	58
		Trimethyol propane triglycidyl ether	52
Diaryliodonium hexafluoroantimonate	Anthracene	Octyl glycidyl ether	95
		Butyl glycidyl ether	85
		Phenyl glycidyl ether	98
		1,4-butanediol diglycidyl ether	55

5.2.4. Conclusions

The method of Transform Fourier Infrared (FTIR) spectroscopy was used in this research effort primarily for confirming the conversion values obtained by the PDSC experiments. As described in the experimental set-up, essentially two FTIR absorption spectra were used to calculate the percent conversion of a cationic photopolymerization. The results in Table 5.23 show a great deal of similarity in terms of conversion and general trends with respect to monomer structure and functionality as those obtained by PDSC experiments.

5.3. References

1. J. G. Kloosterboer, *Adv. Polym. Sci.*, **84**, 1 (1988).

2. K. S. Anseth, C. M. Wang and C. N. Bowman, *Macromolecules*, **27**, 650 (1994).

3. T. Doornkamp and Y. Y. Tang, *Polym. Commun.*, **31**, 362 (1990).

4. K. S. Anseth, C. M. Wang and C. N. Bowman, *Polymer*, **35**, 3243 (1994).

5. C. Dekker and K. J. Moussa, *Coatings Tech.*, **62**, 55 (1990).

6. J. V. Crivello, J. L. Lee and D. Conlon, *J. Rad. Curing*, **10**, 6 (1983).

7. E. W. Nelson, T. P. Carter, and A. B. Scranton, *J. of Poly. Sci., Poly. Chem Ed.*, **33**, 247 (1995).

8. E. W. Nelson, T. P. Carter, and A. B. Scranton, *Macromolecules.*, **33**, 247 (1995).

9. C. Priou, A. Soldat, J. Cavezzan, F. Castellanos and J. P. Fouassier, *J. of Coatings Tech.*, **67**, 851:71, (1995).

10. J. M. Barton, *Adv. Polym. Sci.*, **72**, 111 (1985).

11. J. V. Crivello and S. S. Liu, *J. Polym. Sci., Part A: Polym. Chem.*, **37**, 1199 (1999).

12. Y. Toba, M. Saito, and Y. Usui, *Macromolecules*, **32**, 3209 (1999).

13. J. V. Crivello, S. Liu, *Chem. Mater.*, **10**, 3724 (1998).

14. S. K. Rajaraman, W. A. Mowers, and J. V. Crivello, *Macromolecules*, **32**, 36 (1999).

15. R. Narayan and J. V. Crivello, *Macromolecules*, **29**, 439 (1996).

16. W. A. Patterson, *Anal. Chem.*, **26**, 823 (1954).

17. J. P. Kennedy, and E. Marechal, Carbocationic Polymerization, John Wiley & Son, N. Y. 1982.

18. S. P. Pappas, L. R. Gatechair, and J. H. Jilek, *J. Polym. Sci.: Polym. Chem. Ed.*, **22**, 77 (1984).

19. E. W. Nelson, T. P. Carter and A. B. Scranton, *J. Polym. Sci.: Polym. Chem. Ed.*, **33**, 247 (1995).

Chapter 6

Conclusions and Recommendations

This research effort has contributed to the fundamental understanding of the reaction kinetics of cationic photopolymerization of epoxide monomers. The results from the PDSC experiments of these UV-initiated cationic photopolymerizations presented in this thesis will complement the more macroscopic studies currently in literature and are imperative if the potential of these reactions is to be realized. In addition, the experimental techniques used in this research can be readily applicable in high-speed polymerization reactions. This chapter also provides some conclusions and recommendations for future work.

6.1. Summary of Results

The technique of Photo-differential scanning calorimetry (PDSC) has proven to be quite a useful tool to systematically characterize the reaction kinetics of cationic photopolymerization for a series of epoxide monomers with three distinct photoinitiators, and two different photosensitizers over a temperature range from 30°C to 40°C and finally to 50°C. Table 6.1 provides a summary of all the constituents that make up different combinations of reaction formulations. Basically, there are 42 total distinct reaction mixtures, each of which contains an epoxide monomer and a photoinitiator and may contain a photosensitizer. Several parameters that can affect the rate of polymerization and the ultimate limiting monomer conversion have been studied. The

parameters are initiating light intensity, type and concentration of photoinitiator, type and concentration of photosensitizer, and temperature. The kinetics results may be correlated with monomer structure and functionality and reaction conditions to provide insight into the underlying fundamental reaction processes.

Table 6.1. Summary of distinct reaction formulations in the kinetic studies of cationic photopolymerizations of epoxide monomers.

Photoinitiator	Photosensitizer	Epoxide monomer
Tolycumyl iodonium tetrakis (pentafluorophenyl) borate	1-chloro-4-propoxy - 9H-thioxanthen-9- one (CPTX)	Butyl glydidyl ether
		Octyl glycidyl ether
		Phenyl glycidyl ether
		1,4-butanediol diglycidyl ether
		Cyclohexane dimethanol diglycidyl ether
		Trimethyol propane triglycidyl ether

Note: Two other photoinitiators are: *diaryliodonium hexafluoroantimonate* and *triarylsulfonium hexafluorophosphate*, and another photosensitizer *anthracene*.

The two significant kinetics aspects of cationic photopolymerizations are the rate of polymerization, R_p, and the final monomer conversion, both of which can be affected by the parameters with the results presented in the following sections.

6.1.1. Effect of the Incident Light Intensity on Polymerization Kinetics

Our studies show that the incident (initiating) light intensity can affect tremendously the rate of polymerization. For example, when light intensity is raised from 35 mW/cm^2 to 90 mW/cm^2, the reaction rate for mono-epoxy octyl glycidyl ether with 8.0 x 10^{-3} molal diaryliodonium hexafluoroantimonate at 50°Ca reaction, the reaction rate more than doubles and the final conversion increases from 81% to 83%

(Table 5.1). This general trend with huge increase in rate of polymerization and relatively smaller increase in final conversion was also found in the case with di-epoxy 1,4-butanediol diglycidyl ether under the same initiator concentration and reaction temperature.

6.1.2. Effect of Photoinitiator and Photoinitiator Concentration on Cationic Photopolymerization Kinetics

The effect on the rate of polymerization is for the most part comparable for both photoinitiators diaryliodonium hexafluoroantimonate and tolycumyl iodonium tetrakis (pentafluorophenyl) borate, although there is some variability when it comes to monomers with a different number of epoxide rings in the monomer molecule. With the antimonate salt, the effect is a little more pronounced with the mono-epoxide monomers than with the di- and tri-epoxide monomers probably because of the crosslinking which severely limits the mobility of the active polymer chains from propagating with other epoxide groups. For a given photoiniatator at the same reaction temperature and initiating light intensity, the rate of polymerization is almost the same for tri and di-epoxide monomers and slowest for the mono-epxide monomer. The final conversion is in the reverse trend: mono-di-epoxide > di-epoxide > tri-epoxide (~ 85 %, ~ 76 % and ~ 60 % respectively). The effect of photoinitiator concentration was studied to show that the concentration of 8.0 x 10^{-3} molal would make the most sensible choice because the reaction rate was high and the final conversion reached the limiting point in most cases. The further increases in initiator concentration only result in small increase of the rate of polymerization and improve very little in conversion.

6.1.3. Effect of Photosensitizer and Photosensitizer Concentration on Polymerization Kinetics

The photosensitizer is added to the reaction mixture in order to increase the spectral sensitivity of the photoinitiator to the initiating light, which has strong emission peaks in the 300 – 380 nm region (near UV). The photosensitizer causes a remarkable increase in the rate of polymerization by increasing the active centers at the initial phase of the reaction. As a result, the final conversion also increases. Overall, CPTX was determined to be a better photosensitizer than anthracene because CPTX absorbs more strongly of the initiating light (Figure 4.11). The efficiency of the photosensitizer CPTX was studied by changing its concentration in a series of reaction mixtures containing butyl glycidyl ether and 8.0×10^{-3} molal of diaryliodonium hexafluoroantimonate. Our studies indicate that at sensitizer concentration of $8.0 \times 1{-}4$ molal, the reaction rate more than doubles, but the conversion only increases from ~ 71 % to ~ 73%. When raised to 8.0×10^{-3} molal (a tenfold increase), the reaction rate only increased by about 22% and the conversion changed from ~73 % to ~75 %.

6.1.4. Effect of the Monomer Structure and Functionality on Polymerization Kinetics

Monomer molecular structure (as illustrated in Table 4.1) was determined to affect the reaction kinetics of cationic photopolymerization. Among the three mono-epoxide monomers in this research, the monomer phenyl glycidyl ether is most reactive and consequently has the highest final conversion; the monomer butyl glycidyl ether was a little more reactive than octyl glycidyl ether, but has lower conversion. This

observation may be attributed to butyl glycidyl ether's low glass transition temperature. Between the two di-epoxide monomers, 1,4-butanediol diglycidyl ether was observed to generally have a slightly higher reaction rate and conversion as compared to those of the cyclohexane dimethanol diglycidyl ether. With respect to functionality (number of epoxide rings in a monomer molecule), monomer reactivity is ranked as follows: di-epoxides > tri-epoxides > mono-epoxides; and for final conversion: mono-epoxides > di-epoxides > tri-epoxides.

6.1.5. Effect of the Temperature on Polymerization Kinetics

As expected, reaction temperature was observed to affect the both the rate of polymerization and final conversion. The effect of temperature by itself in general is smaller than with the addition of a photosensitizer and a given photoinitiator. For example, for a reaction mixture containing butyl glycidyl ether with 8.0×10^{-3} molal photoinitiator tolycumyl iodonium tetrakis (pentafluorophenyl) borate, the reaction rate increases from 0.0044 mol/L*sec at 30°C to 0.0316 mol/L*sec at 50°C for the control sample , whereas the rate increases from 0.0138 mol/L*sec at 30°C to 0.0551 mol/L*sec at 50°C with the photosensitizer CPTX at 8.0×10^{-4} molal (Table 5.9).

In general, as the reaction temperature increases, the rate of polymerization also increases rather significantly, however the final conversion does not necessarily increase with the same magnitude due to the difference in monomer structure and functionality.

6.2. Recommendations for Future Works

The focus of this research effort is on the final outcomes with respect to the rate of polymerization and final limiting conversion. Further investigation can be implemented in the following areas:

- The mechanism on the rate of the active centers generation.

- Determination of the propagation rate constant and elucidate its behavior throughout the course of the reaction.

- Determination of the termination rate constant.